COMPOSITE BEAMS WITH FLEXIBLE CONNECTIONS

THE BEHAVIOUR OF COMPOSITE BEAMS WITH FLEXIBLE CONNECTIONS

by

IVAN HAMILTON ARCHER, B.Sc.

A Thesis

Submitted to the Faculty of Graduate Studies

in Partial Fulfilment of the Requirements

for the Degree

Master of Engineering

McMaster University

February, 1966

MASTER OF ENGINEERING
(Civil Engineering)

McMASTER UNIVERSITY
Hamilton, Ontario.

TITLE: The Behaviour of Composite Beams With Flexible Connections

AUTHOR: Ivan Hamilton Archer, B.Sc. (University of Manitoba)

SUPERVISOR: Dr. H. Robinson

NUMBER OF PAGES: x, 154

SCOPE AND CONTENTS: Two types of tests are reported in this thesis: (1) tests of push-out specimens and (2) tests of composite rectangular beams. These tests were conducted to provide information regarding the behaviour of composite beams with flexible connections, and also to investigate the suitability of the Newmark and Stussi theories for composite beam analysis.

ACKNOWLEDGEMENTS

The author feels especially indebted to Dr. H. Robinson who suggested the problem, and who provided encouragement and guidance throughout the tests and the analysis of the test results.

Gratitude is extended to Dr. G.A. Oravas for the general assistance and advice given from time to time during the course of this study.

Thanks are also due to the National Research Council whose financial assistance made it possible to carry out the work.

CONTENTS

Chapter		Page
1	INTRODUCTION	1
	1.1 Introduction	1
	1.2 Object and Scope of Investigation	2
	1.3 Definitions	5
2	THEORETICAL ASPECTS	7
	2.1 General	7
	2.2 The Newmark Theory	7
	2.3 The Stussi Theory	11
3	PUSH-OUT TESTS	14
	3.1 Description of Specimens and Materials	14
	3.2 Preparation of Specimens	16
	3.3 Instrument and Loading Apparatus	16
	3.4 Test Procedure	17
	3.5 Test Results and Observations	17
4	COMPOSITE RECTANGULAR BEAM TESTS	27
	4.1 Description of Specimens and Materials	27
	4.2 Manufacture of Specimens	29
	4.3 Instrument and Loading Apparatus	30
	4.4 Testing Procedure	32
	4.5 Deflection Characteristics of Beams	34
	4.6 Strain Measurements	37
	4.7 Slip Measurements	39
	4.8 Modes of Failure and Comparison of the Behaviour of Beams	41
5	DISCUSSION AND SUMMARY	98
	5.1 Discussion	98
	5.2 Comparison Between the Newmark and Stussi Theories	102
	5.3 Summary	104

CONTENTS (Continued)

Chapter		Page
6	CONCLUSIONS AND RECOMMENDATIONS	127
	6.1 Conclusions From Tests on Composite Beams	127
	6.2 Recommendations for Future Studies	128
APPENDIX A		130
	A.1 Notation	130
	A.2 Analysis by the Newmark Theory	132
	A.3 Sample Calculations	138
APPENDIX B		
	B.1 Notation	142
	B.2 Analysis by the Stussi Theory	144
	B.3 Sample Calculations	149
REFERENCES		154

LIST OF FIGURES

Figure		Page
2.1	Variation of q/q' and F/F' for Simply Supported Beam with Two-Point Load	12
2.2	Variation of q, q/q', F and F/F' for Simply Supported Composite Beam with Uniformly Distributed Loading	13
3.1	Details of Push-Out Specimens	21
3.2	Loading Position of Push-Out Specimen with 3/8" and 5/16" Diameter Connectors	22
3.3	Loading Position of Push-Out Specimen with 1/4" Diameter Connectors	23
3.4	Load-Slip Curves for Specimens with 3/8" Diameter Connectors	24
3.5	Load-Slip Curves for Specimens with 5/16" Diameter Connectors	25
3.6	Load-Slip Curves for Specimens with 1/4" Diameter Connectors	26
4.1	Connector Spacings and Loading Configurations	46
4.2	Details of Shear Connections	47
4.3	Loading Position of B1, B2, B3 and B4	48
4.4	Typical Failure for B1, B2, B3 and B4	49
4.5	Loading Position of Encastre Beam	50
4.6	Loading Position of B6	51
4.7	Position of Gauges on B1, B2, B3, B4 and B6	52
4.8	Position of Gauges on B5	53
4.9	Load-Deflection Curves for B1	54
4.10	Load-Deflection Curves for B1	55

LIST OF FIGURES (Continued)

Figure		Page
4.11	Load-Deflection Curves for B2	56
4.12	Load-Deflection Curves for B2	57
4.13	Load-Deflection Curves for B1 and B2	58
4.14	Load-Deflection Curves for B3	59
4.15	Load-Deflection Curves for B3	60
4.16	Load-Deflection Curves for B4	61
4.17	Load-Deflection Curves for B4	62
4.18	Load-Deflection Curves for B3 and B4	63
4.19	Load-Deflection Curves for B5	64
4.20	Moment- Deflection Curves for B6	65
4.21	Load-Strain Curves for Bottom of B1	66
4.22	Load-Strain Curves for Bottom of B1	67
4.23	Load-Strain Curves for Bottom of B1	68
4.24	Load-Strain Curves for Bottom of B1	69
4.25	Load-Strain Curves for Top of B1	70
4.26	Load-Strain Curves for Top of B1	71
4.27	Load-Strain Curves for Bottom of B2	72
4.28	Load-Strain Curves for Top of B2	73
4.29	Load-Strain Curves for Bottom of B3	74
4.30	Load-Strain Curves for Bottom of B3	75
4.31	Load-Strain Curves for Bottom of B3	76
4.32	Load-Strain Curves for Bottom of B4	77

LIST OF FIGURES (Continued)

Figure		Page
4.33	Load-Strain Curves for Bottom of B5	78
4.34	Strain Distribution Curves for Bottom of B5 at 600 lbs. Load Level	79
4.35	Strain Distribution Curves for Bottom of B5	80
4.36	Cross-Sectional Strain Distribution for B1	81
4.37	Cross-Sectional Strain Distribution for B2	82
4.38	Cross-Sectional Strain Distribution for B3	83
4.39	Cross-Sectional Strain Distribution for B4	84
4.40	Slip Distribution for B1 (2nd. Loading)	85
4.41	Slip Distribution for B2 (2nd. Loading)	86
4.42	Slip Distribution for B3 (2nd. Loading)	87
4.43	Slip Distribution for B4 (2nd. Loading)	88
4.44	Slip Distribution Curves for B5	89
4.45	Slip Distribution Curves for B6	90
4.46	Load-Slip Curves for B1	91
4.47	Load-Slip Curves for B2	92
4.48	Load-Slip Curves for B1 and B2	93
4.49	Load-Slip Curves for B3	94
4.50	Load-Slip Curves for B4	95
4.51	Load-Slip Curves for B3 and B4	96
4.52	Variation of Slip in B2 after Ultimate Load	97
5.1	Variation of 1/C in Beam B1	106

LIST OF FIGURES (Continued)

Figure		Page
5.2	Variation of k in Beam B1	107
5.3	Variation of 1/C in Beam B2	108
5.4	Variation of k in Beam B2	109
5.5	Variation of 1/C in Beam B3	110
5.6	Variation of k in Beam B3	111
5.7	Variation of 1/C in Beam B4	112
5.8	Variation of k in Beam B4	113
5.9	Load-Slip Curves for Connectors in Beam B1	114
5.10	Load-Slip Curves for Connectors in Beam B2	115
5.11	Load-Slip Curves for Connectors in Beam B3	116
5.12	Load-Slip Curves for Connectors in Beam B4	117
5.13	Slip Distribution for Beam B1	118
5.14	Slip Distribution for Beam B3	119
5.15	Slip Distribution for Beam B6	120
5.16	Slip Distribution Curves for Beam B1	121
5.17	Slip Distribution Curves for Beam B3	122
5.18	Variation of Connector Load in Beam B5	123
5.19	Efficiency Curves for Composite Beams (Based on Deflection Calculations)	124
5.20	Deformed Position of B6 at 1,000 lb. Load Level	125
5.21	Deformed Position of B6 at 9,000 lb. Load Level	126

LIST OF TABLES

Table		Page
3.1	Results of Push-Out Tests	19
4.1	Description of Composite Rectangular Beams	28
4.2	Modulus of Elasticity of Steel	31
A.1	Results of Beam B1	141
B.1	Results of Beam B2	153

CHAPTER 1

INTRODUCTION

1.1 Introduction

A composite structure is one which consists of two or more components which are held together so as to act as one unit.

During the past two decades the behaviour of composite structures has been the subject of an intensive theoretical and experimental study. Although a great deal of understanding has been obtained, there are still many aspects relating to this type of structure to be investigated. For example, it has not yet been possible to measure the magnitude of the load on a shear connector.

A conventional composite beam is one consisting of a concrete deck slab and steel beam, which may be called the major components, and which are held together through the medium of shear connectors. If during loading there is no slip or relative movement between the slab and beam, then complete interaction is achieved. However, even in the best practical case there is

normally some relative movement which is brought about by the development of horizontal shear forces in the components. Hence, one may generally conclude that there is a loss of interaction whenever a composite beam undergoes flexural loading. Since the shear connectors also serve the purpose of resisting horizontal forces, the control of slip depends greatly on the overall performance of these connectors.

Many different types of mechanical connectors have been used. These included angles, channels, plates, tees, hooked bars, spirals and studs. Of these the stud connector has been used most extensively, perhaps on account of its easy method of installation.

The intrinsic merit of the conventional composite T-beam lies in the dual utilization of the slab (as in reinforced concrete construction), in the rational disposition of the two materials in respect of their tensile and compressive strength and stability, and in the advantages of their prefabrication.

1.2 Object and Scope of Investigation

Since a knowledge of the behaviour of a beam under a given loading configuration is a design prerequisite, then a theoretical method of analysis becomes

desirable so as to provide basic information regarding such behaviour. N.W. Newmark[1] and Fritz Stussi[2] have both developed theoretical methods whereby composite beams may be analyzed; and the main object of this investigation was to verify various aspects of these theories by experimental observations. It was also the purpose of this project to draw certain comparisons between the two theories, and to observe the influence of connector spacing on the overall performance of a composite beam.

Robinson[8] observed that there was good agreement between the experimental behaviour of his fourteen beams tested and that predicted by the Newmark theory. This was thought to be due, in large part, to a more flexible connection brought about by the incorporation of a cellular zone, compared to the more conventional composite beam with a distinct interfacial plane which may result in a stiff connection. Hence, the beams tested in this investigation were made with flexible connectors.

Push-out tests were used to determine the moduli of the shear connectors. However, it should be borne in mind that the loading conditions of push-out tests do not fully simulate those of flexural loading;

and therefore, the performance of a connector in a push-out test may not be truly representative of its behaviour in a composite member undergoing flexural loading. Some of the differences may be attributed to the following:-

1) The slab in the push-out test is not in overall compression as may be the case in the beam.
2) The stress distribution over the slab thickness is different from that in the beam.
3) The uplift force which has been observed in beam tests may be restricted in a push-out test.

Despite these differences, push-out tests have been widely used as a means of evaluating the shear strength and load-slip characteristics of different types of shear connectors[5].

The experimental work of this investigation consisted of the testing of nine push-out specimens and six small-scale composite rectangular beams. In the push-out tests only load and slip were measured, whereas in the beam tests slip, strain and deflection were recorded at various points along the beam and at diffe-

rent load levels.

Comparisons were made between the experimental results and those derived from the theoretical solutions of Newmark and Stussi. These theories are presented in the Appendices.

Use was made of an I.B.M. 7040 digital computer to facilitate some of the computations.

1.3 Definitions

The following is a list of terms used throughout the investigation. Some of these definitions may be peculiar to this presentation alone, and have been used so as to make this dissertation more easily readable.

A COMPOSITE RECTANGULAR BEAM refers to a beam composed of two rectangular sections interconnected in such a way that they act together as one unit.

AN INTERFACE is the area of contact between the two components.

A SLAB COMPONENT is the element above the interface.

A BEAM COMPONENT is the element below the interface.

A SHEAR CONNECTOR is a device for transmitting horizontal shear between the slab and beam components,

and for preventing the separation of these components.

A FLEXIBLE CONNECTOR is one which deforms under loading.

SLIP is the relative horizontal movement between the slab and beam components at a particular section.

THE MODULUS of a shear connector is that load on the connector which produces a unit slip.

THE CONNECTOR LOAD is the horizontal shear force transmitted by the connector from one component to the other.

COMPLETE INTERACTION exists between the slab and beam components when there is no relative movement between these compon nts. However, if slip does take place, there is a loss of interaction; and INCOMPLETE INTERACTION is said to exist.

The condition of NO INTERACTION exists when the slab and beam components act independently of each other, and no horizontal force is transferred between these two components. Under this condition slip takes place freely at the interface.

THE INTERACTION COEFFICIENT, 1/C, is a dimensionless expression indicating the degree of interaction. It is a function of the modulus of the connector, the connector pitch, the elastic and geometric properties of the slab and beam components and the span of the composite beam.

CHAPTER 2

THEORETICAL ASPECTS

2.1 General

If a two-point, quarter-point loaded, simply supported beam is made to bear the same total external load as a simply supported beam carrying a uniformly distributed load, then the vertical end shear and the midspan moment in both beams would be the same. Accordingly, in the past it was a common assumption that a two-point loading applied at quarter-span of a simply supported beam was a good simulation of a uniformly distributed loading on a simply supported beam.

2.2 The Newmark Theory

An application of the above assumption to a composite flexural member led to the belief that measurements taken at, or close to, midspan in this type of two-point loaded composite beam would provide true information concerning the effects of a uniformly distributed loading on a simply supported composite member. However, the Newmark theory suggests that such a belief may hold true for composite beams with low degrees of interaction; but that when there is a high degree of interaction, there

is a marked difference in the behaviour of these two types of structures.

Figs. 2.1 and 2.2 show the theoretical predictions of Newmark for these beams. The F/F' curves may be interpreted as an indication of the loss of interaction along the beams. One notes that for 1/C = 100.0 both beams reveal little loss of interaction, as the F/F' curves show relatively high values throughout the length of these members. However, it is observed that there is a marked loss of interaction along both members when the interaction coefficient decreases to a value of 1.0, and that this loss of interaction varies in a similar manner for both beams.

In Fig. 2.1 the q/q' curves give an idea of the variation of the horizontal shear flow along the beam, while this is shown by the q curves in Fig. 2.2. It can be seen that for the two loading configurations there is a significant difference in the variation of the unit horizontal shear per unit length of beam for a high degree of interaction. As an example, when the value of 1/C is 100.0 the shape of the q/q' curve in Fig. 2.1 is different from that of the q curve in Fig. 2.2. For the quarter-point loading in Fig. 2.1 the magnitude of q/q' decreases by approximately 100% between x/L = 0.125 and x/L = 0.375, whereas in Fig. 2.2 the magnitude of q decreases by 68%

over the same range of x/L. However, for 1/C = 1.0, that is to say for a very flexible connection, there is a similarity in the variation of the horizontal shear flow for both types of loading. The q/q' curve in Fig. 2.1, which is the same as the q curve for the two-point loading, has a shape similar to that of the q curve in Fig. 2.2. Between x/L = 0.125 and x/L = 0.375 the magnitude of q/q' decreases by 67.5%, while the magnitude of q decreases by 62.2% over this same range of x/L in Fig. 2.2.

Other points of interest arising out of these theoretical curves are shown in Fig. 2.1. Here it is evident that the greatest loss of interaction takes place at the load points. Also, as the points of application of the load moves towards the points of support, there is a more pronounced breakdown of interaction at the load points as indicated by the F/F' curves, a greater loss of interaction in the shear spans, and a decrease in the loss of interaction towards midspan.

One assumption of the Newmark theory is that the values of 1/C and k are constant throughout the length of the beam and throughout the elastic range. In this investigation these quantities were computed on the basis of slips measured along the length of the beam, and were found to vary from point to point and at different load levels as shown in Figs. 5.1 to 5.8. It is likely that the theory in its present form is inadequate for computing

these quantities in this manner.

Since 1/C was found to vary along the beam, two different values of the interaction coefficient were used in the analyses of beams B1 and B3. These were called 1/C constant and 1/C varying, and were derived on the basis of slips measured along these members. The constant coefficient of interaction was obtained by taking the average value of the different interaction coefficients for the end connection in the elastic range. This elastic range was conservatively determined from the load-deflection curves of the member. The end connection was selected over the others since it was felt that a connector at this point was a good representation of a connector in a push-out test, as the end of a simply supported beam has zero moment, and may be thought of as a region of pure shear.

The varying interaction coefficient was derived by taking the average of the different coefficients of interaction at a given load level as the coefficient for that load. Therefore, since the interaction coefficients varied as the load was changed, it meant that a different value of 1/C was applied in the analysis for each load increment. However, this was not done for B5, as the value of 1/C for this member was based upon the value of k which was obtained from the push-out tests for ¼" diameter connectors.

2.3 The Stussi Theory

It is important to note that while Newmark has provided a theoretical method of evaluating composite beam deflections, Stussi has not directly developed a procedure for this type of computation. However, since the Stussi theory does provide for the computation of the horizontal force, F, along the beam, a theoretical method of deflection computations becomes possible. This is done by postulating that the horizontal force acts at the centroids of both the slab and beam components, and does not contribute to the deflection of the composite beam. Accordingly, in the computations the external moment was reduced by the couple generated by the horizontal force at each connector location along the beam, and then conjugate beam methods were used to calculate the deflection of the member. This method of evaluation is referred to as the Stussi method for deflection calculations, and an example of its application has been included in Appendix B.

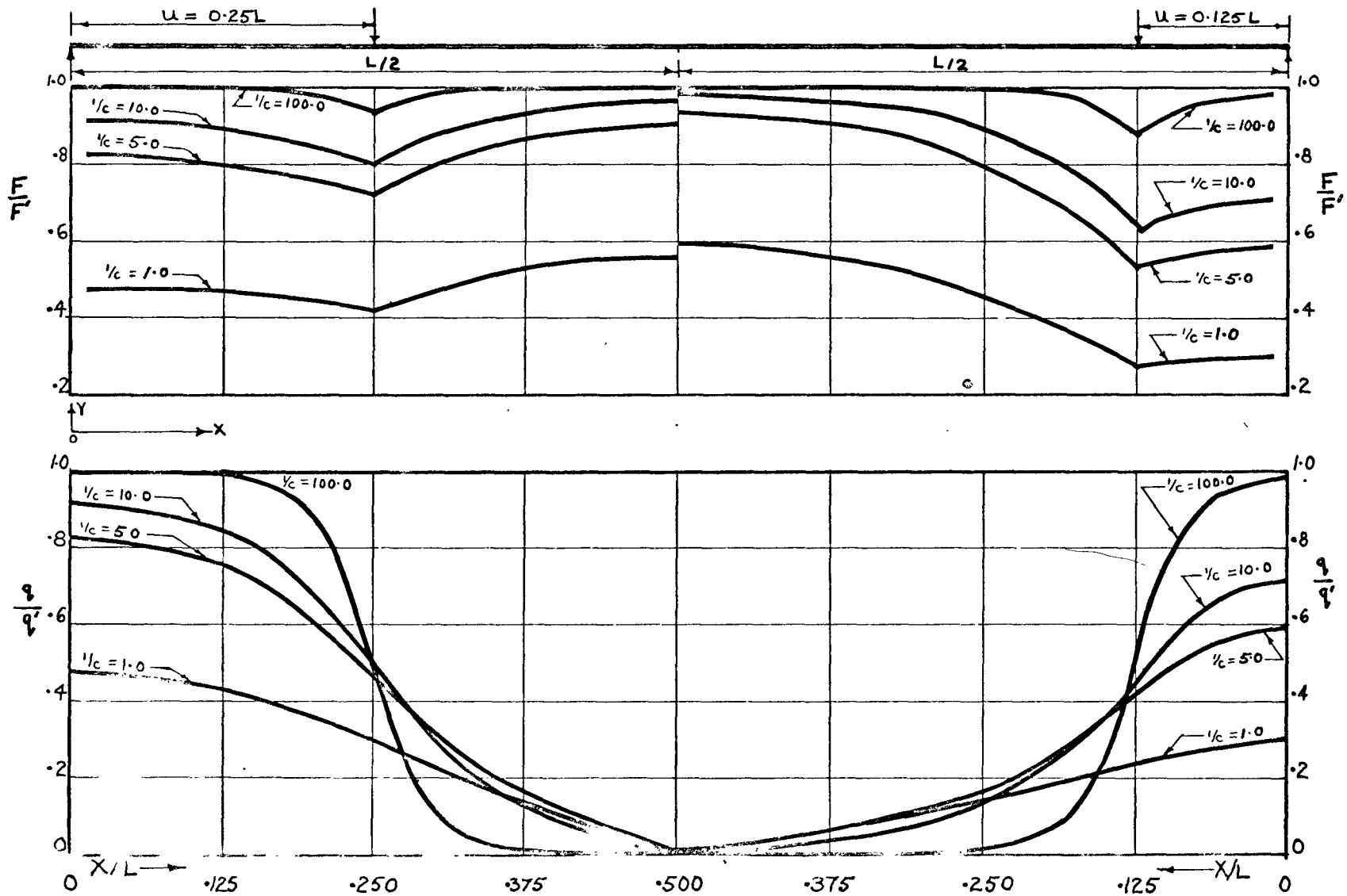

Fig. 2.1 Variation of q/q' and F/F' for Simply Supported Composite Beam with Two-Point Ld.

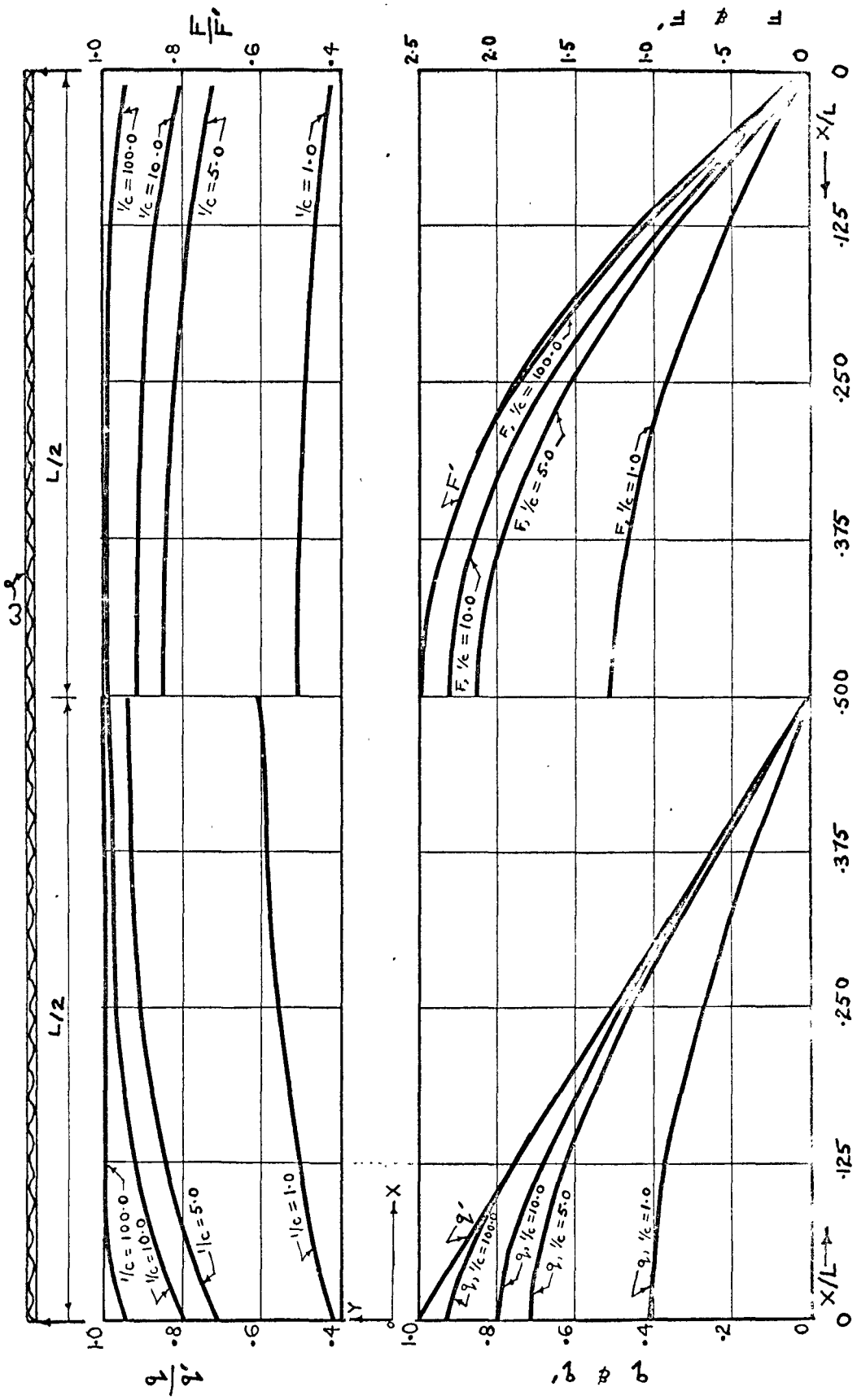

Fig. 2.2 Variation of q, q/q', & F/F' for Simply Supported Concrete Beam with U.D.L.

CHAPTER 3

PUSH-OUT TESTS

3.1 Description of Specimens and Materials

An attempt was made to contain the connectors in the same depth of material as they were in the beam specimens. The push-out specimens are shown in Figs. 3.1, 3.2 and 3.3. Each specimen consisted of a rectangular steel slab in the middle with two similar slabs attached at each edge so as to form an H-section. The outer steel slabs° were connected to the central one* by means of shear connectors. Lateral movement of the outer slabs was prevented by having these components securely connected to a base plate 1¼" thick.

In most push-out tests for conventional composite beams only one pair of connectors is used in each specimen. However, in these tests each specimen was provided with two pairs of connectors. It was surmised that since there was no bond between the outer slabs and the connectors, rotational movement of the central slab could occur if there was any eccentricity in loading with

° Referred to as slab component in Figs. 3.4, 3.5 and 3.6

* Referred to as beam component in Figs. 3.4, 3.5 and 3.6

respect to the vertical plane at mid-thickness of the central slab, and if only one pair of connectors were used. It was assumed that there would be an even distribution of the load among the four connectors in each specimen.

The main purpose of the push-out tests was to determine the shear strength and load-slip characteristics of the shear connectors. The variables included the diameter and length of the connectors, and the thickness and width of the rectangular steel slabs. The 3/8" and 5/16" diameter connectors were tested in specimens made up of 1¼" x 6" x 14" steel slabs; while the ¼" diameter connectors were tested in specimens of which the rectangular slabs were ¾" x 4" x 12".

Connectors of the same diameter were tested in the same housing; and in addition, for 3/8" and 5/16" diameter connectors the same housing was used. However, the holes were positioned in such a way that for different sets of connectors of a specific diameter, each corresponding pair of connectors had its longitudinal axes at a constant distance apart. Also, for each set of connectors different holes were used. Table 3.1 contains a summary of specimen details and push-out test results.

The rectangular slabs and base plates were made from cold-rolled steel plates, while the connectors were prepared from cold-rolled steel rods.

3.2 Preparation of Specimens

The connectors were cut to length from steel rods and rounded at their ends. The threads were then carefully prepared in a threading machine, and a threaded nut was fitted at one end of each connector.

The rectangular slabs were cut to size from steel plates. For each specimen these slabs were clamped together, and remained clamped until all the holes were drilled, tapped and threaded. This measure was to ensure a proper line-up of the components in the final assemblage of the specimen. Two $\frac{1}{2}$" deep grooves were cut in each base plate to such widths as to provide a tight fit for the outer rectangular slabs.

The contact surfaces of the steel slabs were machined to a smooth finish and coated with oil so as to reduce friction. The outer slabs were then placed in the base plate grooves, and the central member was put into position and attached to the outer ones by the shear connectors. The shear connectors were passed through the holes in the outer slabs and were screwed tight into the threaded holes of the middle slab. The threaded nuts were then screwed fingertight against the outer slabs.

3.3 Instrument and Loading Apparatus

The specimens were tested on a Tinius-Olsen Universal four-screw testing machine with a capacity of

120,000 lbs. The load was applied to the central slab through a ball platen in an attempt to achieve an equal distribution of the load.

Interfacial slip between the central and outer slabs was measured with dial indicators having 0.0001 inch graduations. These gauges were positioned as shown in Figs. 3.1, 3.2 and 3.3. Two gauges were fitted on the central slab, and small brackets were attached to the outer slabs in such a way as to engage the dial stems during loading.

3.4 Test Procedure

Prior to the main test, the load on specimens with 3/8" and 5/16" diameter connectors was cycled in small increments between zero and 4,000 lbs. until such time as it was discovered that there was no residual slip when the load was reduced to zero. The same was done in the case of specimens with $\frac{1}{4}$" diameter connectors except that the load was not allowed to exceed 1,500 lbs.

During testing the load was applied to each specimen in 1,000 lb. increments until the maximum load was reached. The dial gauges were read at each load increment to the nearest 0.0001 inch.

3.5 Test Results and Observations

Results of the push-out tests are presented in

Table 3.1. In Figs. 3.4, 3.5 and 3.6 load-slip curves for the specimens are shown. For each curve in these figures the values of the slips plotted were obtained by averaging the slips measured by both indicators on the same specimen. The ordinates of the load-slip curves are equal to one-quarter the actual loads applied on the specimens, since there were four connectors in each specimen. Generally, the elastic slopes of the curves in each figure show best agreement at the central portions of these curves, and it was from these portions that the connector moduli were determined.

Prior to testing, the assumption had been made that there would have been an equal distribution of the total load among the four connectors in each specimen. During the tests the two dial indicators on each specimen recorded different readings; also the early portion of each load-slip curve generally followed a different path, thus indicating that there was unevenness in the load distribution among the connectors. However, the inaccuracies brought about by the uneven distribution of the load were partly compensated for by averaging the slip readings.

Another possible source of inaccuracy might have been due to friction at the contact surfaces between the central and outer slabs. However, because of the smoothness of these surfaces, and the fact that the nuts on the shear connectors were only fingertight, it is believed

TABLE 3.1

RESULTS OF PUSH-OUT TESTS

Specimen Set No.	Dimensions in inches			Avg. Ult. Load per Connector (kips)	Connector Modulus in 10^5 lbs/in.	Avg. Connector Modulus in 10^5 lbs/in.
	Central Slab	Outer Slab	Shear Connector			
1	¾ x 4 x 12	¾ x 4 x 12	¼ x 1 3/8	2.78	2.59	
2	¾ x 4 x 12	¾ x 4 x 12	¼ x 1 3/8	2.80	2.56	
3	¾ x 4 x 12	¾ x 4 x 12	¼ x 1 3/8	2.76	2.59	2.58
1	1½ x 6 x 14	1½ x 6 x 14	5/16 x 1 7/8	4.72	3.67	
2	1½ x 6 x 14	1½ x 6 x 14	5/16 x 1 7/8	4.63	3.76	
3	1½ x 6 x 14	1½ x 6 x 14	5/16 x 1 7/8	4.53	4.04	3.82
1	1½ x 6 x 14	1½ x 6 x 14	3/8 x 1 7/8	5.80	2.99	
2	1½ x 6 x 14	1½ x 6 x 14	3/8 x 1 7/8	5.86	4.35	
3	1½ x 6 x 14	1½ x 6 x 14	3/8 x 1 7/8	5.95	2.98	3.44

that errors due to this cause were negligible.

Once the ultimate load was reached, the applied load began to drop off, while excessive slip continued to take place. This went on until the connectors started to shear off. In most of the specimens two connectors sheared off in quick succession on one side; in the others, connectors sheared off alternately on both sides. Whenever two connectors had sheared off on any one side of a specimen, the test was discontinued.

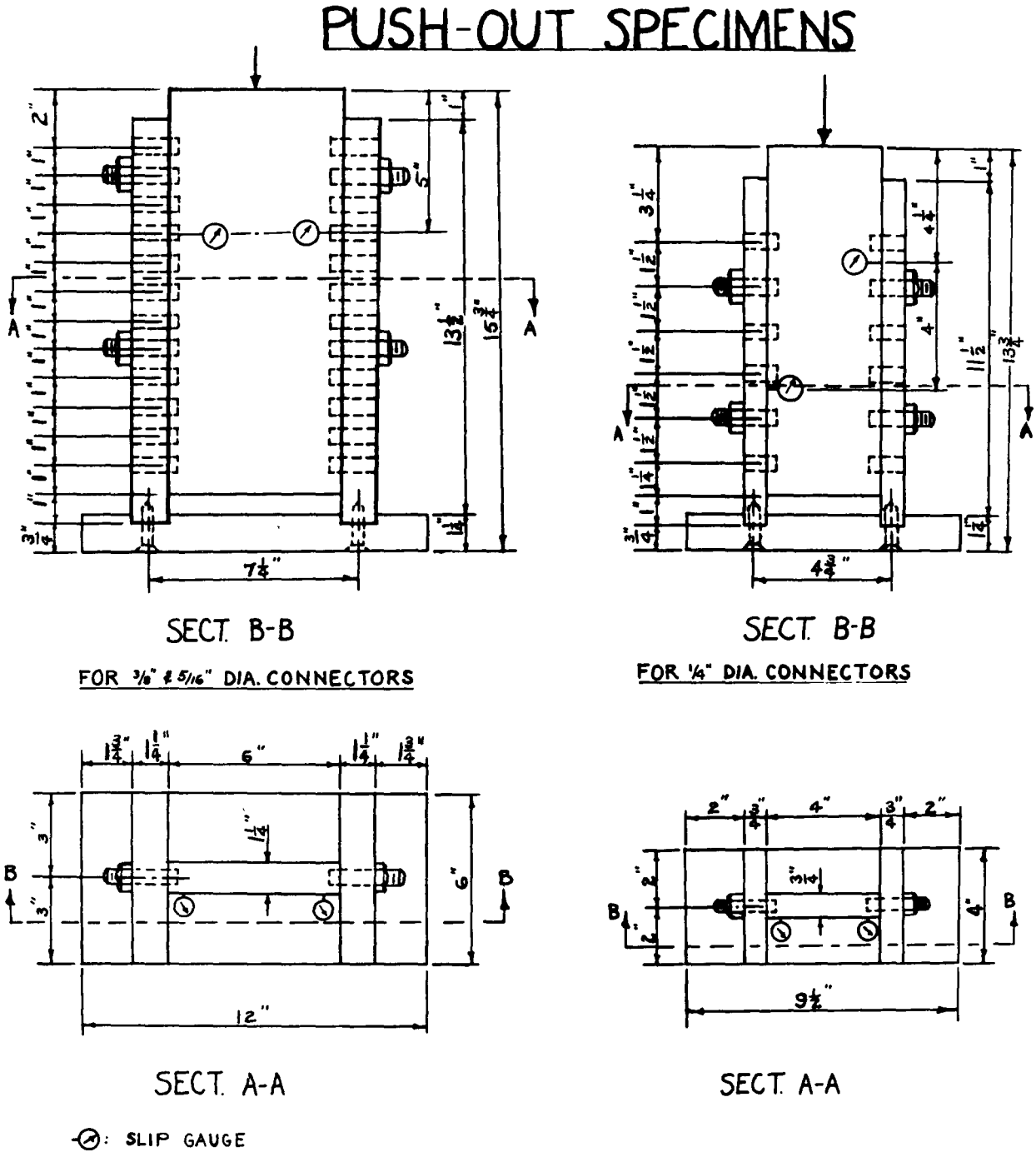

Fig. 3.1 Details of Push-out Specimens

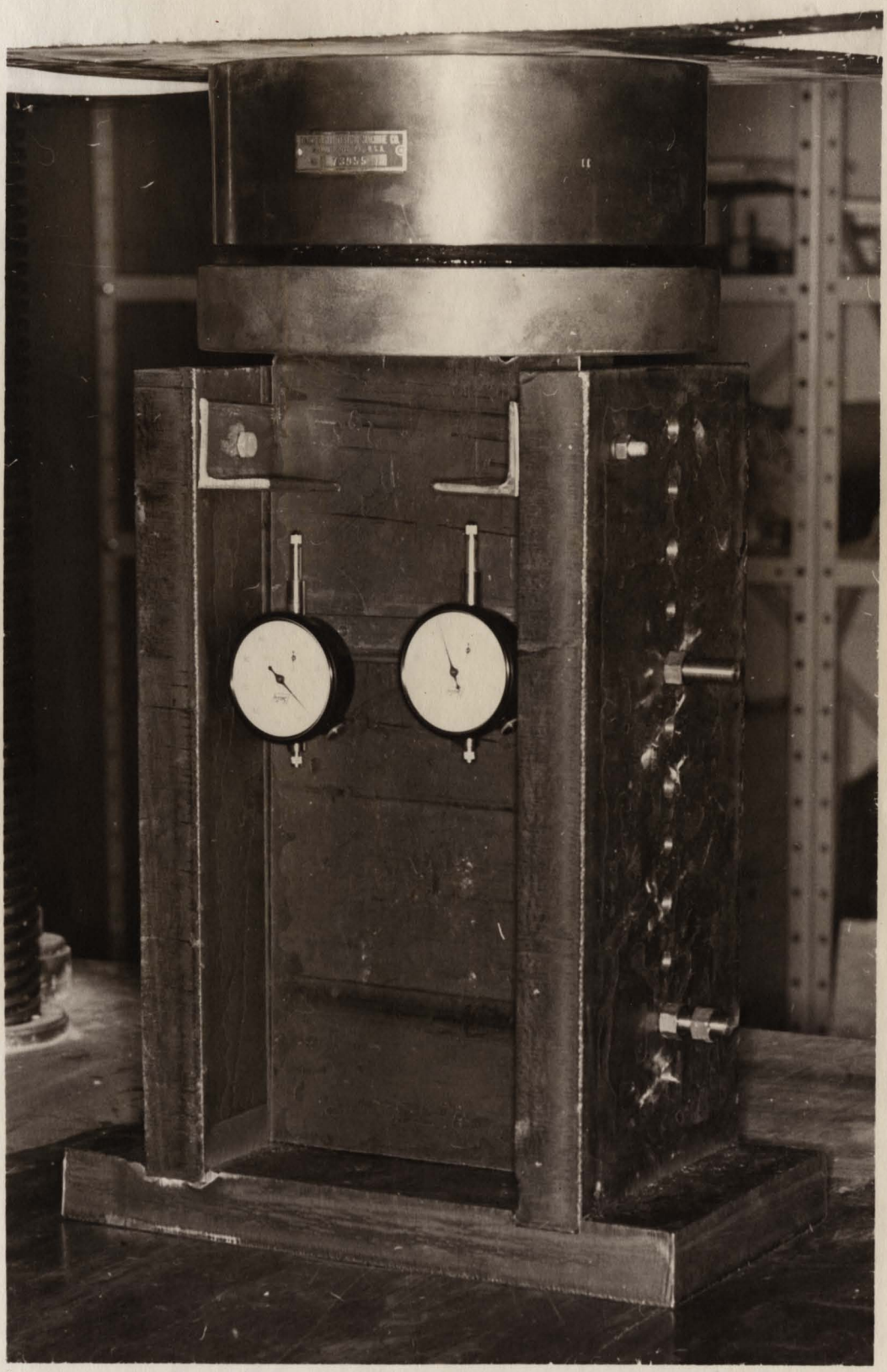

Fig. 3.2 Loading Position of Push-Out Specimen with 3/8" and 5/16" Diameter Connectors

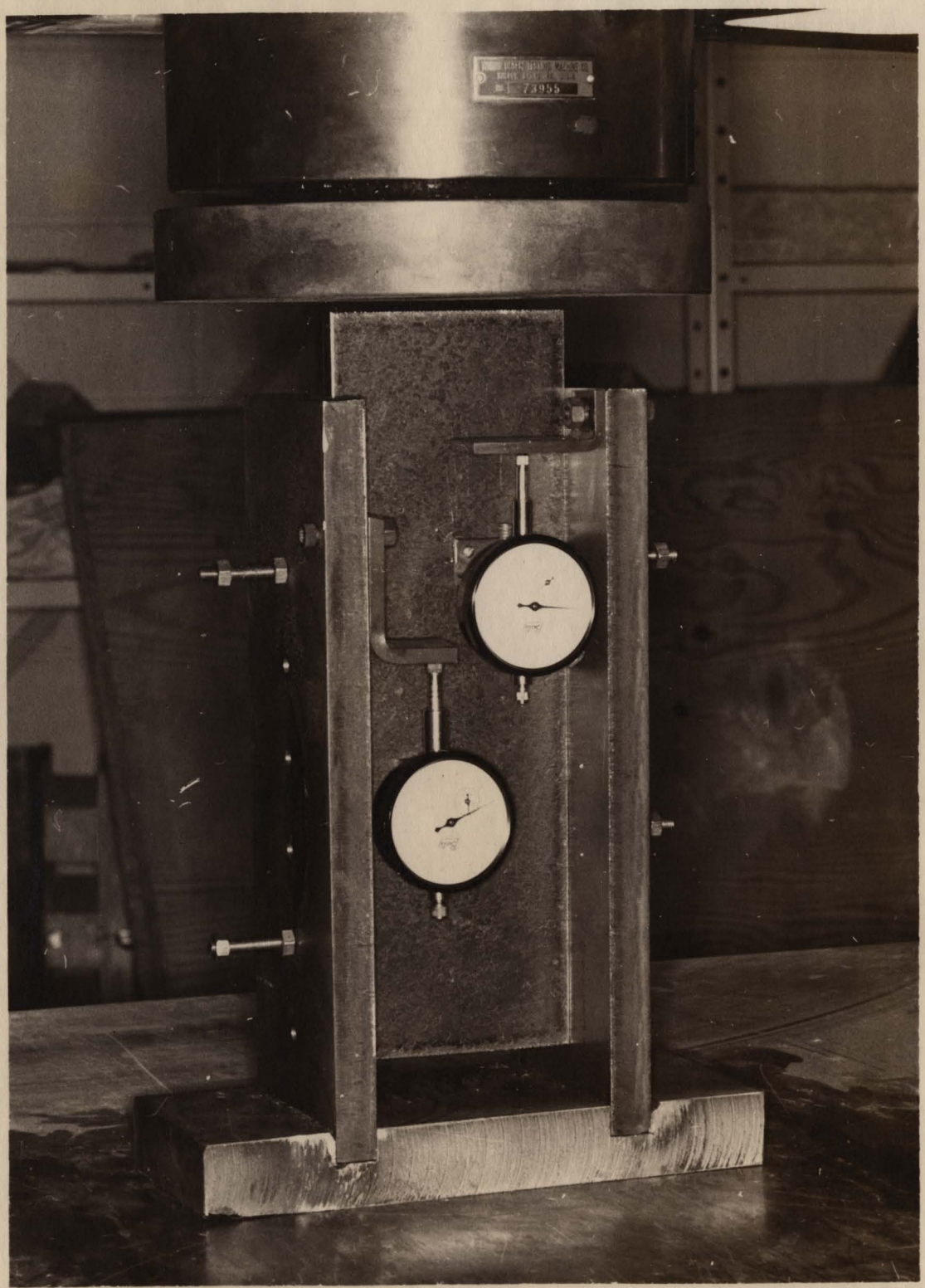

Fig. 3.3 Loading Position of Push-Out Specimen with 1/4" Diameter Connectors

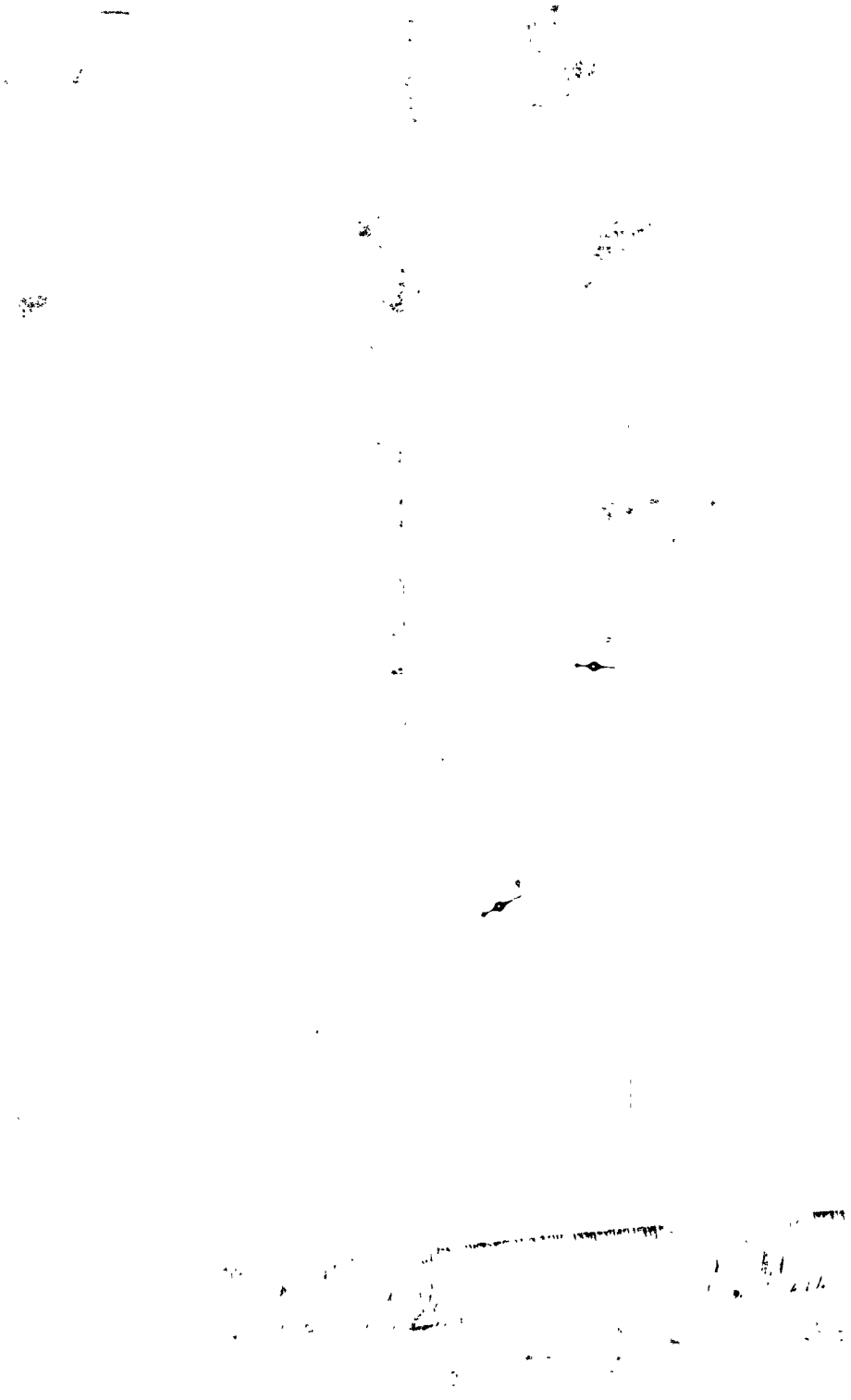

Fig. 3.3 Loading Position of Push-Out Specimen with 1/4" Diameter Connectors

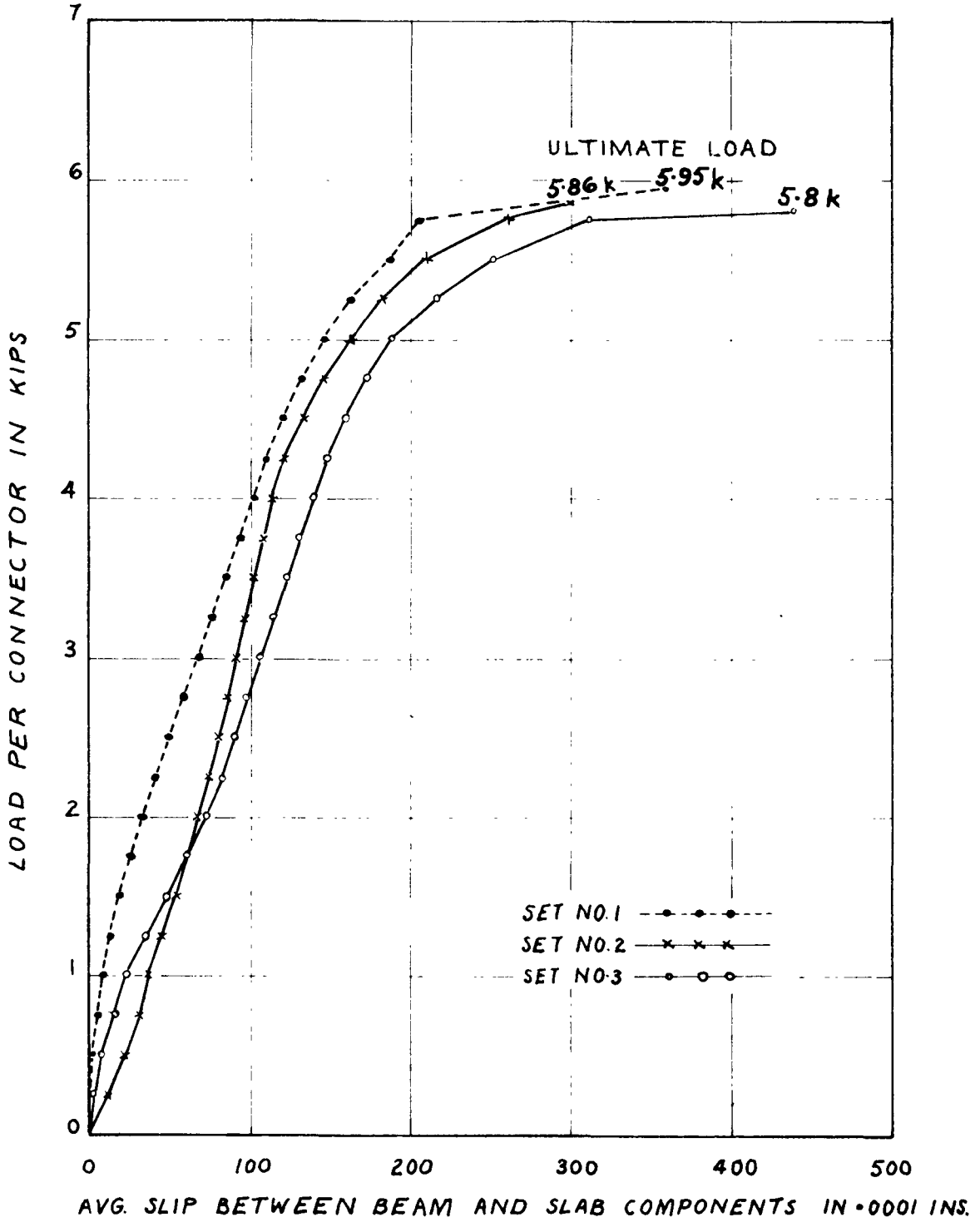

Fig. 3.4 Load-Slip Curves for Specimens with 3/8" Diameter Connectors

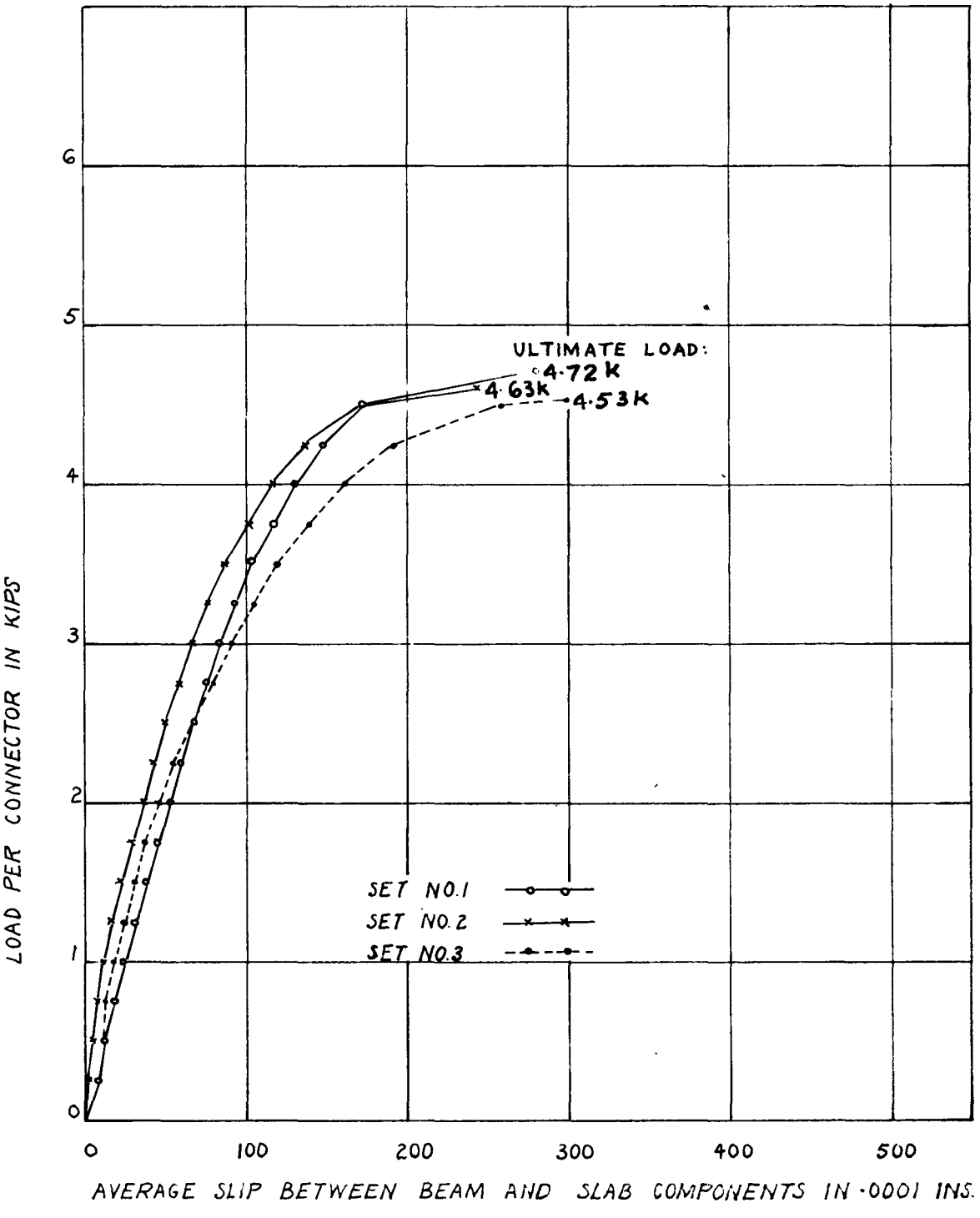

Fig. 3.5 Load-Slip Curves for Specimens with 5/16" Diameter Connectors

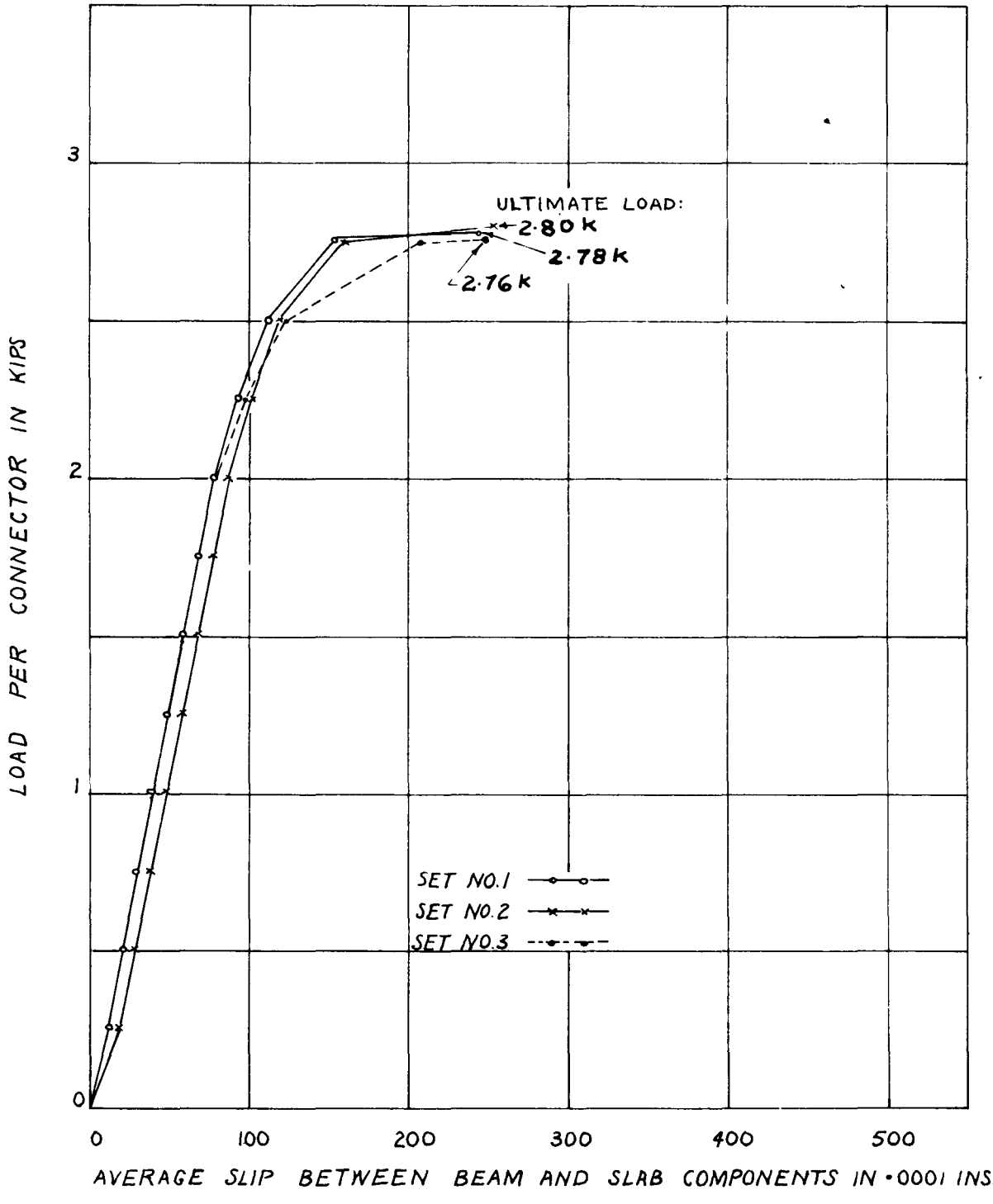

Fig. 3.6 Load-Slip Curves for Specimens with 1/4" Diameter Connectors

CHAPTER 4

COMPOSITE RECTANGULAR BEAM TESTS

4.1 Description of Specimens and Materials

Six composite rectangular beams were tested in the investigation. They are designated B1, B2, B3, B4, B5 and B6. All these beams were fabricated from cold-rolled steel. Dimensions are given in Table 4.1. Connector spacing and load arrangements are shown in Fig. 4.1.

Beams B1, B2, B3, B4 and B5 were provided with shear connectors which were made from cold-rolled steel rods, and which were intended to simulate the headed stud type shear connector. The holding down effect of these connectors was achieved by having the lower end of each connector screwed into the beam component and then tightening the holding down nut against the slab component. A typical connector arrangement is shown in Fig. 4.2.

Beam B6 had a continuous rubber connection which was made of 3/8" thick rubber strips. Details of this connection are given in Fig. 4.2. This beam was tested to note the influence of the load positions on the deflection and slip distribution of the member; and also for

TABLE 4.1

DESCRIPTION OF COMPOSITE RECTANGULAR BEAMS

Beam	Overall Length	Width of Beam Component	Thickness of Beam Component	Width of Slab Component	Thickness of Slab Component	Length* of Connectors	Connector Diameter	Number of Connectors
B1	64 in.	2 in.	1.25 in.	2 in.	1.25 in.	1 7/8 in.	3/8 in.	21
B2	64 in.	2 in.	1.25 in.	2 in.	1.25 in.	1 7/8 in.	3/8 in.	21
B3	64 in.	2 in.	1.25 in.	2 in.	1.25 in.	1 7/8 in.	5/16 in.	31
B4	64 in.	2 in.	1.25 in.	2 in.	1.25 in.	1 7/8 in.	5/16 in.	31
B5	40 in.	0.75 in.	0.75 in.	0.75 in.	0.75 in.	1 3/8 in.	1/4 in.	37
B6	40 in.	2 in.	0.75 in.	2 in.	0.75 in.	Continuous Rubber Connection°		

° See details of this connection in Fig. 4.2

* See Fig. 4.2

the purpose of making visual observations of the deformation of the connection during loading. White rectangular meshes were painted on the black rubber; and ½" diameter ball bearings were seated in 1/8" deep spherical indentations at 6-inch intervals along the length of the beam to avoid compression of the rubber, and therefore to keep the slab and beam components at a constant distance apart.

4.2 Manufacture of Specimens

The shear connectors were prepared as described in the case of the push-out specimens. For each composite rectangular beam specimen, the slab and beam components were first cut to their approximate lengths, placed together and tack welded at the ends. The holes were then drilled, tapped and threaded. In making these holes attempts were made to avoid tolerances between the shear connectors and the slab component. Afterwards the components were taken apart by having the tack welds removed. The interface was cleaned, filed and treated with oil so as to permit good contact between both components throughout the length of the beam, and also to reduce friction. The connectors were then screwed tight into the beam component, the slab component was fitted into position, and the holding down nuts were attached to the shear connectors

and tightened fingertight against the top of the slab component.

Beam B5 was an encastré beam, and details of the end supports are shown in Fig. 4.5. There was no gap between the end of the beam and the back-up plate of the housing.

Tensile test coupons were prepared from additional lengths of the same material as beams B1, B2, B3, B4 and B5. The purpose of these tensile tests was to evaluate the modulus of elasticity of the steel. The values obtained are given in Table 4.2.

4.3 Instrument and Loading Apparatus

All the beams were tested on a Tinius-Olsen Universal four-screw testing machine with a capacity of 120,000 lbs. The load was applied to B1, B2, B3 and B4 through roller edges, B5 was loaded through a knife edge, while B6 was loaded through knife edges supported on steel pads.

Slip between the beam and slab components was measured with dial gauges having 0.0001 inch graduations. The gauges were mounted on the slab components and small brackets were fitted to the beam components to engage the dial stems during loading.

TABLE 4.2

MODULUS OF ELASTICITY OF STEEL

Coupon No.	Applicable to Beam	Modulus of Elasticity (psi)	Average Modulus of Elasticity (psi)
1	B1*	32.3×10^6	
2	B1	32.2×10^6	32.25×10^6
1	B5	30.6×10^6	
2	B5	31.9×10^6	31.25×10^6

* Beams B1, B2, B3 and B4 were made from the same material.

Deflection was measured at midspan for all beams, and also at quarter-span in the case of B1, B2, B3 and B4. Dial gauges reading to 0.001 inch were used to measure deflection.

¼" foil electric strain gauges, model C6-141-B, were used to measure strain in the beams. Strain measurements were taken at midspan and at quarter-span of B1, B2, B3, B4 and B5. In addition, on B5 strain gauges were fitted throughout the length of the lower extreme fibres. The strains were measured by a Datran Digital Recorder.

The positions of slip, deflection and strain gauges are shown in Figs. 4.3, 4.5, 4.6, 4.7 and 4.8.

4.4 Testing Procedure

Beams B1, B2, B3 and B4 were each supported on a 60-inch span and loaded by two equal concentrated loads located 15 inches on either side of midspan. Beam B5 was supported on a 36-inch span and loaded by a point load at midspan. Beam B6 was supported on a 36-inch span and was successively loaded by two equal concentrated loads located 6, 9 and 12 inches on either side of midspan.

Before testing began, the loads on B1, B2, B3 and B4 were cycled between zero and 1 kip in an effort to overcome mechanical interlocking at the interface which

might have arisen through manufacturing deficiencies. During this cycling process, instrumentation was not used except that the slip and deflection gauges were zeroed each time the load was reduced to zero. Cycling was continued until such time as all these gauges read zero when the load was removed. The load on B5 was similarly cycled between zero and 0.25 kip.

During testing B1, B2, B3 and B4 were each loaded in increments of one kip up to the 5 kip level, and then slowly unloaded to zero kips. The load was then reapplied in 1-kip increments up to ultimate load. This reloading phase is referred to as second loading in Figs. 4.40, 4.41, 4.42 and 4.43. Ultimate load was interpreted as the maximum load which each of these beams was able to resist. Shortly after this load was reached there was an instantaneous shearing off of a few shear connectors in one of the shear spans with a reduction in the applied load. The load continued to drop off, while connectors continued to yield until all the connectors over half the length of the beam had sheared off completely. At this stage loading was reduced to zero and the test was discontinued.

For these members deflection, strain and slip measurements were recorded at zero load, at each load increment, at ultimate load and at two other load levels after ultimate.

Beam B5 was loaded from zero to 4.6 kips in 0.2 kip increments. This test was terminated when it was observed that comparatively large deflections occurred with a given load increment. All gauges were read at each load increment.

Beam B6 was loaded in 0.25 kip increments up to 1.25 kips with the load applied at 6 inches on either side of midspan. The load was then removed and reapplied at 9 inches on either side of midspan in the same increments but up to 1.5 kips. Finally, the load was removed and reapplied at 12 inches on either side of midspan up 9 kips in increments of 0.25 kip. Deflection and slip readings were recorded at each load increment.

4.5 Deflection Characteristics of Beams

Deflection curves for all the beams are shown in Figs. 4.9 to 4.20. Along with the measured curves are presented theoretical curves calculated on the bases of the Newmark and Stussi theories. Applications of these theories are presented in the Appendices. The curves indicate incomplete interaction in the beams, since the actual deflections lie between the theoretical curves for complete and zero interaction in the elastic range.

It can be seen from the load-deflection curves

that in the elastic range there was generally good agreement between the theoretical and measured values. However, it may be observed that for two-point loading better agreement was obtained for deflections at the load points than for those at midspan. This is thought to be partly attributable to the presence of uplift forces in the members. A visual inspection of the interface during loading indicated that in beams B1, B2, B3, B4 and B6 these uplift forces were more effective between the load points than in the shear spans. Such forces have a tendency to produce vertical separation of the interface, and it was evident that there was more separation of the interface between the load poi ts. This type of separation is in contradiction with the theoretical assumption that at all points along the beam the slab and beam components should deflect by equal amounts.

Uplift forces, therefore, must have contributed to the lower degree of agreement obtained between the theoretical and measured deflections at midspan; and it is probable that if better precautions had been taken to prevent separation of the interface, better agreement would have been obtained.

Load vs. midspan deflection curves for B1, B2, B3 and B4 are presented in Figs. 4.10, 4.12, 4.15 and 4.17. These curves show that when the load was released from

5 kips to zero kips, there was a small residual deflection in each of these members. On reloading these beams each load-deflection curve followed a different path but arrived at the original point when the load had again reached the level of 5 kips. This phenomenon was also observed by other researchers[4], and seems to take place when the beam as a whole has not yet reached its yield point.

Fig. 4.20 shows the moment-deflection curves for B6. From these curves it can be deduced that for this member there were better deflection performances, which reflected higher efficiencies of the connection, as the points of application of the load moved closer to mid-span. This is what is to be expected from an interpretation of Fig. 2.1. In this figure the q/q' curves show that the shear connectors are less efficiently utilized when the load points move closer to the end supports. As an example, for the value of l/C = 1.0, when the load is applied at quarter-span the values of q/q' are 0.47 and 0.30 at the end of the beam and at quarter-span respectively. With the load applied at one eighth the span length from the end supports q/q' has the values of 0.29 and 0.14 at the end of the beam and at quarter-span respectively. This being the case, for a given applied moment the slab and beam components carry a greater percentage of the

load when the load points move closer to the end supports, and this results in greater deflection of the composite member.

In all the deflection computations a full cross section was assumed, although the cross sections had been slightly reduced at intervals by the drilled holes; and in making these computations, only flexural deflections were taken into account.

4.6 Strain Measurements

Strain measurements were recorded at the points shown in Figs. 4.7 and 4.8, and strain data are presented graphically in Figs. 4.21 to 4.39. There appeared to be good agreement in the elastic range between the computed and measured values. However, as in the case of deflections, there was generally better agreement at the load points than at midspan for B1, B2, B3 and B4; and perhaps uplift forces might have been responsible for this also.

A review of the load-deflection curves in Figs. 4.9, 4.11, 4.14 and 4.16 shows that for the two-point loadings the loads were almost evenly applied at both points of application, because the load vs. deflection curves for the two load points of each of the beams were almost identical. However, despite this fairly equal distribution of the loads, the measured load-strain curve at

the north load point of some members turned out to be significantly different from that at the south load point. As an example, Fig. 4.29 shows a considerable difference between the measured north and south load-strain curves for beam B3. Partly responsible for this difference could be uneven drilling of connector holes at the load points, which could have caused differential weakening of the member at these points. Uneven straining at the load points is also revealed in Figs. 4.36 to 4.39 which show the cross sectional strains recorded for various loads.

The strain measurements in Figs. 4.36 to 4.39 also indicate that there was incomplete interaction between the slab and beam components by the strain discontinuities at the interfacial planes. However, this is to be expected since the shear connectors were not infinitely stiff.

Fig. 4.34 shows the strain distribution along the bottom fibre of beam B5 when an external load of 600 lbs. was applied. It is important to note that the beam was not strictly encastré; the end restraints were not fully effective, and therefore, the actual points of contraflexure shifted from their theoretical positions towards the end supports. This figure also shows that there was good agreement between the computed and measured strain values.

During the later stages of loading of this beam, a slight lifting of the restraining end cap on the housing was observed, indicating end rotation of the member. This gave rise to an increase in the moment at midspan with an accompanying increase in the strain at the central region. This increase in strain partly reduced the degree of agreement between measured and computed results.

Fig. 4.35 shows that as the load was increased on B5 there was a tendency for the points of contraflexure to shift away from midspan. This is understandable because increased loading caused greater end rotation to take place.

4.7 Measurement of Slip

In all the beams tested slip was observed, indicating that there was a breakdown of interaction. Load-slip curves are shown in Figs. 4.46 to 4.51, and slip distribution curves are presented in Figs. 4.40 to 4.45 and 5.13 to 5.17.

Generally, it can be said that for beams B1, B2, B3, B4 and B6 the actual slip distribution was fairly symmetrical about midspan, and that the greatest slips took place in the shear spans and particularly towards the ends of these members. Figs. 4.46, 4.47, 4.49 and 4.50 indicate that there was good quantitative agreement

between the Stussi theory and measured values in the elastic range. However, an inspection of Figs. 5.13 and 5.14 reveals that the slips computed in accordance with the Newmark theory did not compare favourably with those measured for beams B1 and B3.

From Fig. 4.44 it can be seen that for beam B5 there was great quantitative difference between the measured slip values and those predicted by the Stussi and Newmark theories. However, the shape of these curves for the most part show good qualitative agreement. For this beam Fig. 4.44 shows that prior to the application of 600 lbs. no slip readings were noted, and that after 1,800 lbs. had been applied end slips began to appear. It is possible that when the load was lower than 600 lbs. slip was taking place along the beam but the magnitude of this slip was too small to be indicated by the slip gauges.

For this member both theories assume that no end slip took place. In the case of the Newmark theory this assumption means that there was no load on the end connection. For the Stussi theory it means that there was load on the end connection, but the conditions of end restraint provided an infinitely stiff connection which prevented end slip from taking place. This member was not anchored to the end housing, and it is clear that

increased loading gave rise to deflections which were large enough to pull the ends of the beam towards midspan. This type of behaviour reduced the effectiveness of the end housing in preventing slip, and thus allowed end slips to take place. Fig. 4.44 shows that negative slips occurred at the end of the beam, and also suggests that once such slips began, they had a tendency to change the magnitude of slips in the region of the end of the beam from positive to negative quantities. It is interesting to note that the rate of increase of end slip was rather high; this might have been due to the change in the shear resisting capacity of the end connection once the back-up plate of the housing was no longer effective in the complete prevention of slip.

Fig. 4.45 shows the slip distributions along beam B6 for certain load levels. Here it is seen that the load-slip characteristics of the beam were dependent on the points of application of the load.

4.8 Modes of Failure and Comparison of the Behaviour of Beams

Fig. 2.1 indicates that for a simply supported beam with a two-point load the greatest loss of interaction takes place at the load points. Accordingly, the connector spacing of beam B2 was arranged to resist this

relatively high loss of interaction at such points. Beam B1 had the same number of connectors as did B2; however, while a uniform connector spacing was used in B1, for B2 the connectors were crowded at the load points, and the spacing was relaxed in the central region of the member as shown in Fig. 4.1. In this way it was possible to check, on the basis of the test results, whether any advantage was achieved in B2 over B1 by the redistribution of the shear connectors.

A similar comparison was proposed for beams B3 and B4. These two beams were provided with the same number of connectors. However, there was a uniform spacing in B3, while the studs in B4 were arranged in accordance with the conventional shear force diagram. That is to say, the connectors were crowded in the shear spans and spaced further apart between load points as shown in Fig. 4.1.

Test results showed that in both cases the redistribution of shear connectors enhanced the overall perfomances of the beams. Figs. 4.48 and 4.51 and Figs. 4.13 and 4.18 show better load-slip and load-deflection characteristics for B2 and B4 over B1 and B3 respectively. Moreover, the ultimate loads of B1, B2, B3 and B4 were 11.90 kips, 13.12 kips, 10.64 kips and 12.70 kips respectively; and if the capacity of the beams is characterized

in terms of their ultimate loads, then it can be said that the connector rearrangement in B2 brought about an increase in capacity over B1 of 10.3%, while in B4 it achieved a capacity improvement of 19.3% over B3; thus indicating a more beneficial redistribution of connector spacing in beam B4.

At their ultimate loads the midspan deflections of B1, B2, B3 and B4 were 1.036", 1.163", 0.791" and 0.982" respectively; and at this stage their respective strains at midspan were 2,160, 2,270, 1,424 and 1,974 micro-inches per inch.

There was a similar mode of failure for each of beams B1, B2, B3 and 4. Although their load-strain curves indicate that some yielding had taken place in the beam and slab components at ultimate load, yet it can be said that for these members failure was due to the deformation of the shear connectors. The dropping off of load from ultimate was almost simultaneous with the sudden shearing off of a few connectors in one of the shear spans; and so long as the load was not removed, connectors continued to fracture and the load continued to drop off. This went on until all the connectors over half the length of the beam had sheared off completely, at which point the test was discontinued. This characteristic mode of failure is shown in Fig. 4.4.

It is of interest to note that once the ultimate load was reached all slips took place in one direction; therefore, there was an increase of slip in one half of the beam and a decrease in the other. This was so because the failure of connectors in one shear span tended to cause an imbalance in the horizontal shear force. Accordingly, there was a reduction of the horizontal load and an elastic recovery of those connectors in the other half of the beam which had not yet undergone full plastification. This slip variation after ultimate load is typically shown in Fig. 4.52.

The inelastic deflections observed in B5 were chiefly due to the inelastic behaviour of the steel. Fig. 4.33 shows that at an applied load of 3,800 lbs. large inelastic strains had already taken place in the lower fibres of the beam component at midspan; and at this stage the quarter-span slip was 0.0047 inch as seen in Fig. 4.44. From Fig. 3.6 the magnitude of this slip indicates that the shear connectors were well within the elastic range.

Beam B6 was not allowed to undergo failure since it was tested chiefly for making comparisons in the elastic range, and since it was desired to retain this specimen for future demonstrations.

It is observed from some of the slip curves for B1, B2, B3, B4 and B5 that computed slip values, which were based on connector moduli obtained from push-out tests, were generally greater than those actually measured. It seems therefore, that shear connectors give better load-slip performances in flexural members than in push-out tests. This is possibly due to the fact that in a composite beam each connector is one of a larger system, and consequently, its behaviour is less independent than in a push-out test. Also responsible for this difference in connector performance could be the difference between flexural loading and the loading of a push-out test.

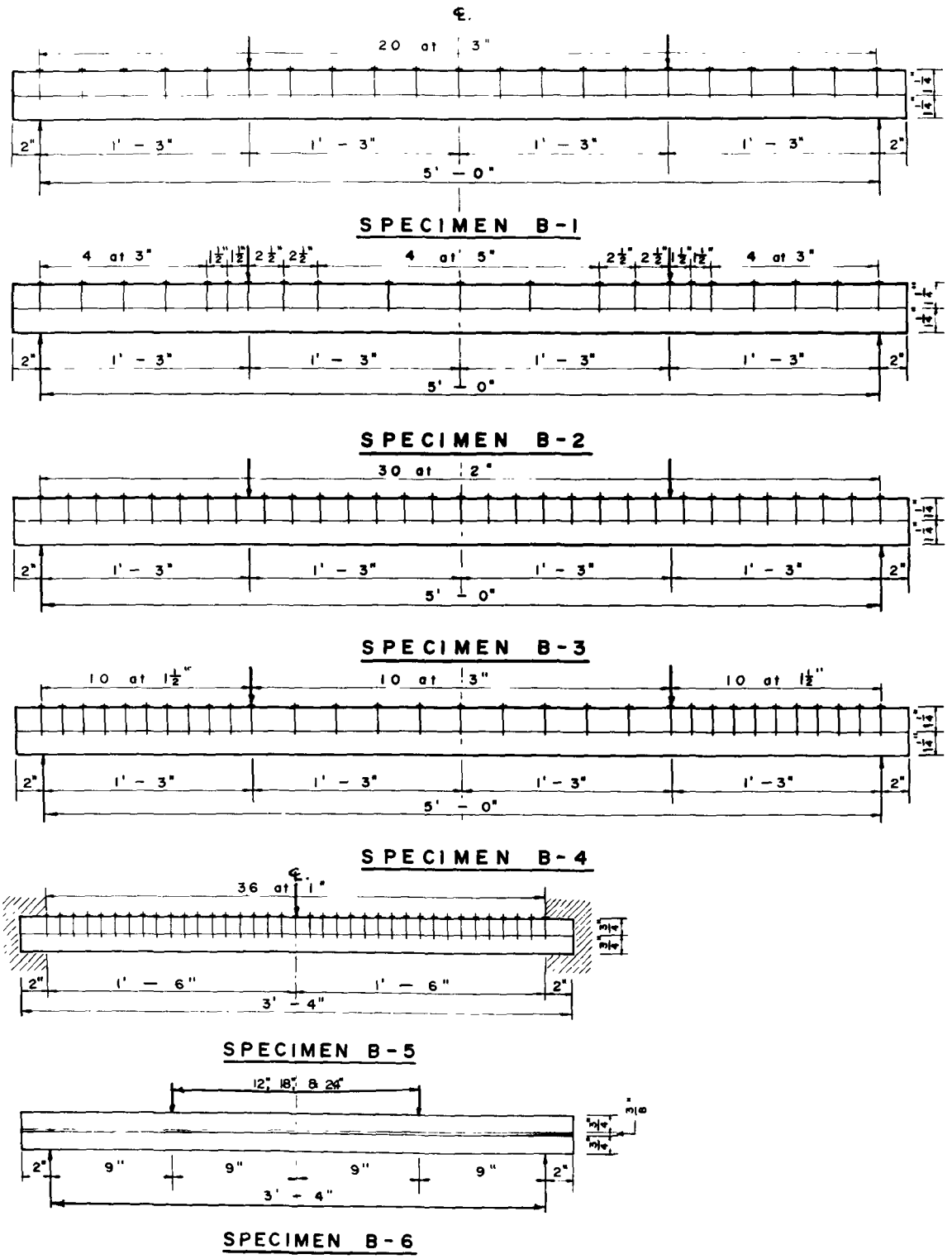

FIG. 4-1

CONNECTOR SPACINGS & LOADING CONFIGURATIONS

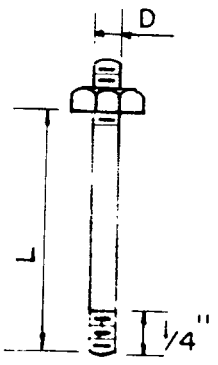

L = length
D = diameter

TYPICAL SHEAR CONNECTOR

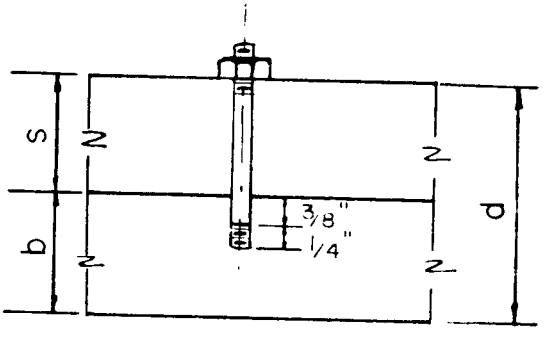

S = depth of slab component

b = depth of beam component

d = beam depth

TYPICAL SHEAR CONNECTION

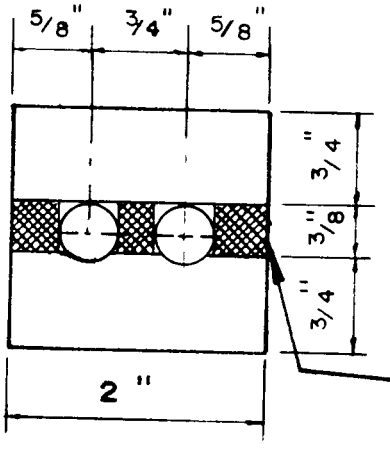

connection (rubber & ball bearings)

CROSS SECTION OF BEAM B6.

FIG. 4·2
Details of Shear Connections

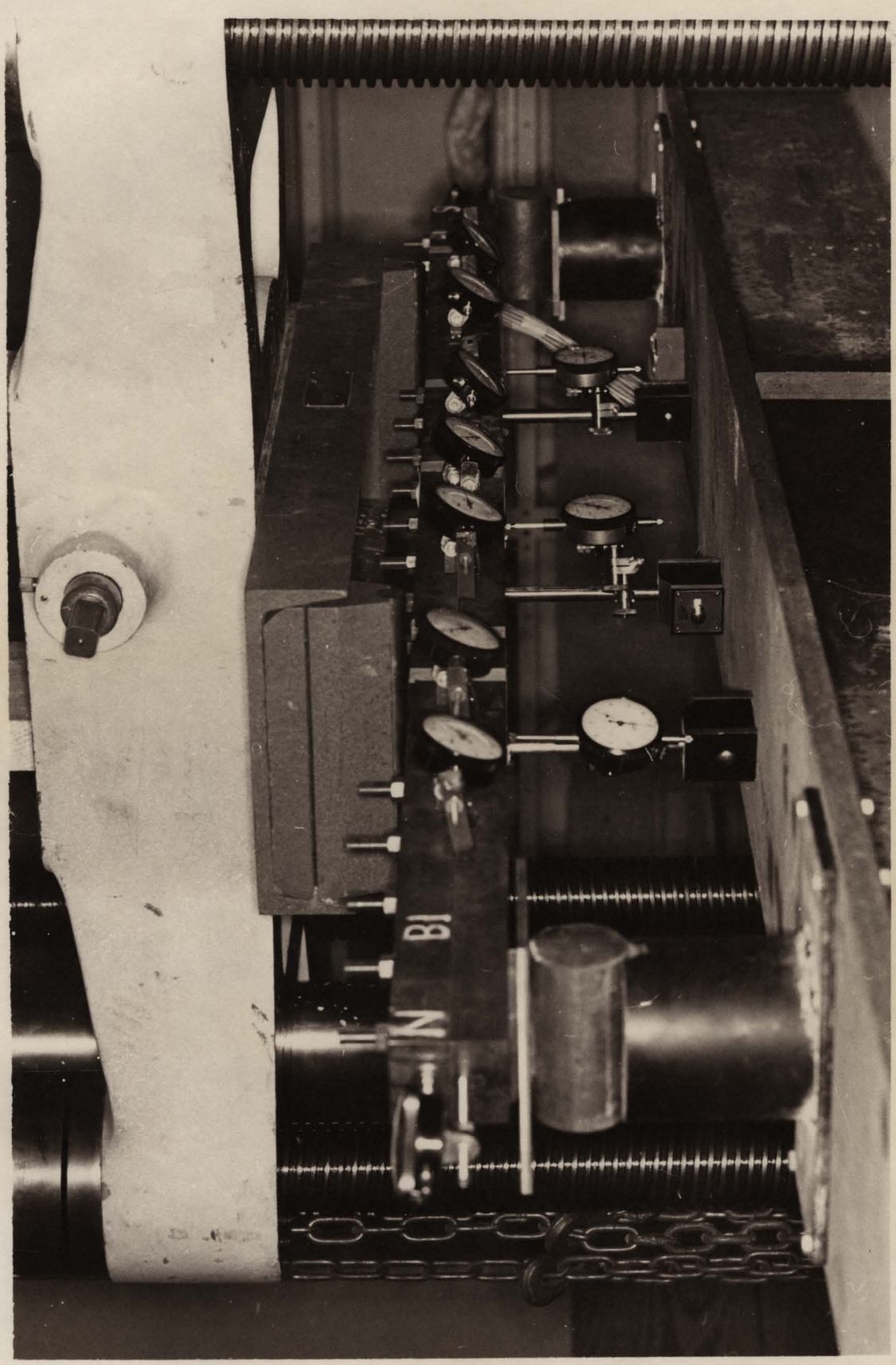

Fig. 4.3 Loading Position of B1, B2, B3 and B4

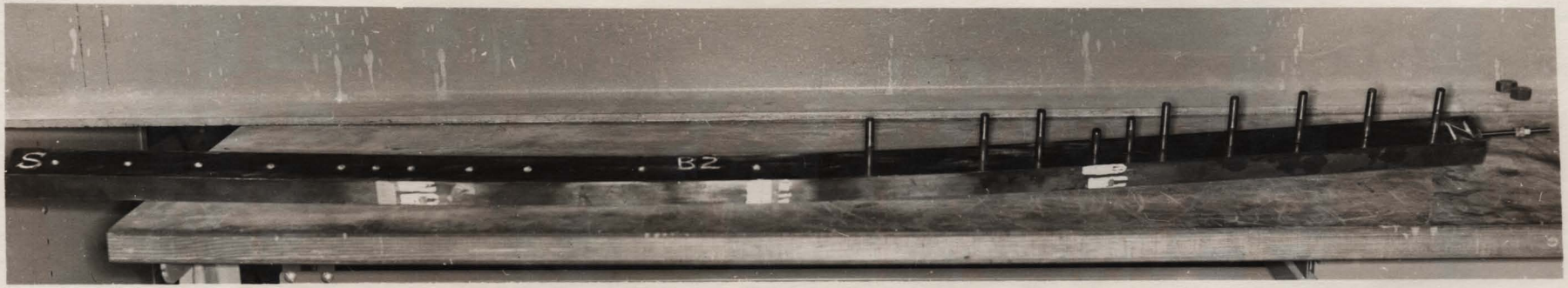

Fig. 4.4 Typical Failure of B1, B2, B3 and B4

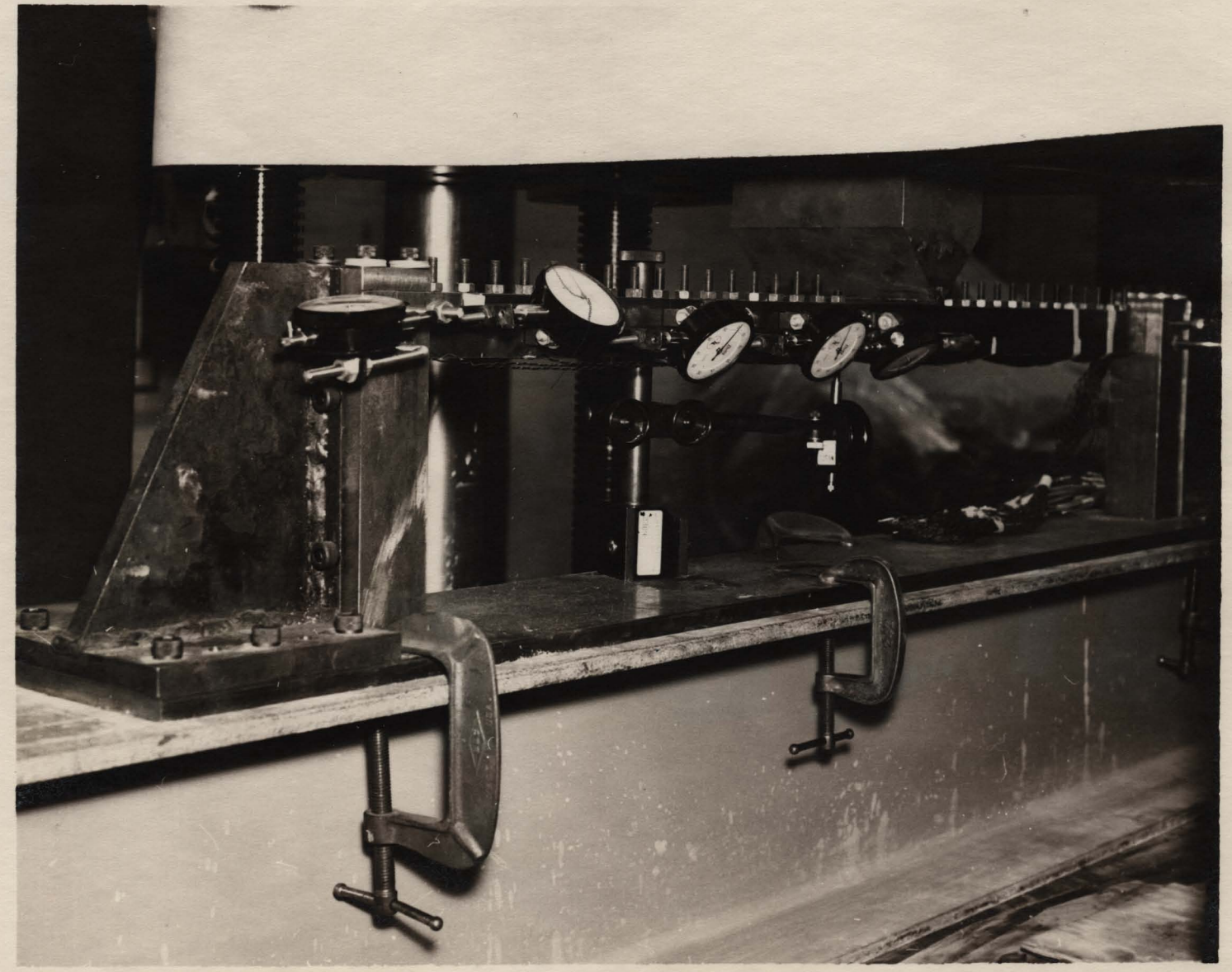

Fig. 4.5 Loading Position of Encastre Beam

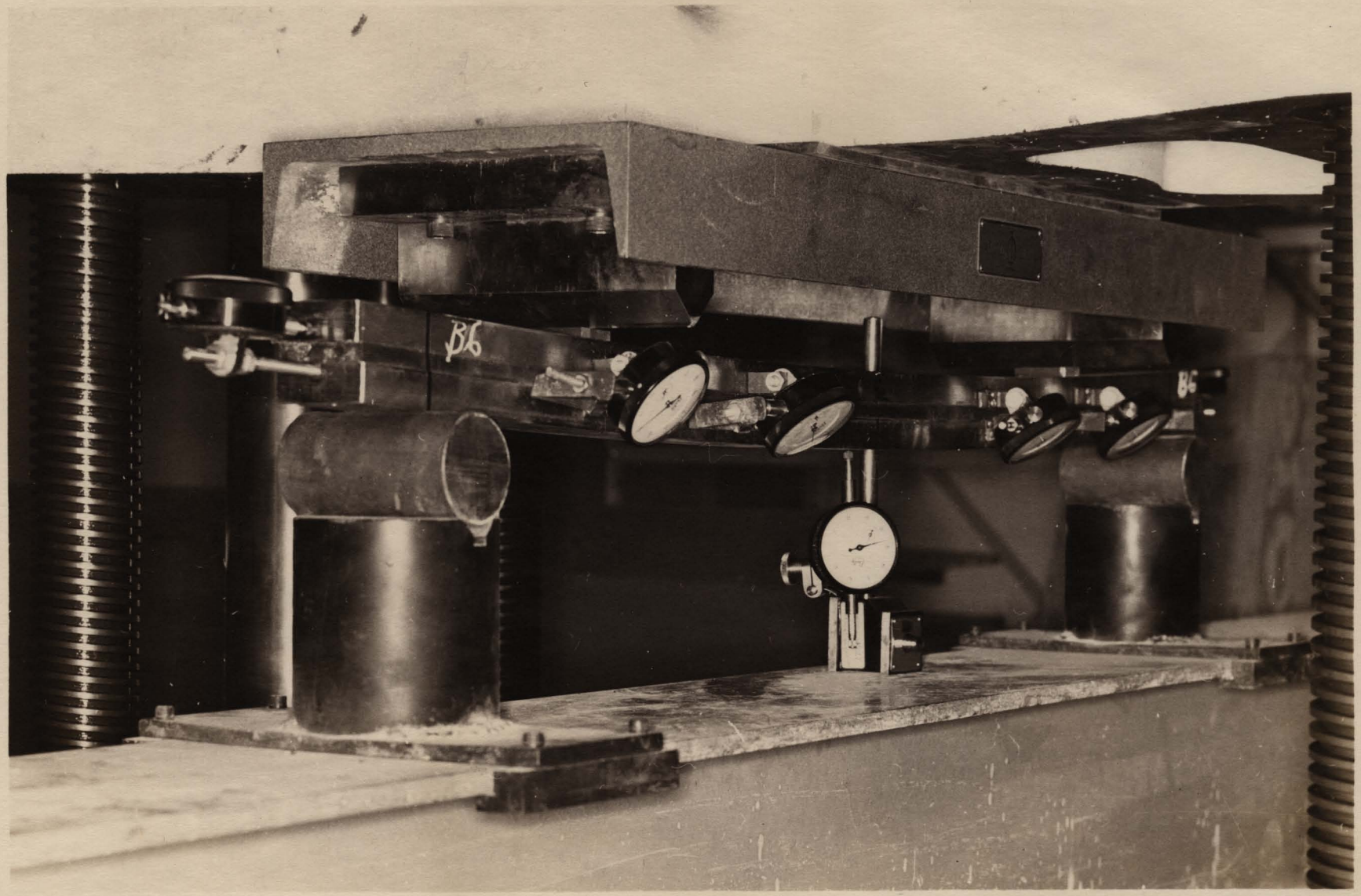

Fig. 4.6 Loading Position of B6

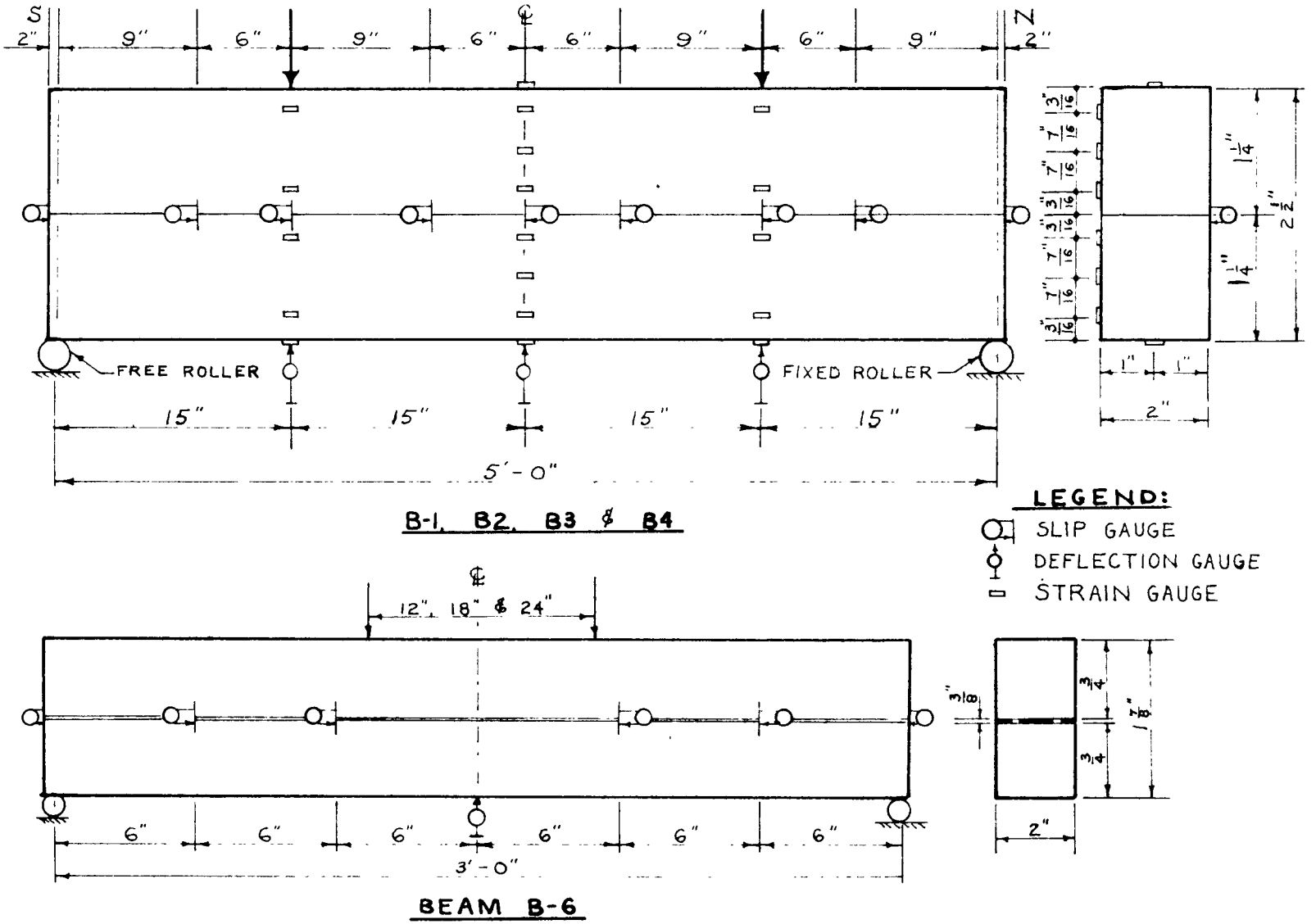

Fig. 4.7 Position of Gauges

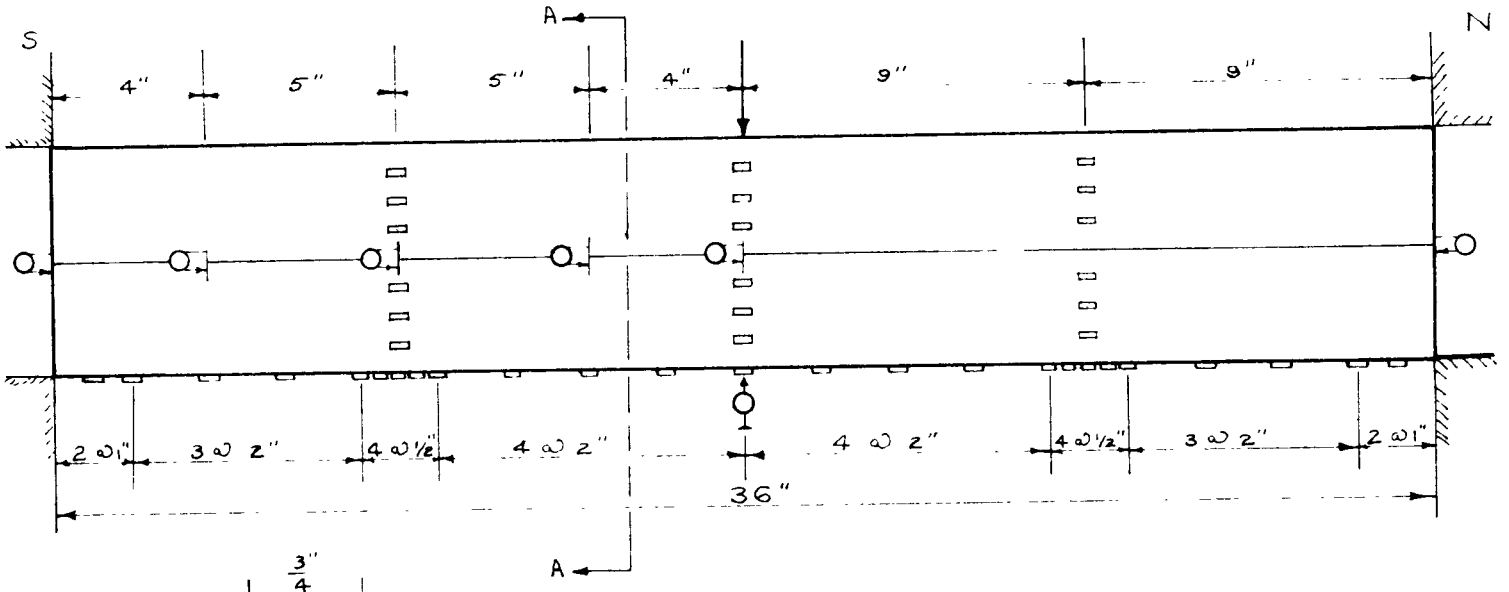

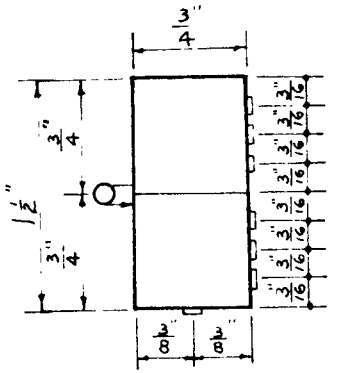

SECT. A-A

LEGEND

- Slip Gauge
- Deflection Gauge
- Strain Gauge

FIG. 4·8 BEAM B-5

Position of Gauges

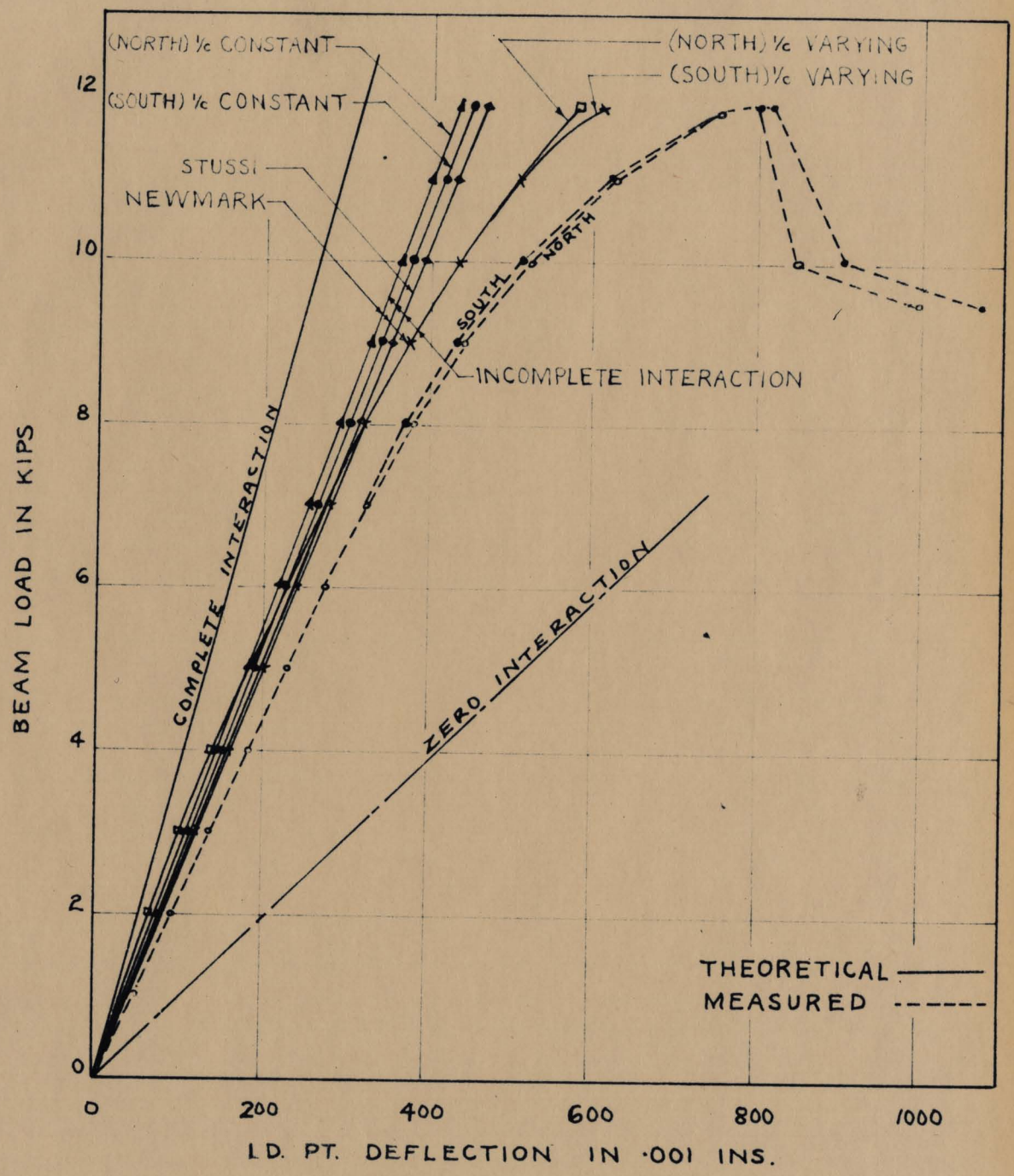

Fig. 4.9 Load-Deflection Curves for B1

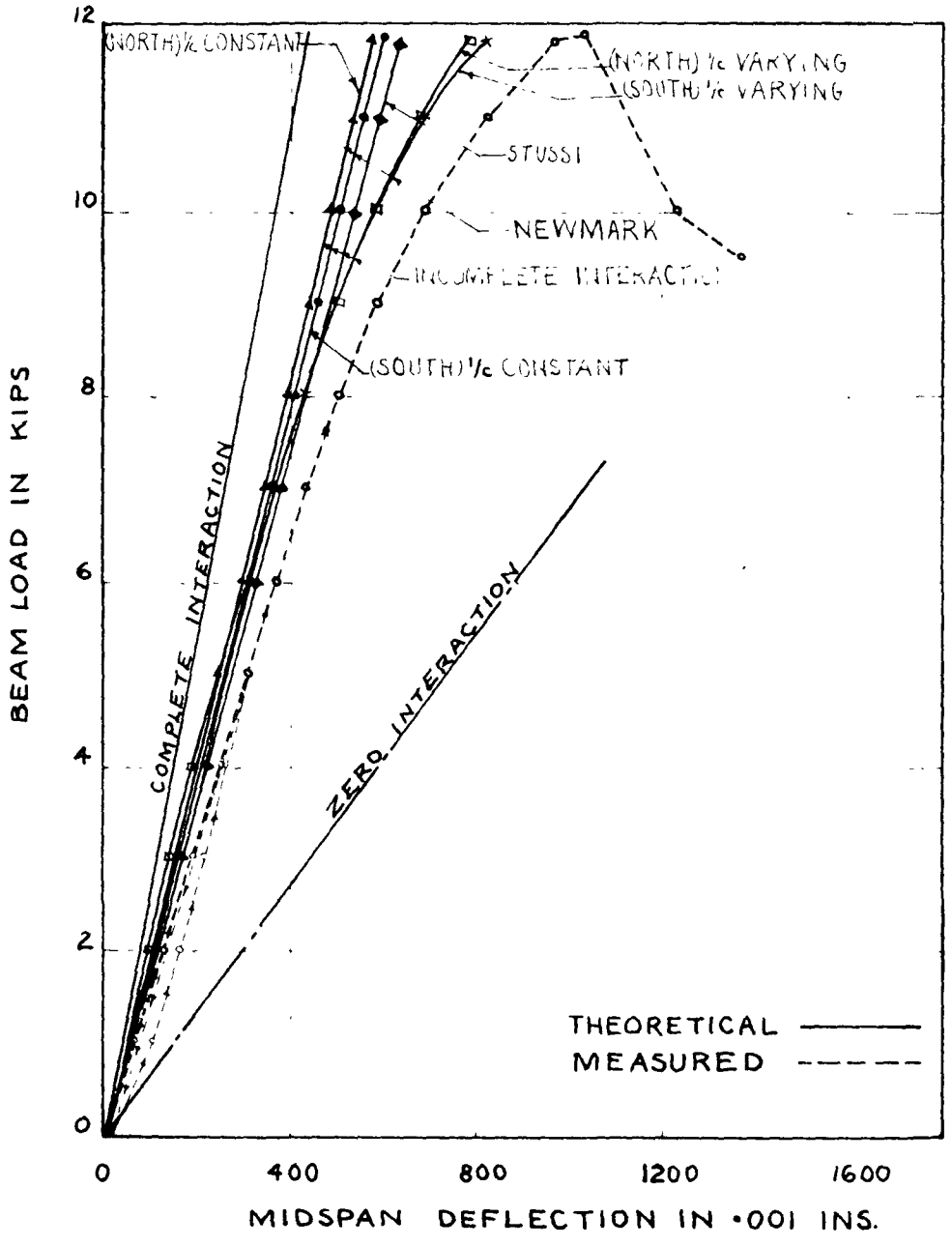

Fig. 4.10 Load-Deflection Curves for B1

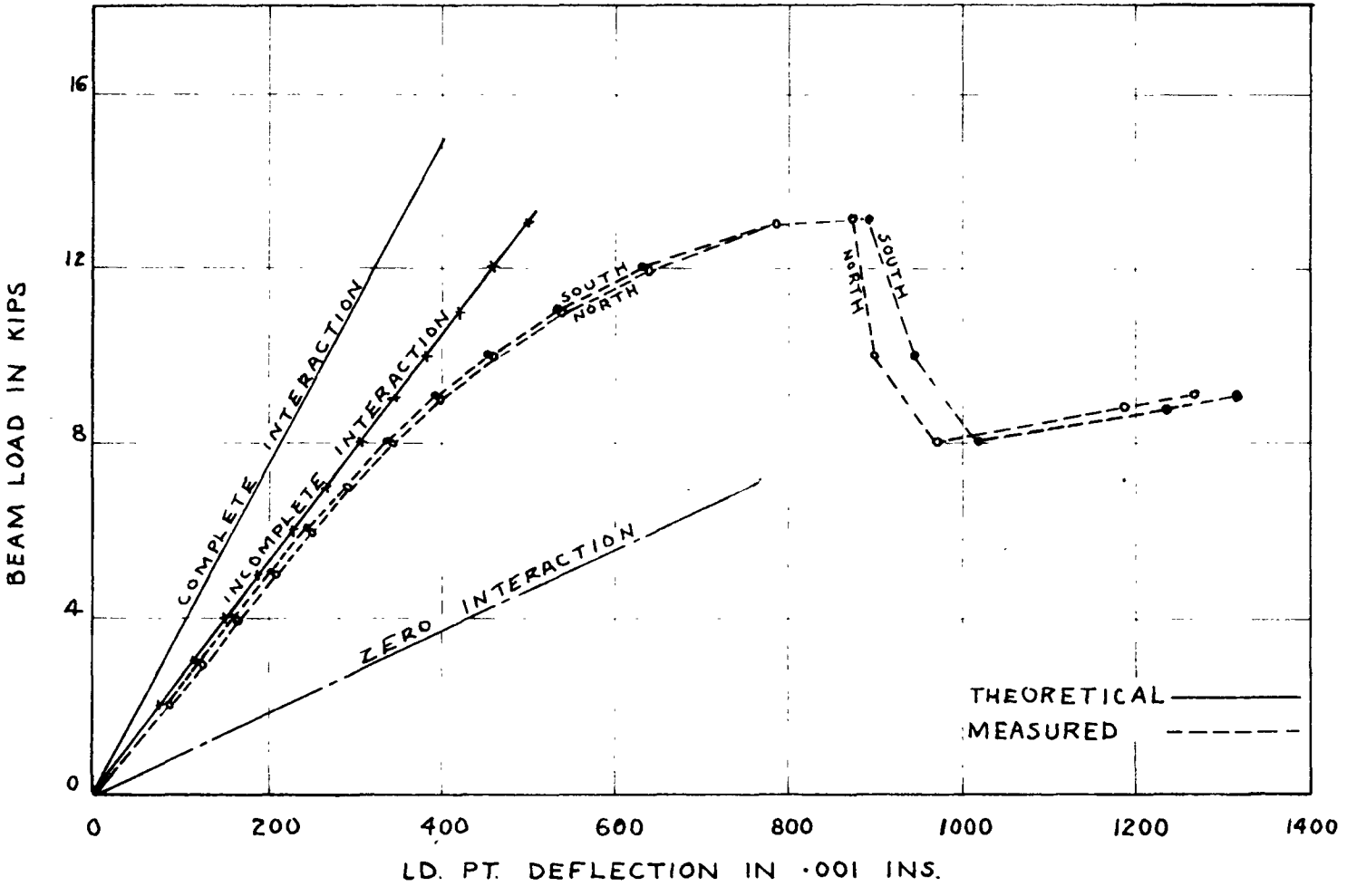

Fig. 4.11 Load-Deflection Curves for B2 (Stussi)

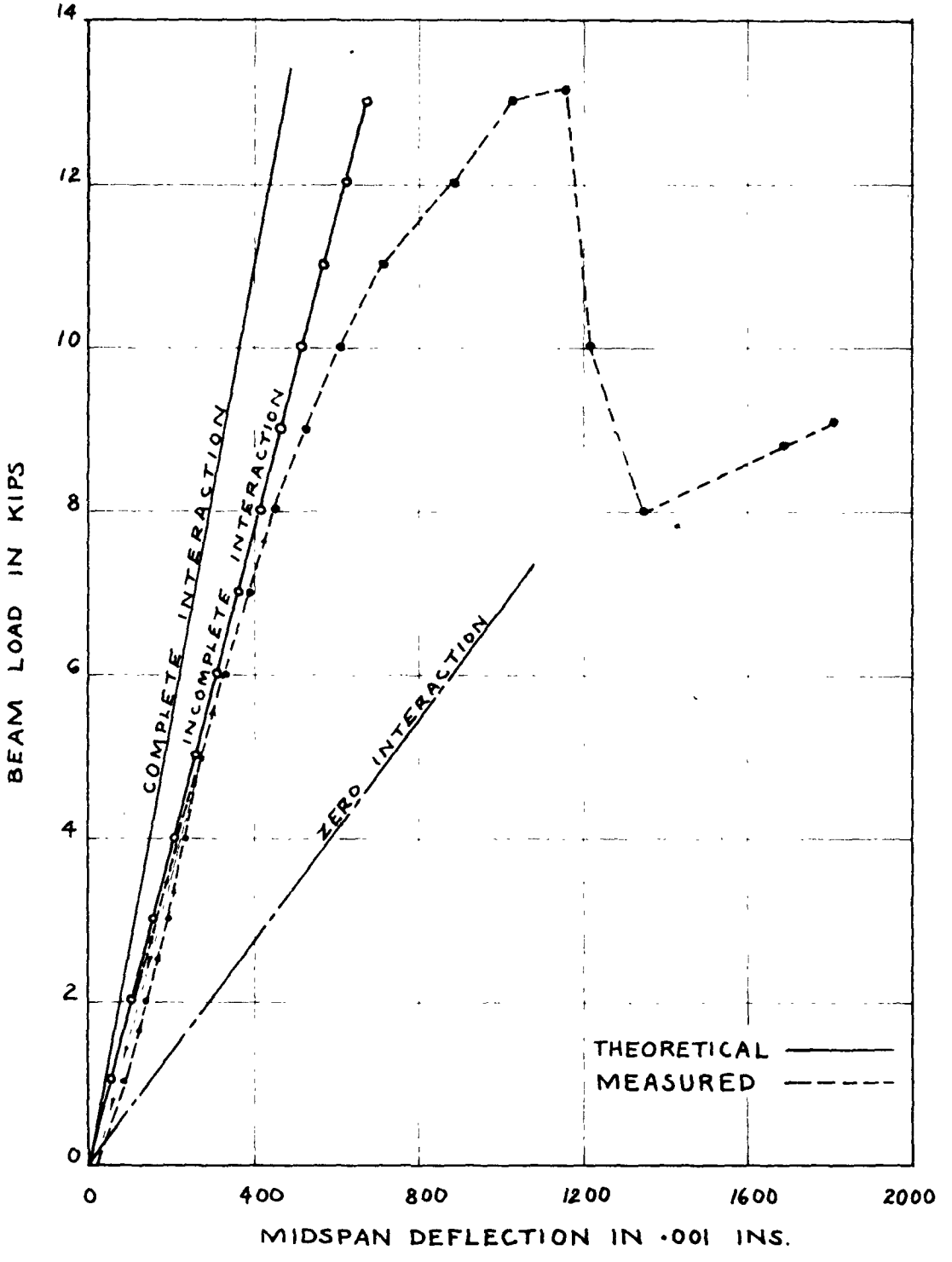

Fig. 4.12 Load-Deflection Curves for B2 (Stussi)

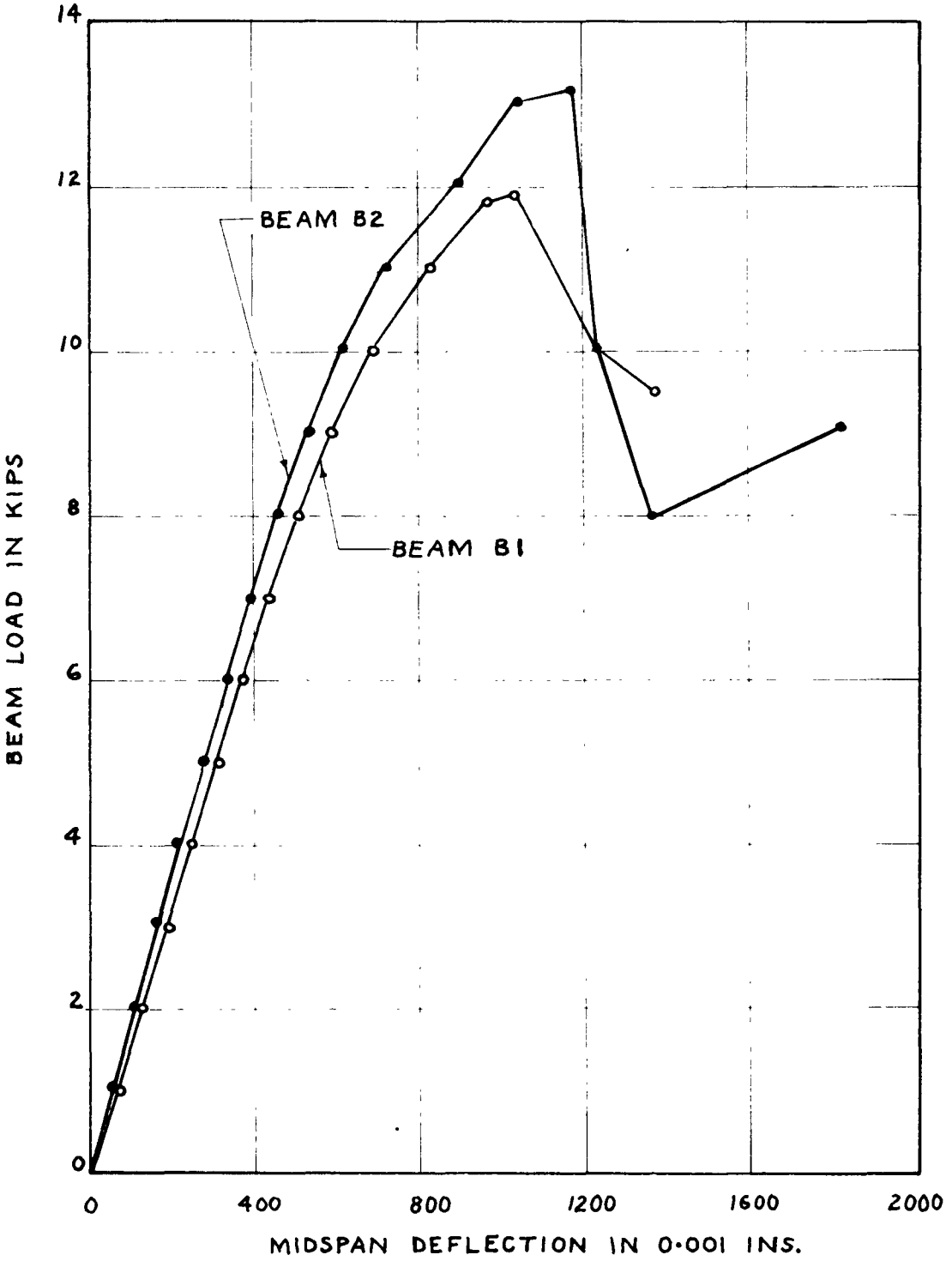

Fig. 4.13 Load-Deflection Curves for B1 and B2

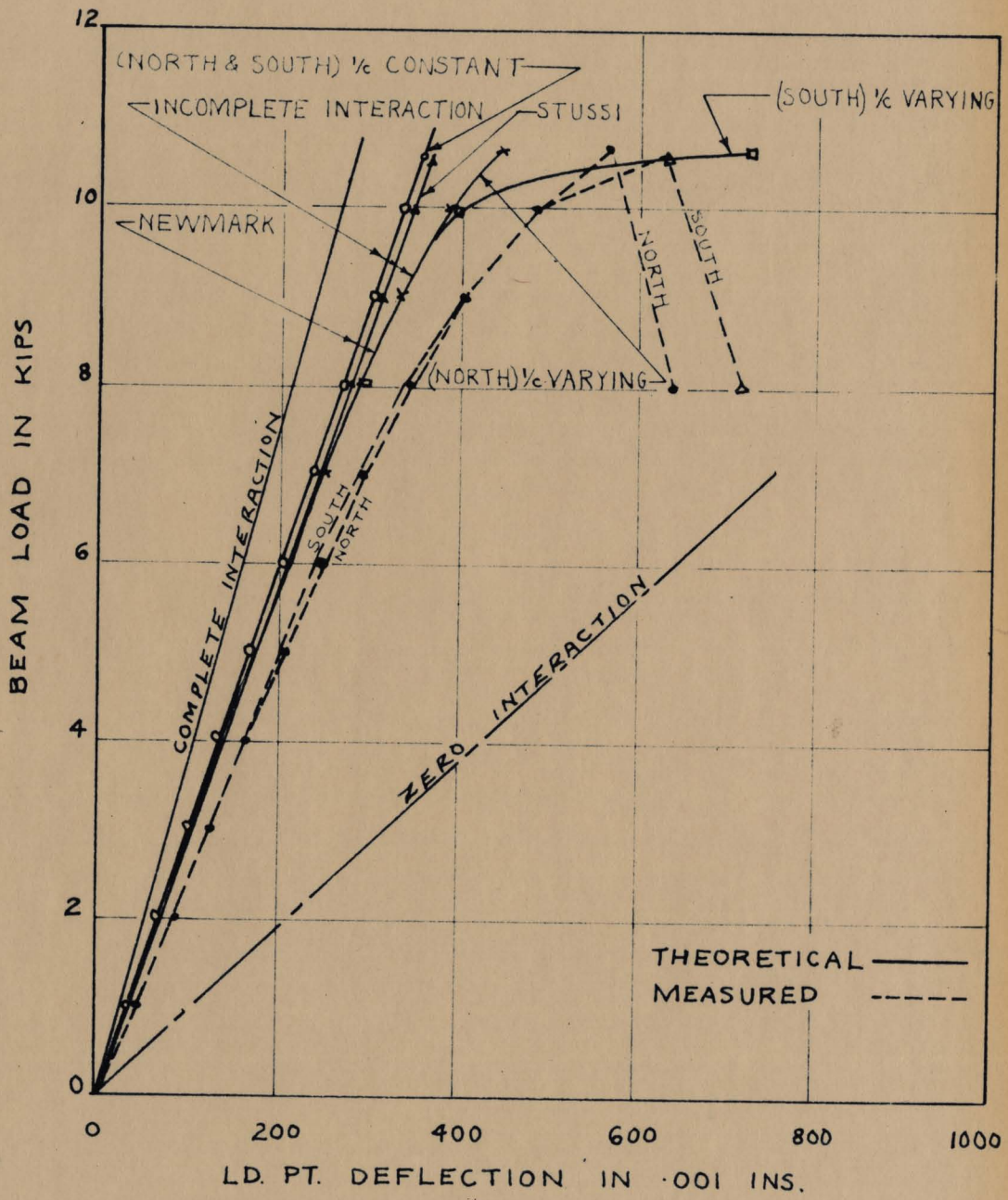

Fig. 4.14 Load-Deflection Curves for B3

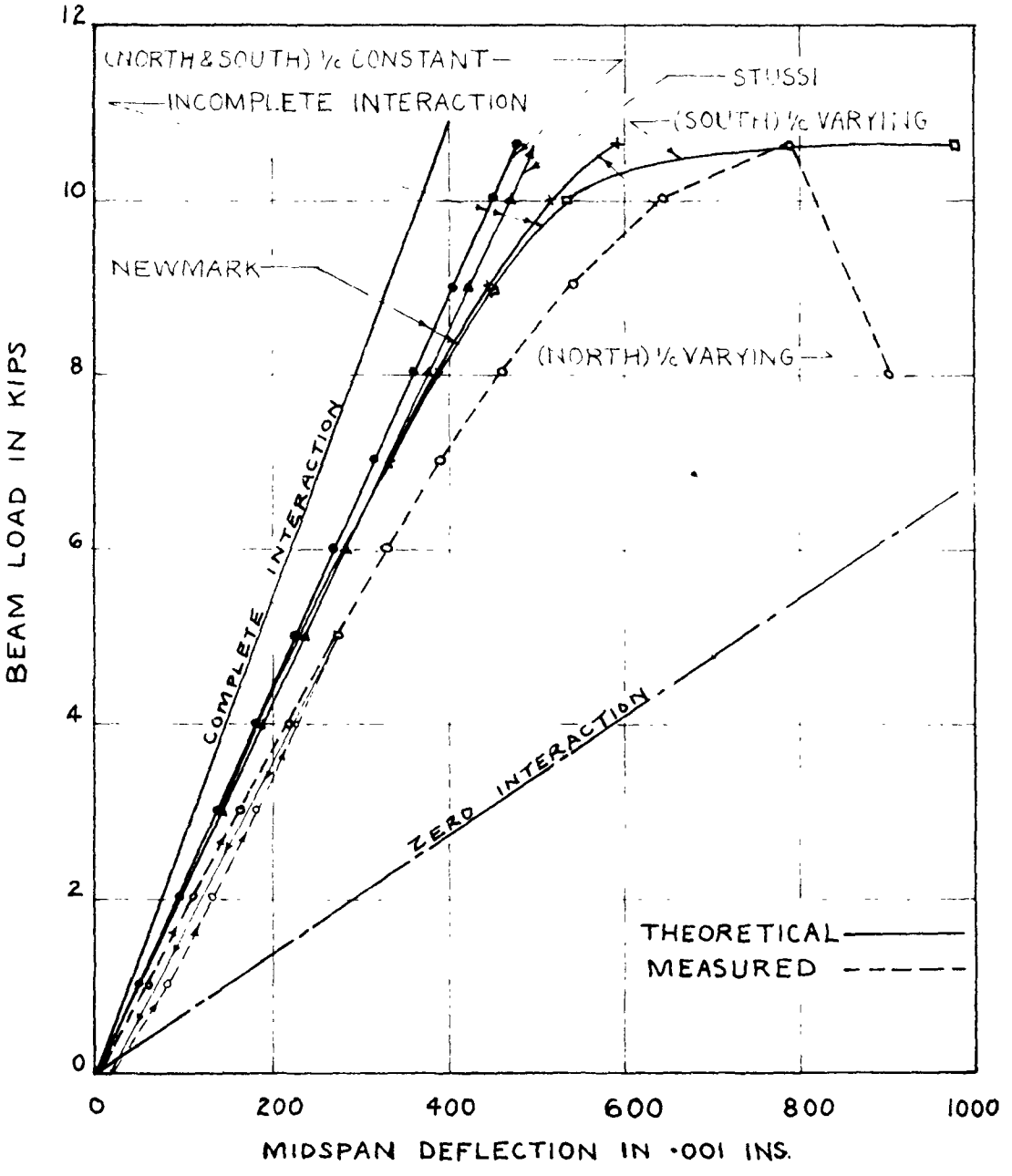

Fig. 4.15 Load-Deflection Curves for B3

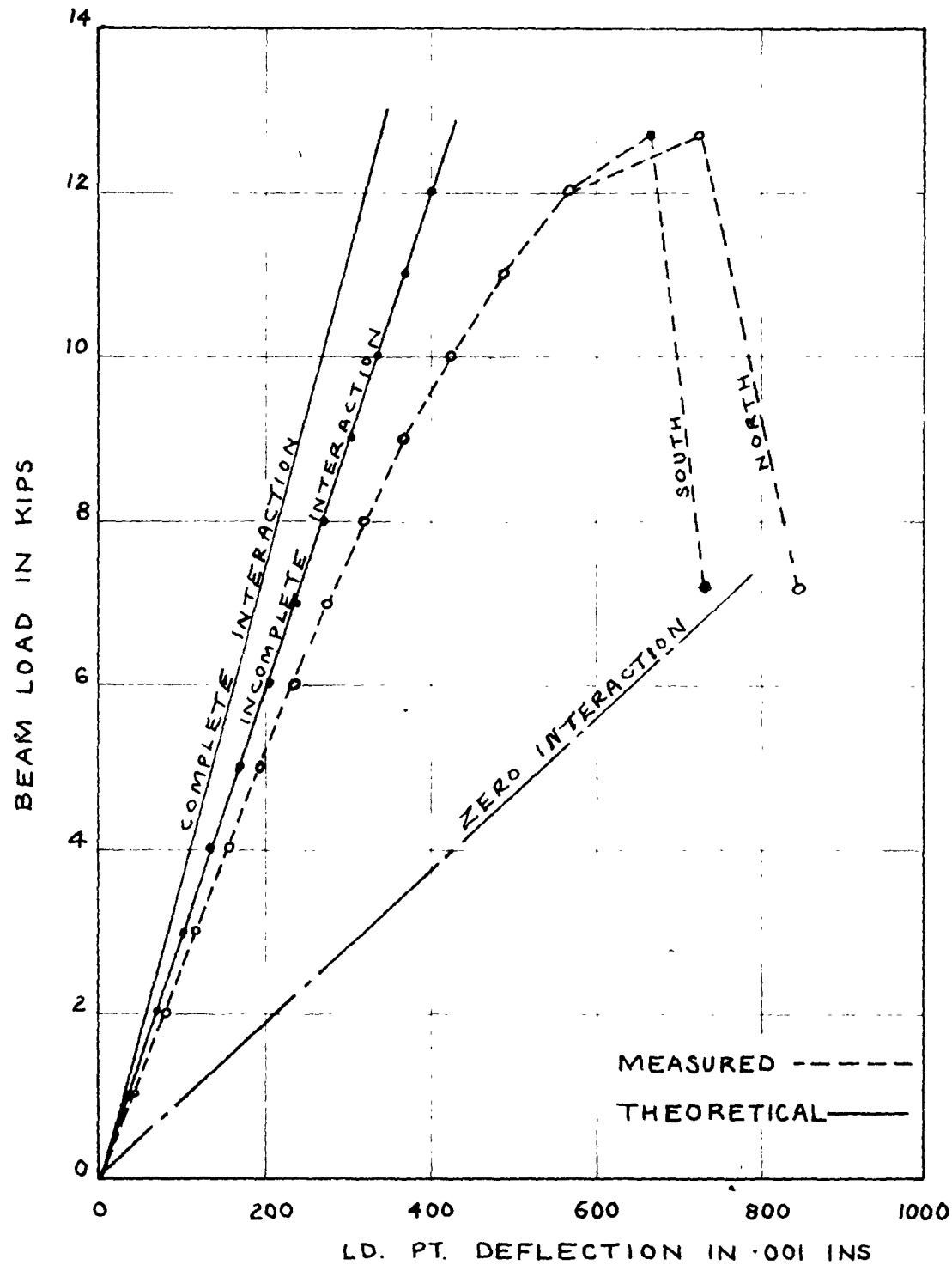

Fig. 4.16 Load-Deflection Curves for B4 (Stussi)

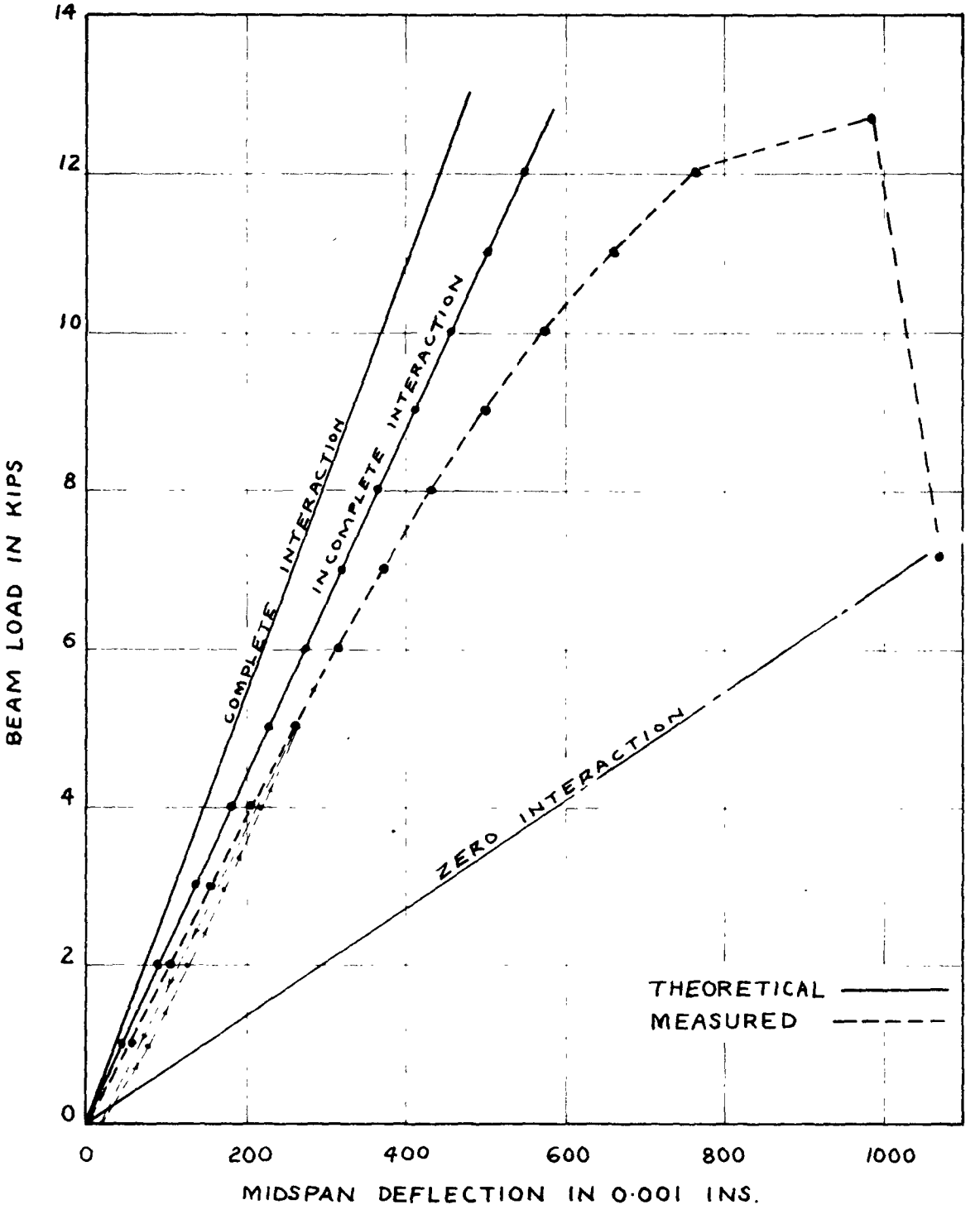

Fig. 4.17 Load-Deflection Curves for B4 (Stussi)

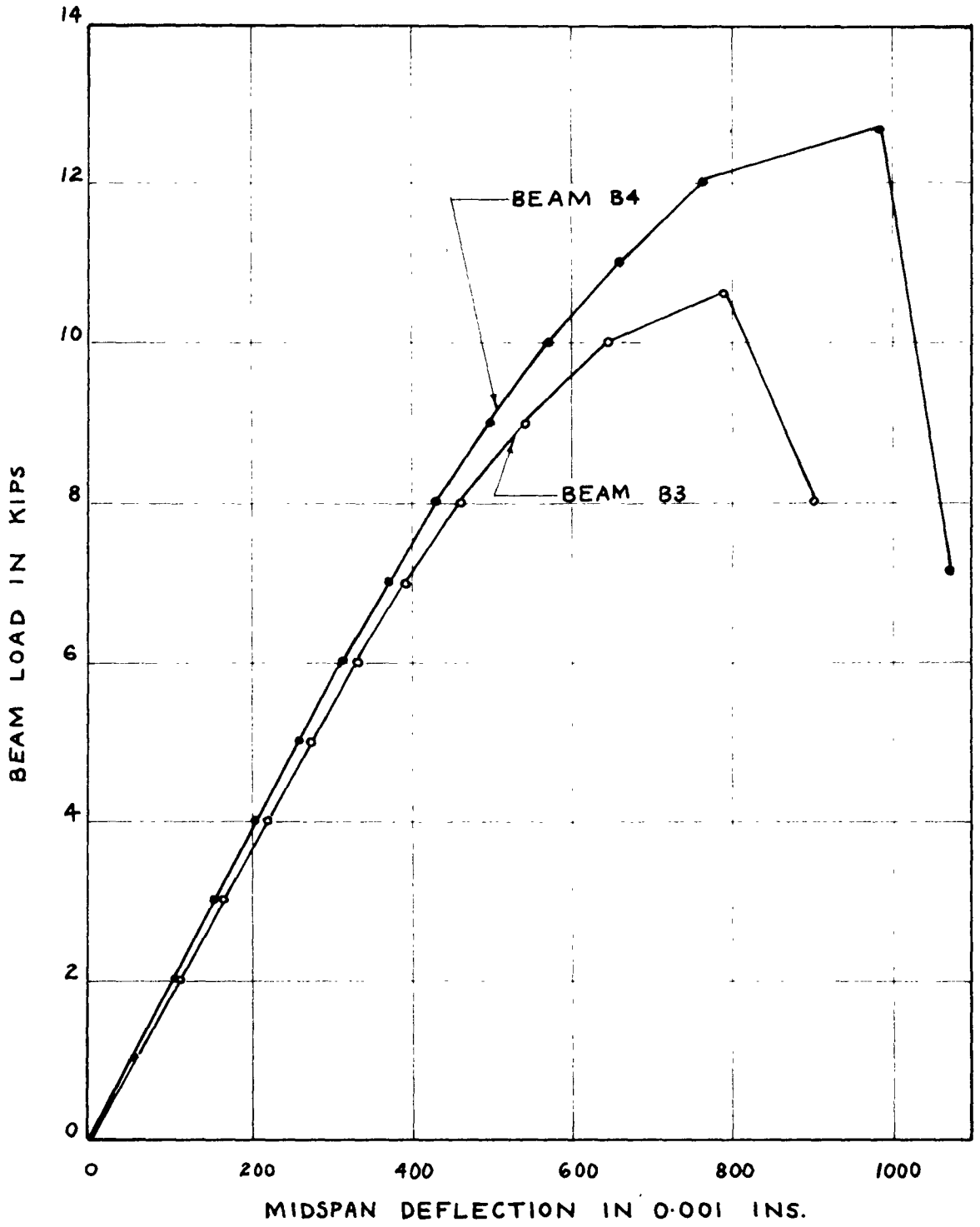

Fig. 4.18 Load-Deflection Curves for B3 and B4

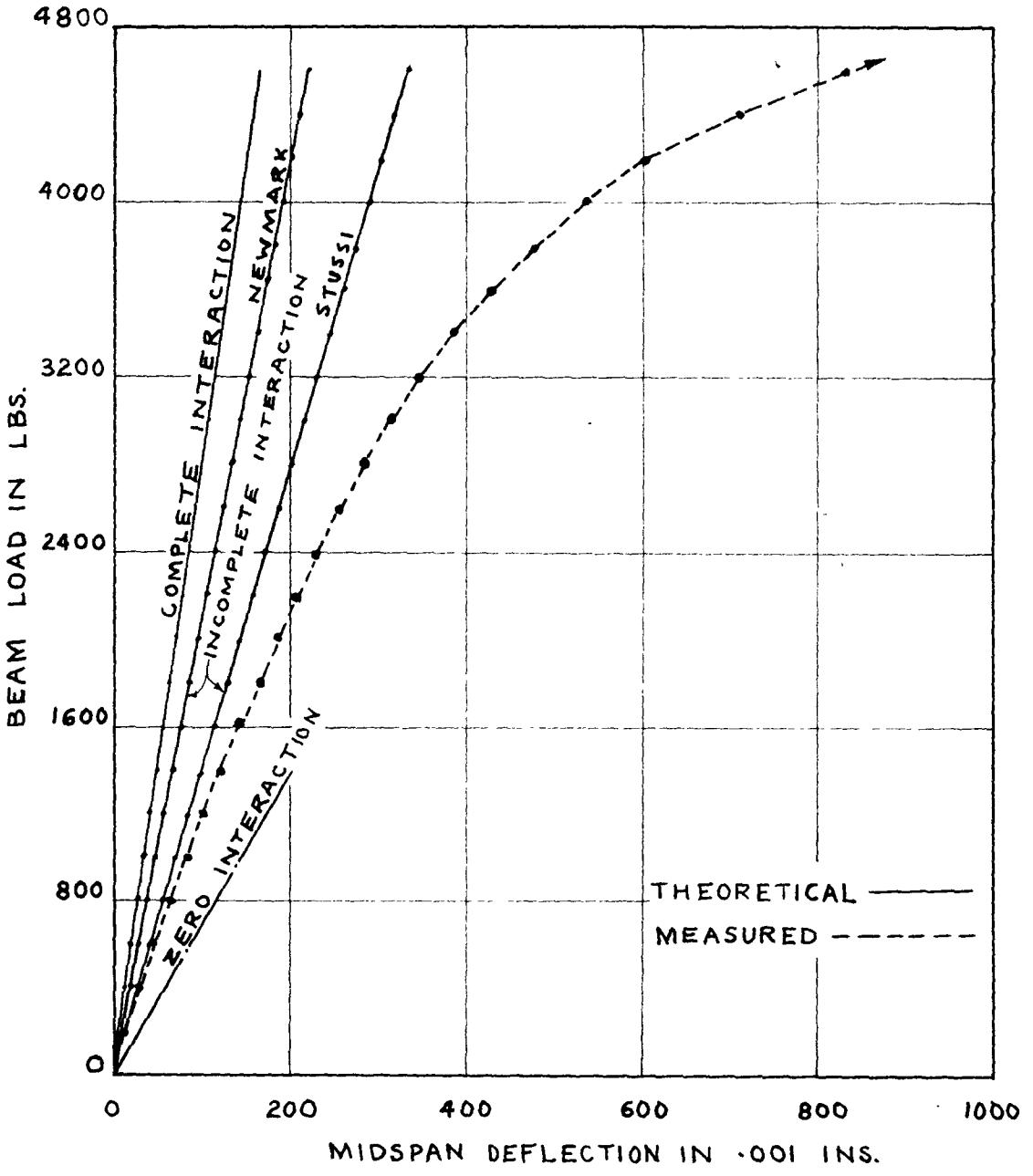

Fig. 4.19 Load-Deflection Curves for B5

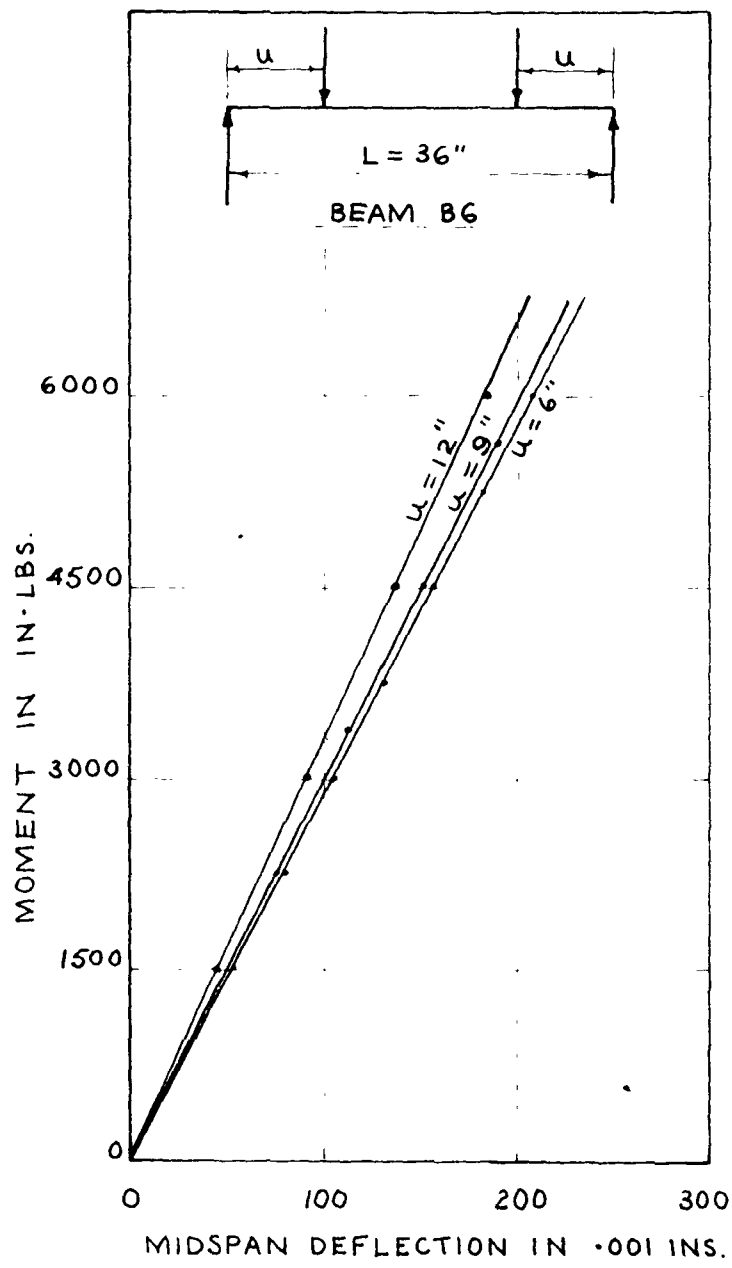

Fig. 4.20 Moment-Deflection Curve for B6

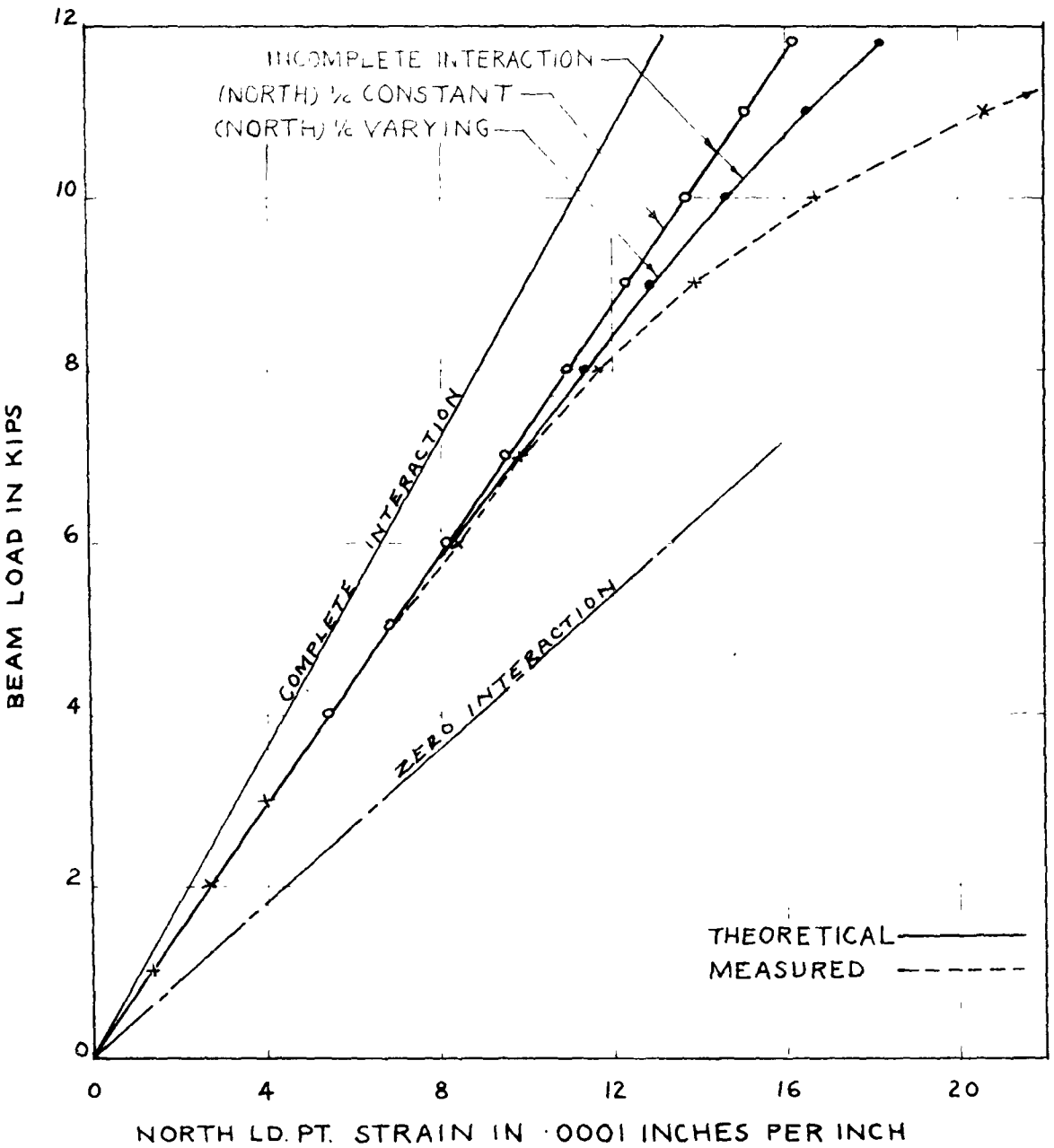

Fig. 4.21 Load-Strain Curves for Bottom of B1
(Newmark)

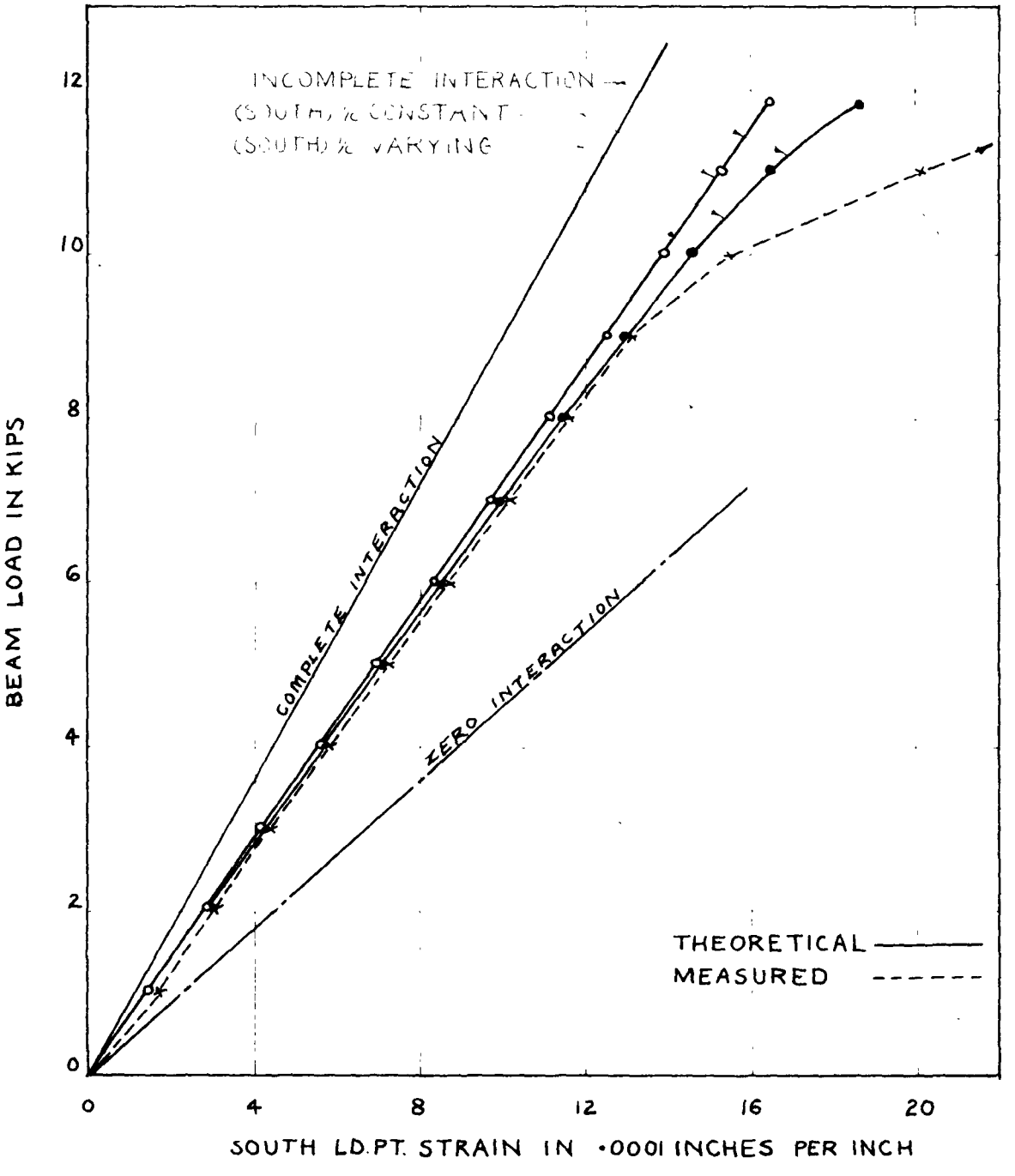

Fig. 4.22 Load-Strain Curves for Bottom of B1 (Newmark)

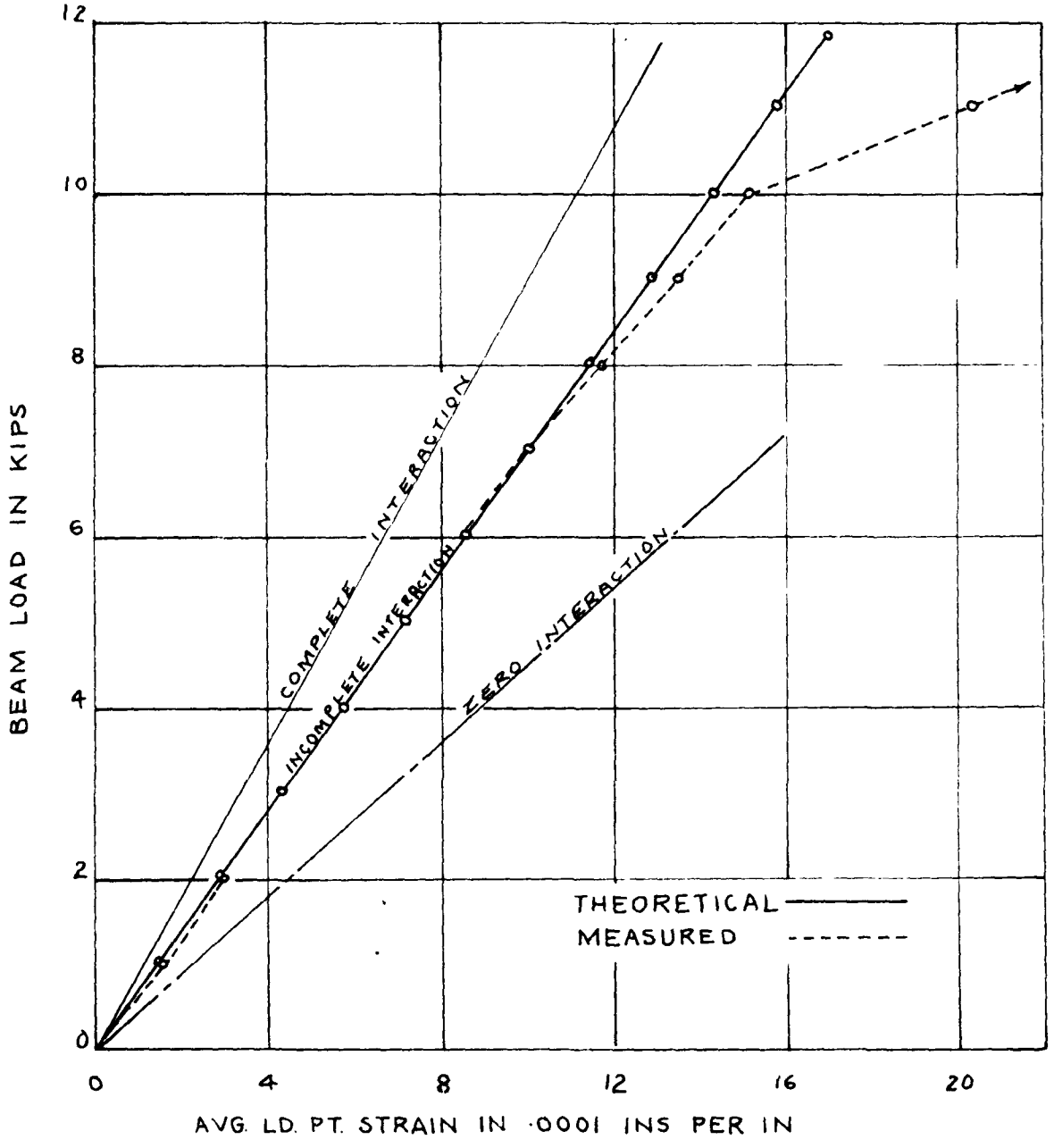

Fig. 4.23 Load-Strain Curves for Bottom of B1 (Stussi)

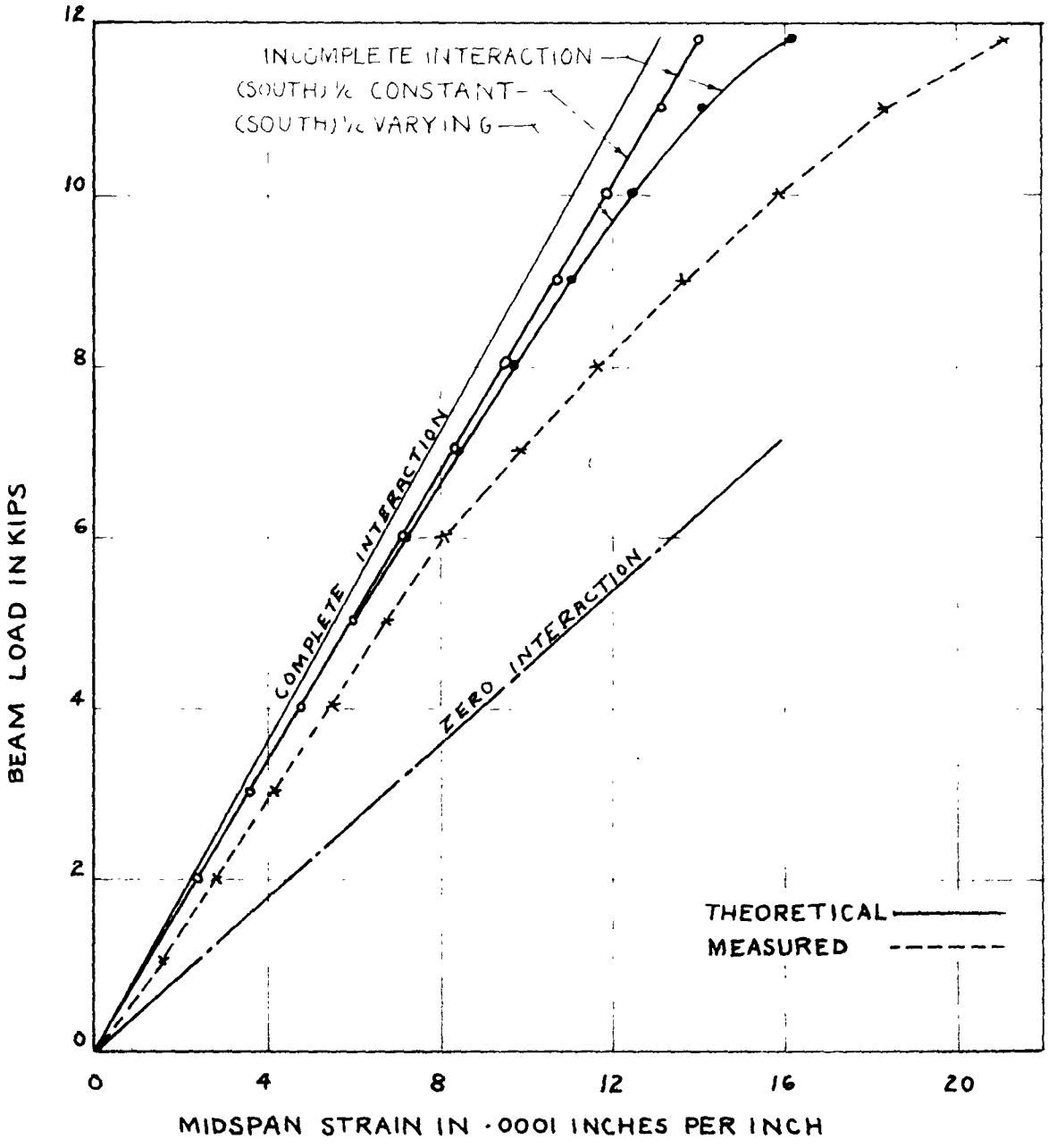

Fig. 4.24 Load-Strain Curves for Bottom of B1 (Newmark)

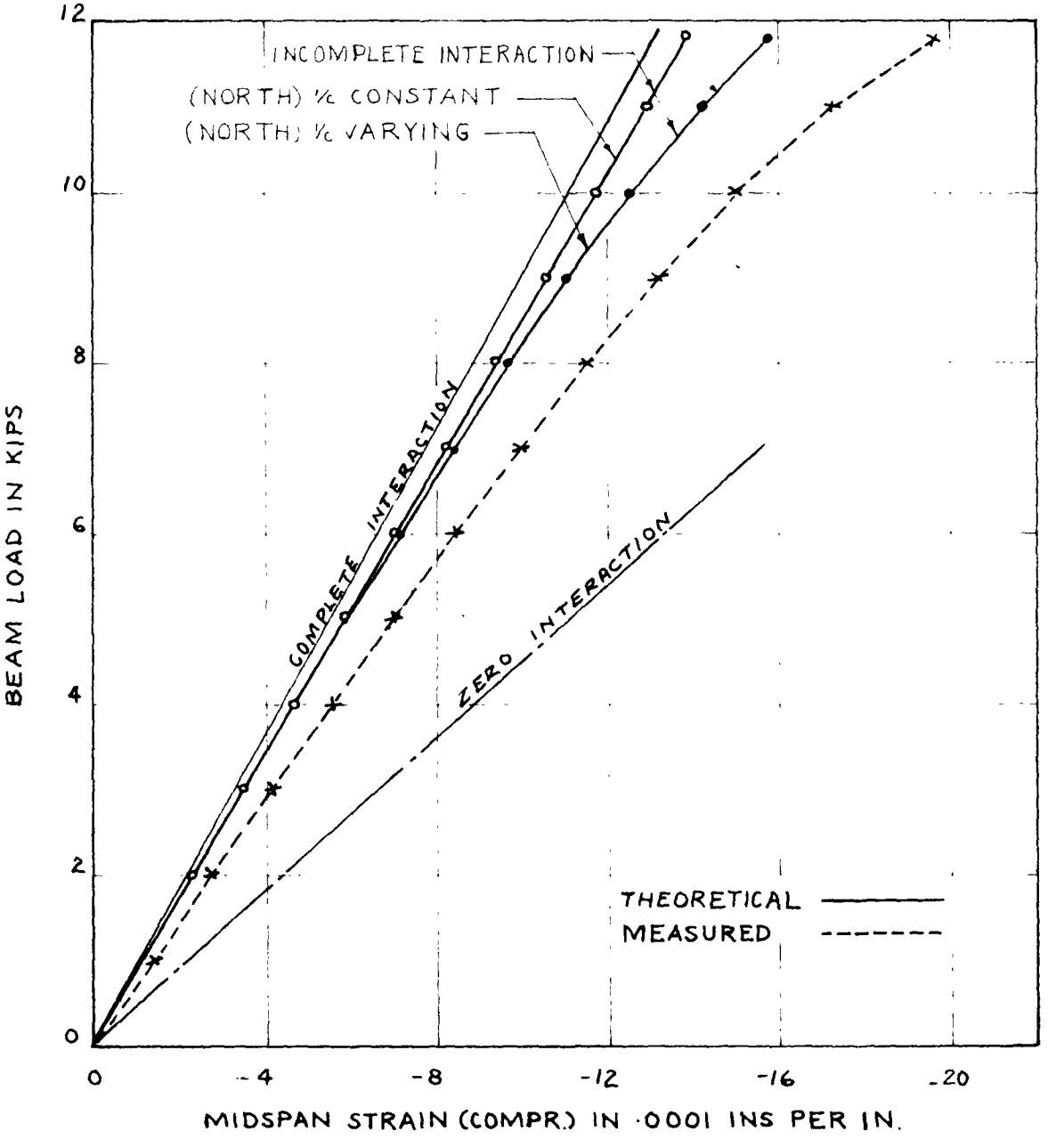

Fig. 4.25 Load-Strain Curves for Top of B1 (Newmark)

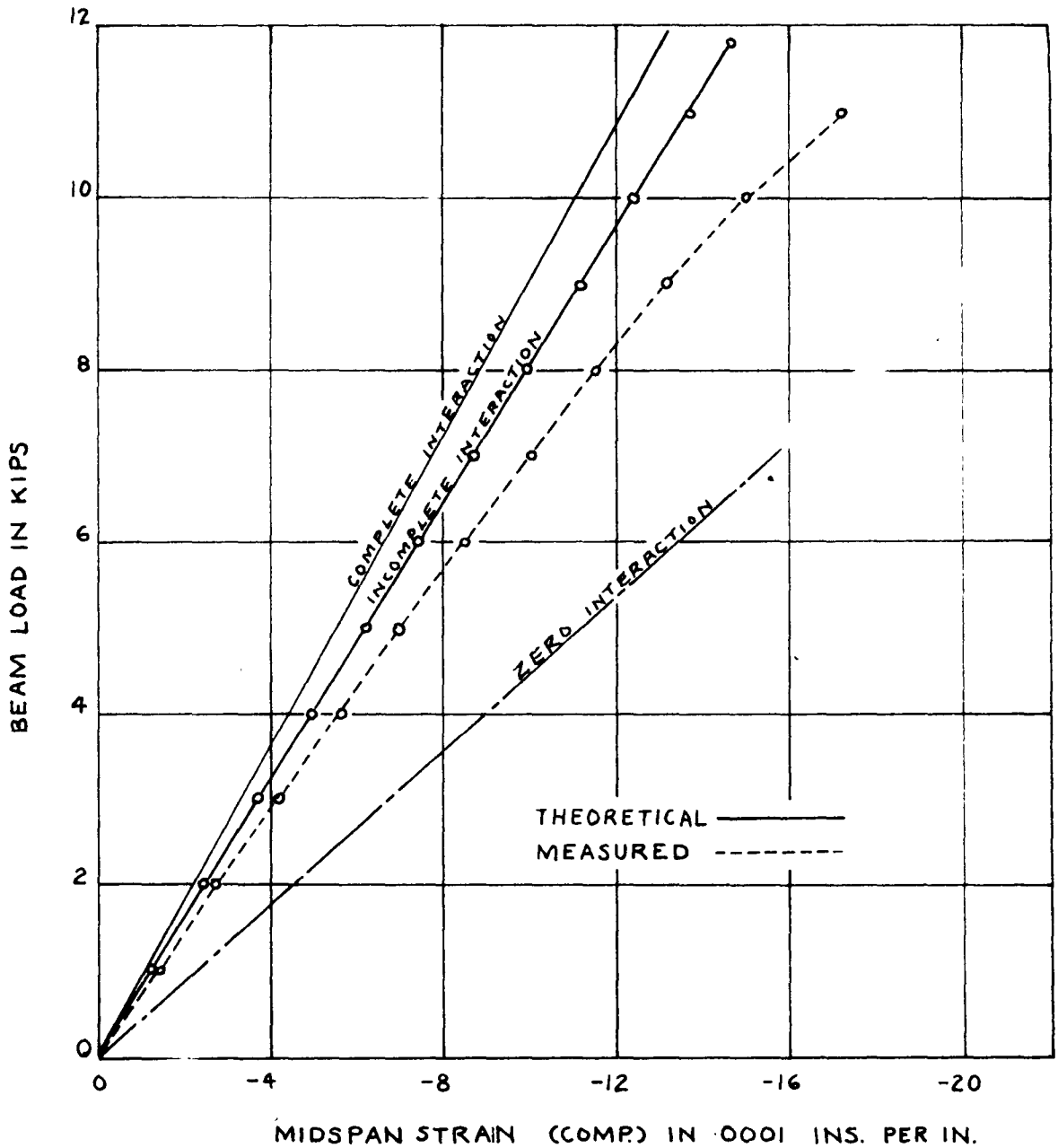

Fig. 4.26 Load-Strain Curves for Top of B1 (Stussi)

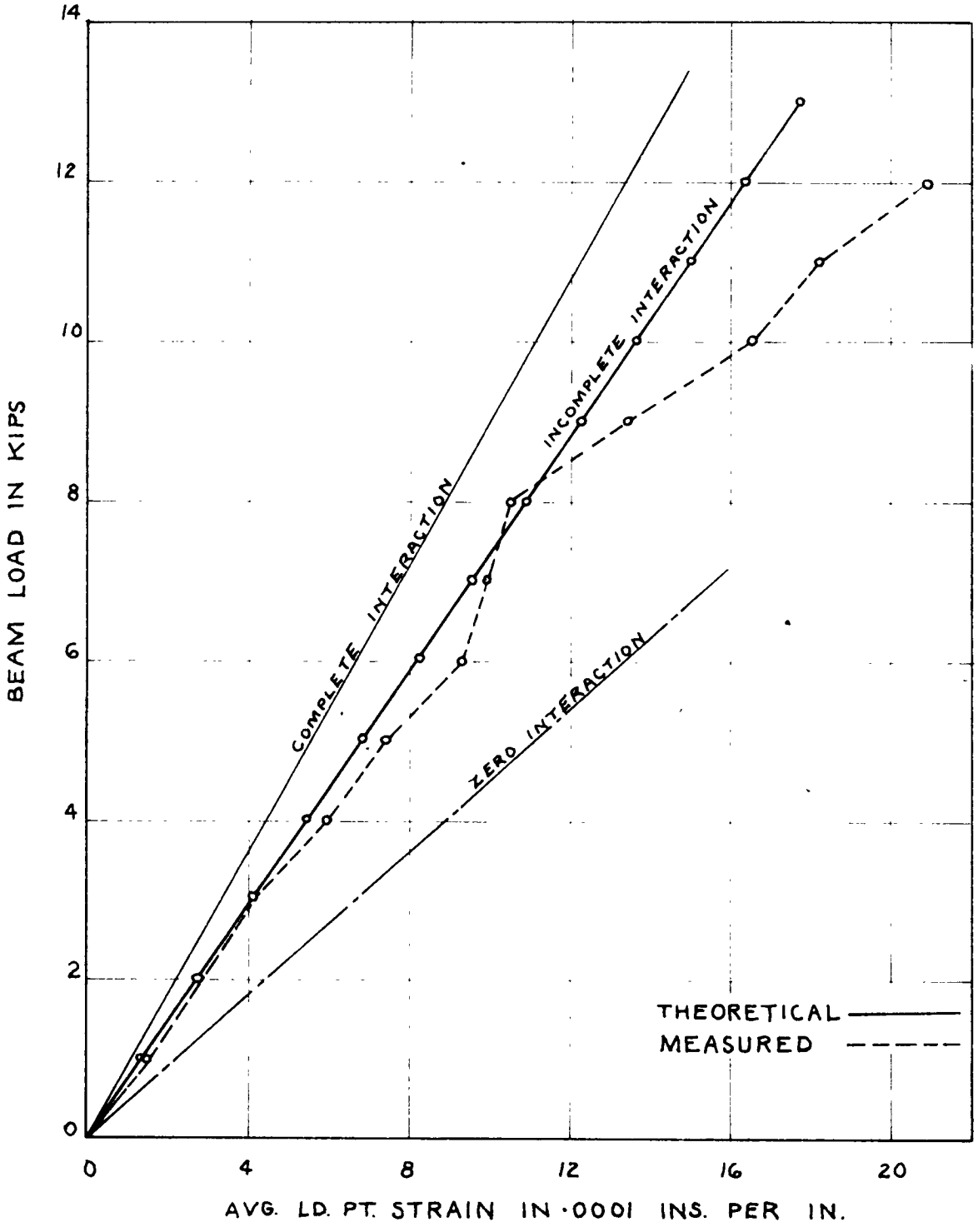

Fig. 4.27 Load-Strain Curves for Bottom of B2 (Stussi)

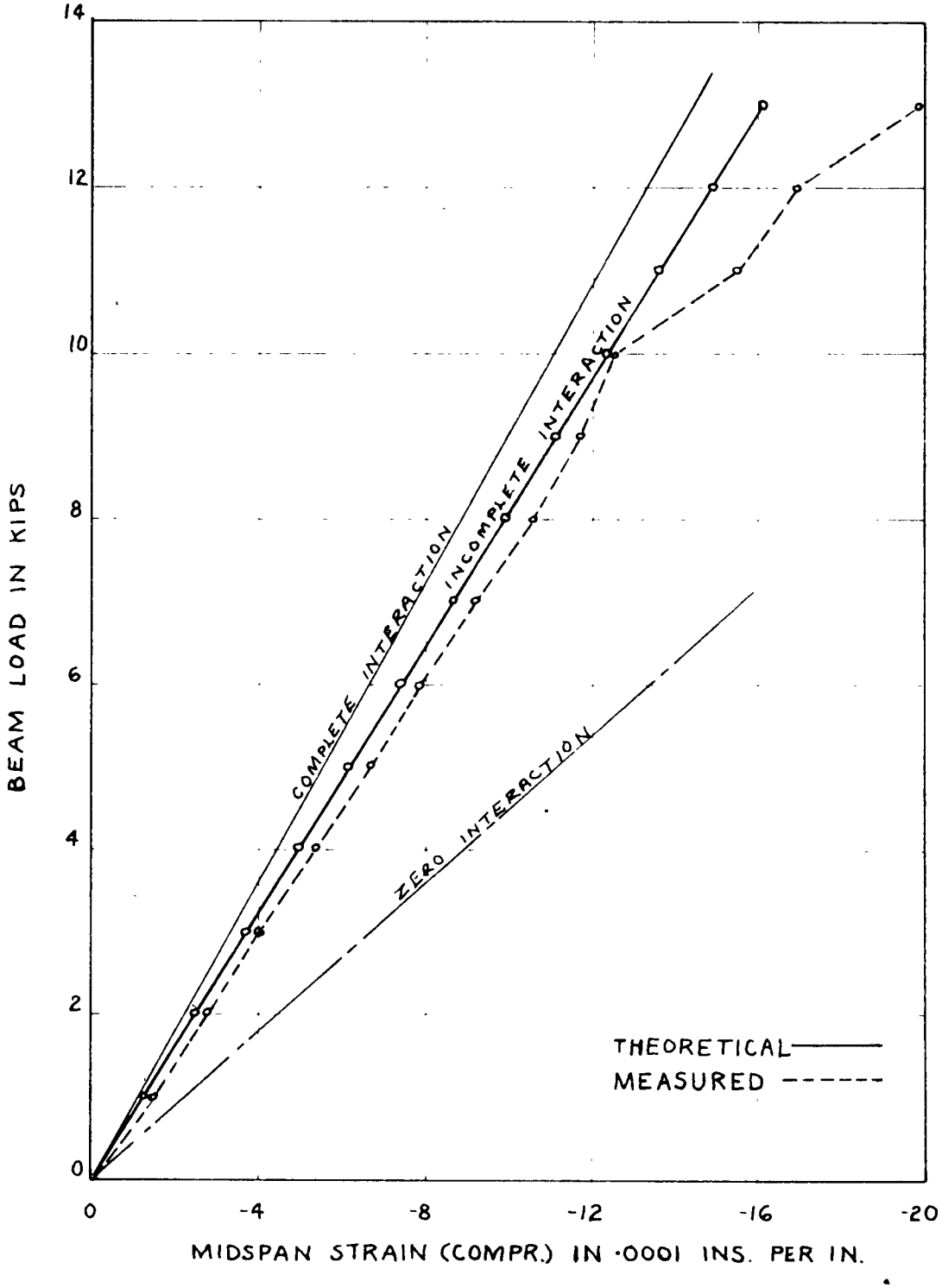

Fig. 4.28 Load-Strain Curves for Top of B2 (Stussi)

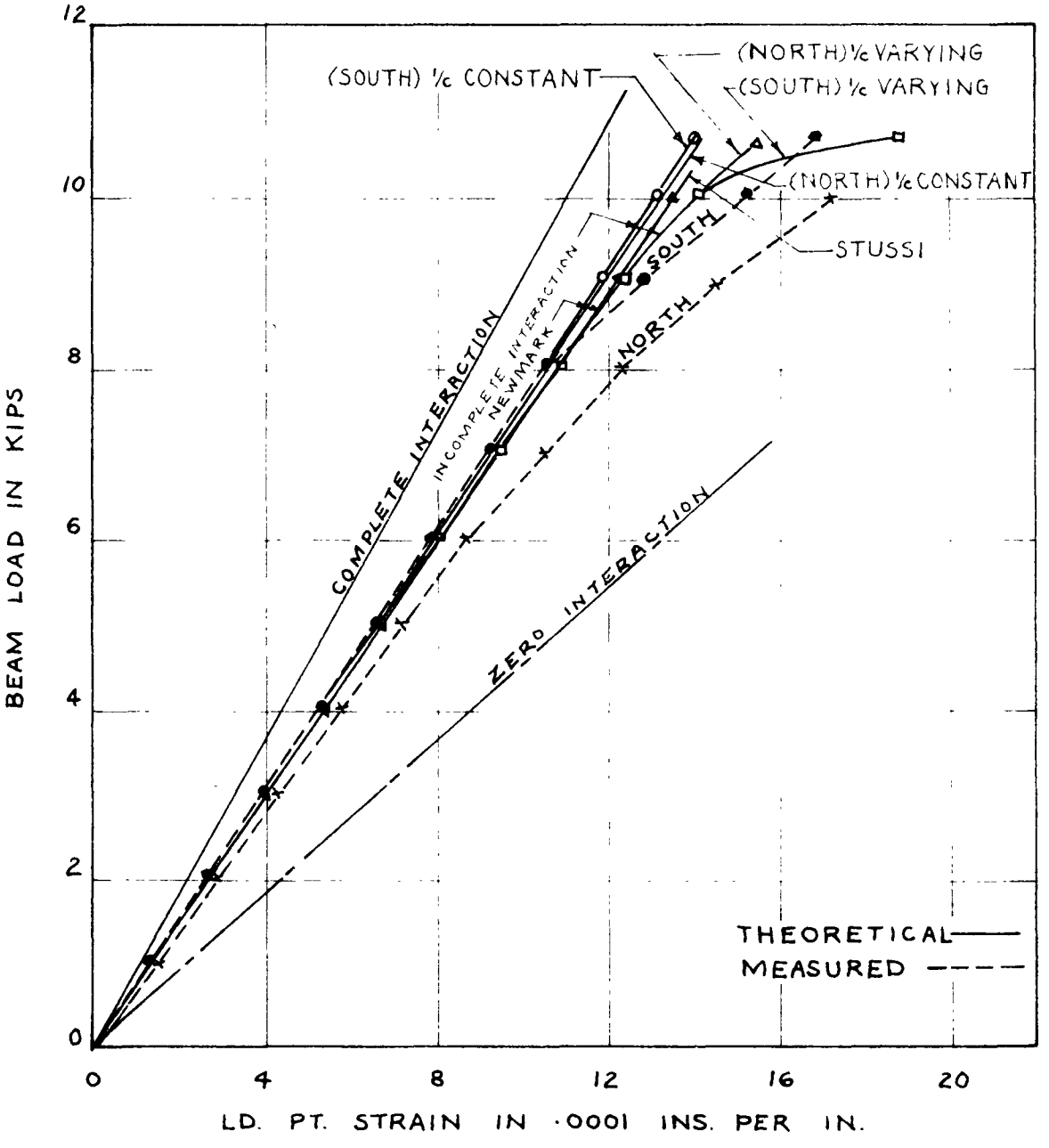

Fig. 4.29 Load-Strain Curves for Bottom of B3

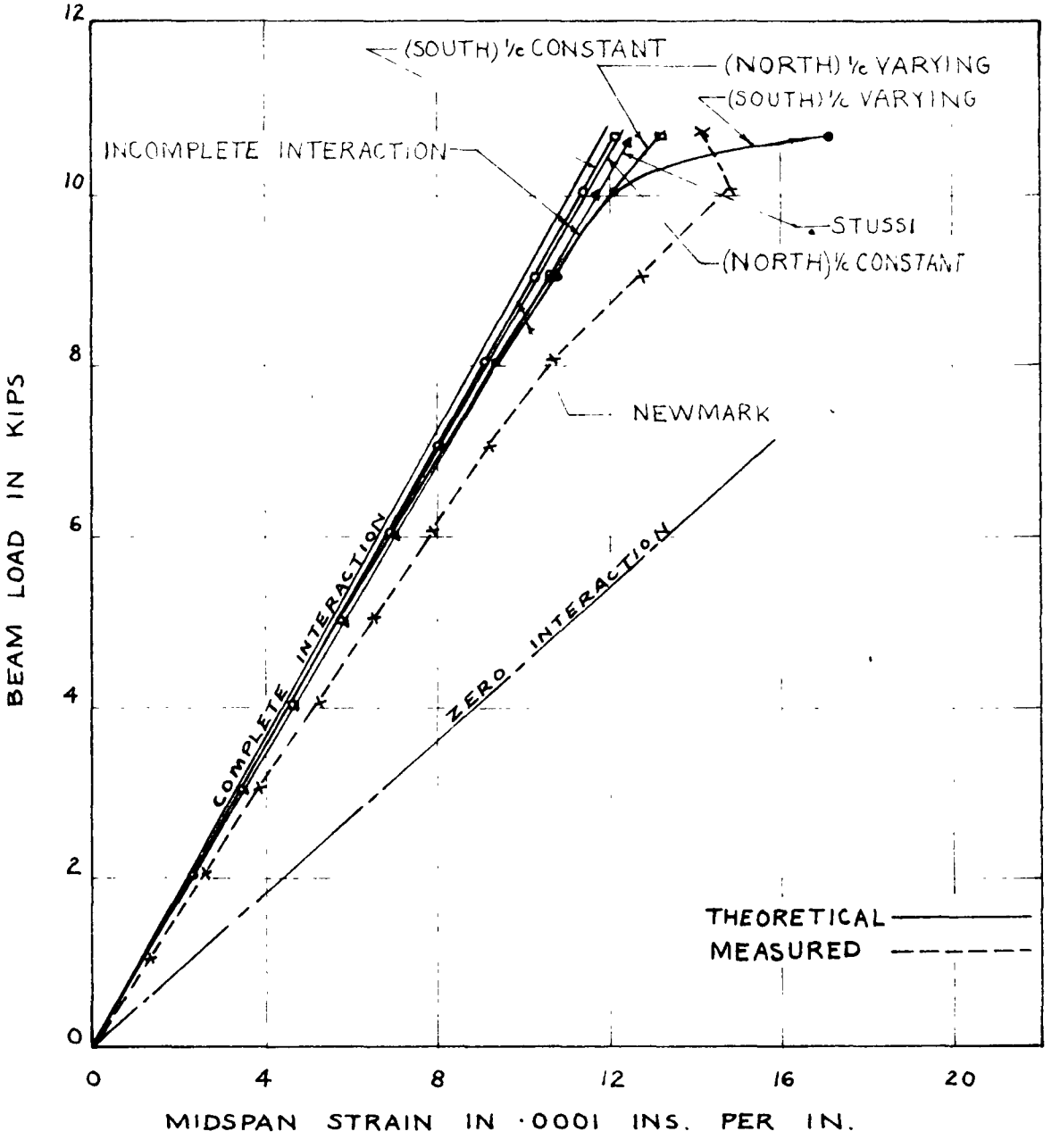

Fig. 4.30 Load-Strain Curves for Bottom of B3

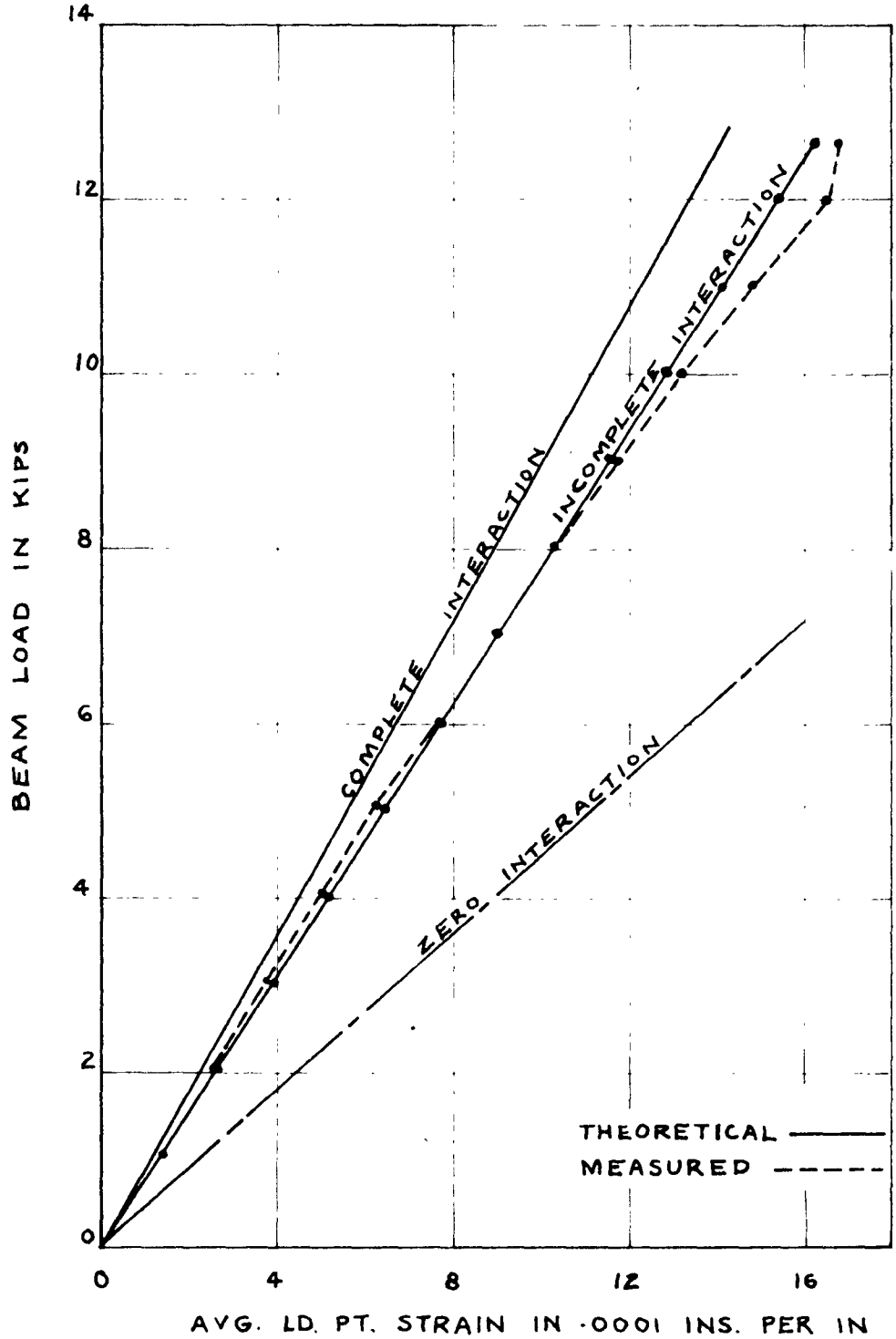

Fig. 4.31 Load-Strain Curves for Bottom of B3

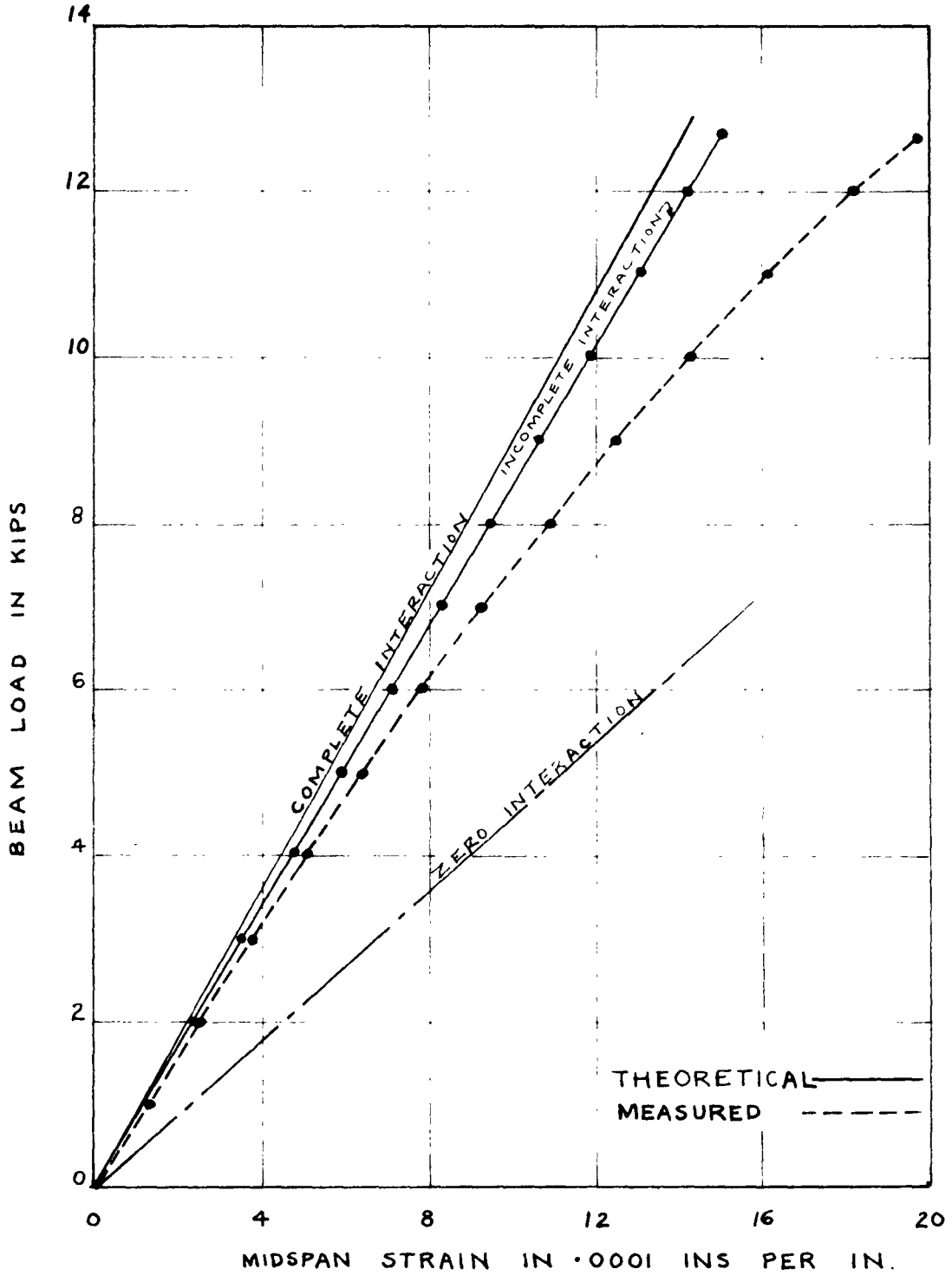

Fig. 4.32 Load-Strain Curves for Bottom of B4 (Stussi)

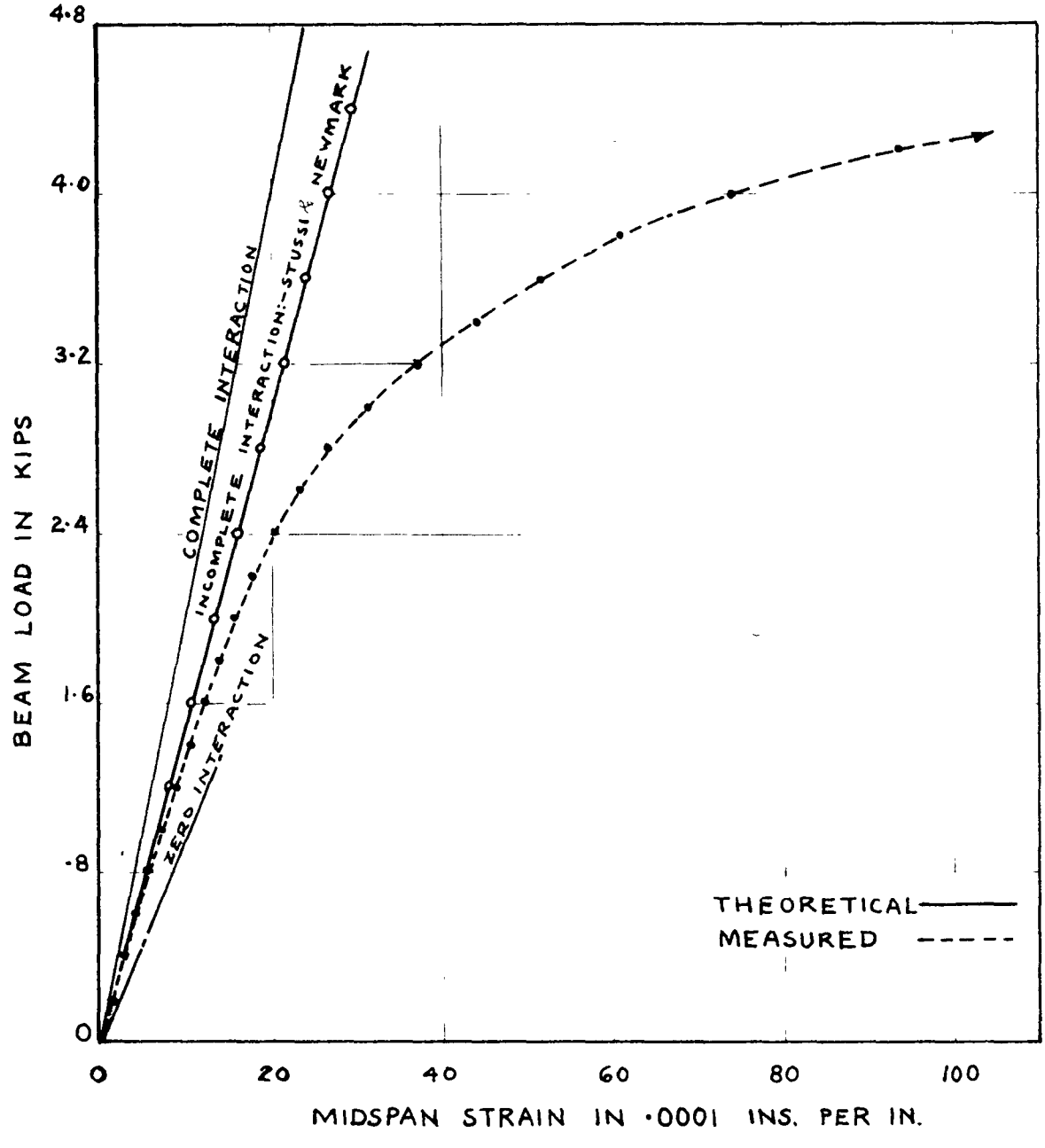

Fig. 4.33 Load-Strain Curve for Bottom of B5

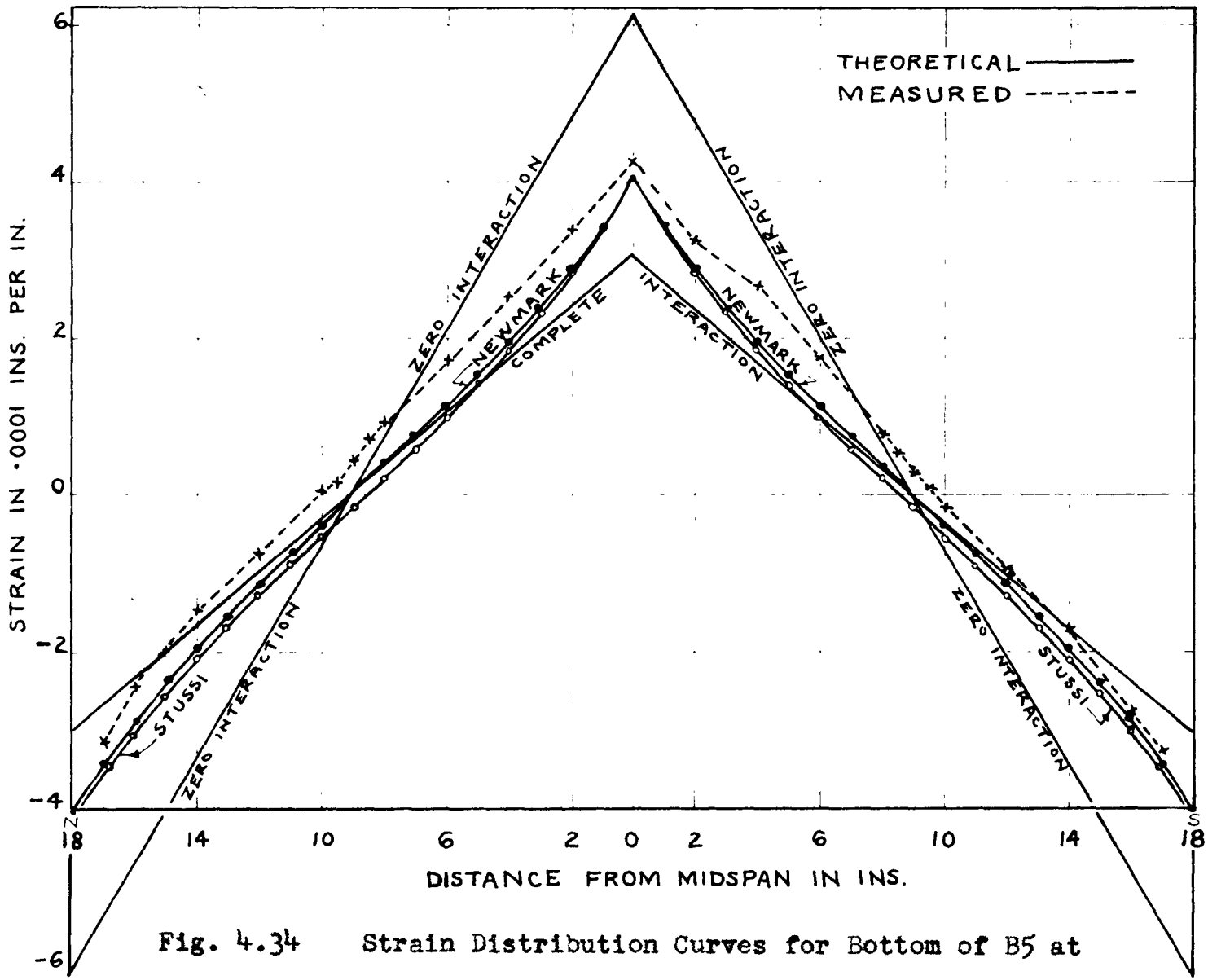

Fig. 4.34 Strain Distribution Curves for Bottom of B5 at 600 lbs. Load Level

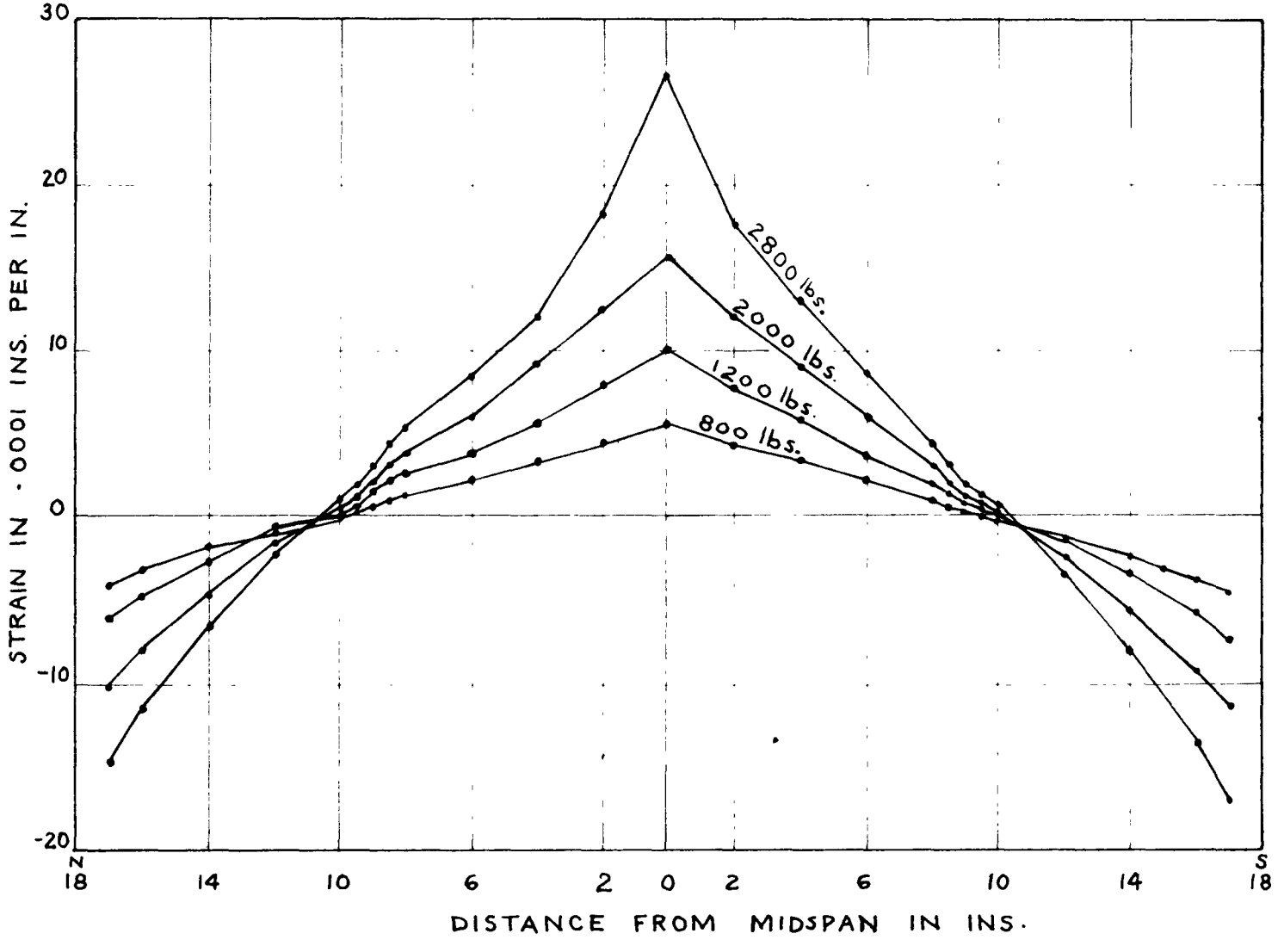

Fig. 4.35 Strain Distribution Curves for Bottom of B5

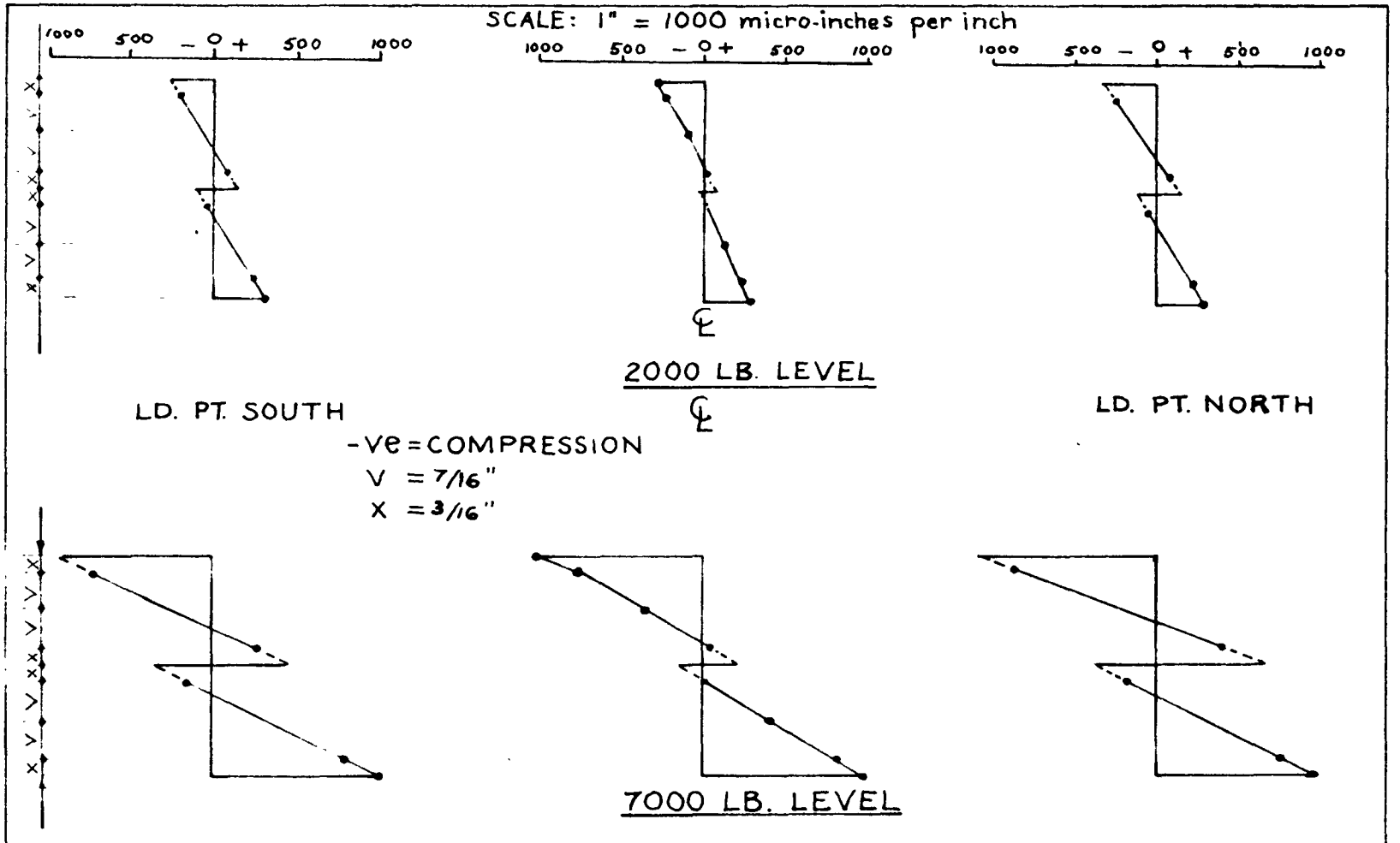

Fig. 4.36 Cross-Sectional Strain Distribution for B1

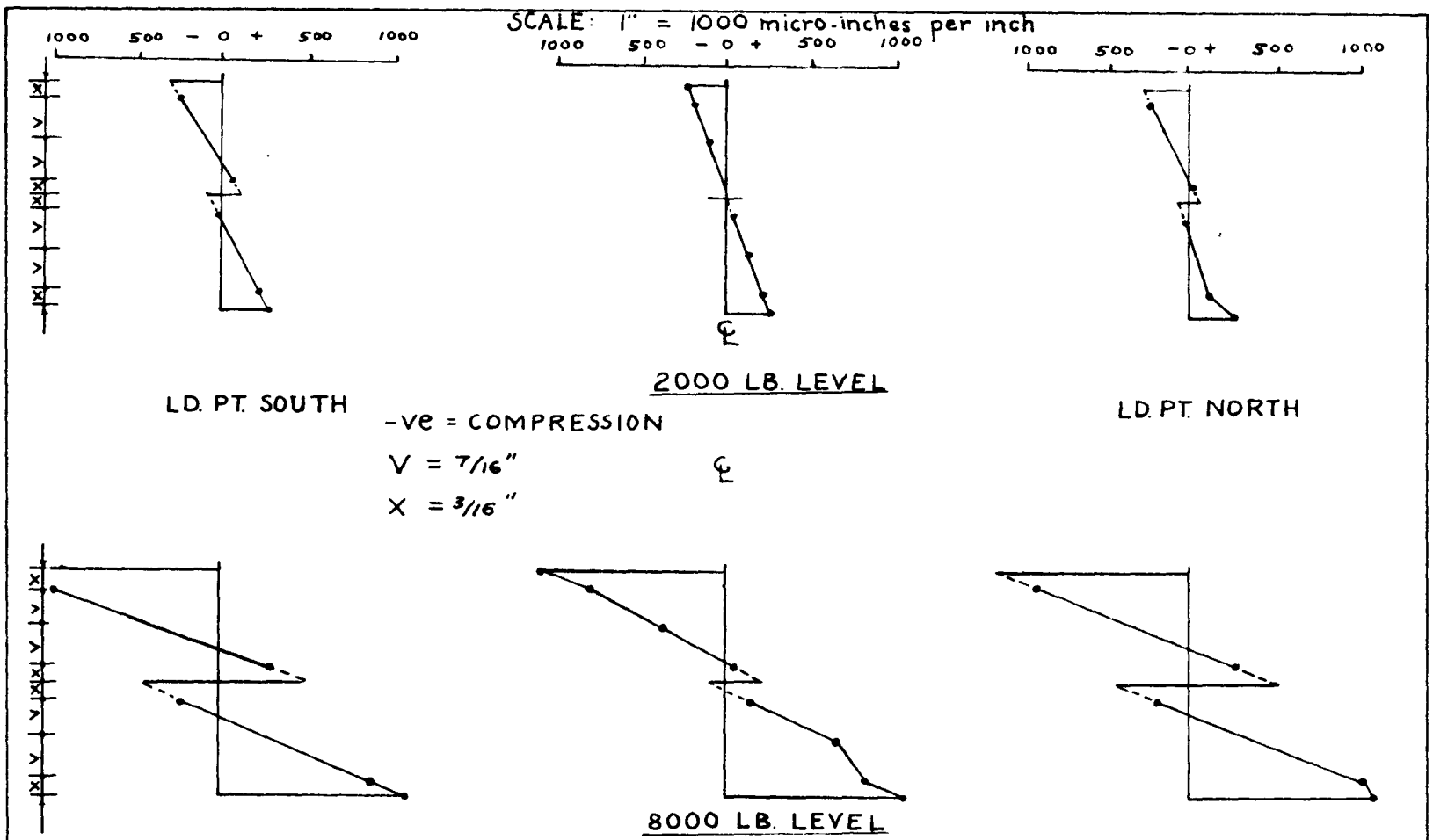

Fig. 4.37 Cross-Sectional Strain Distribution for B2

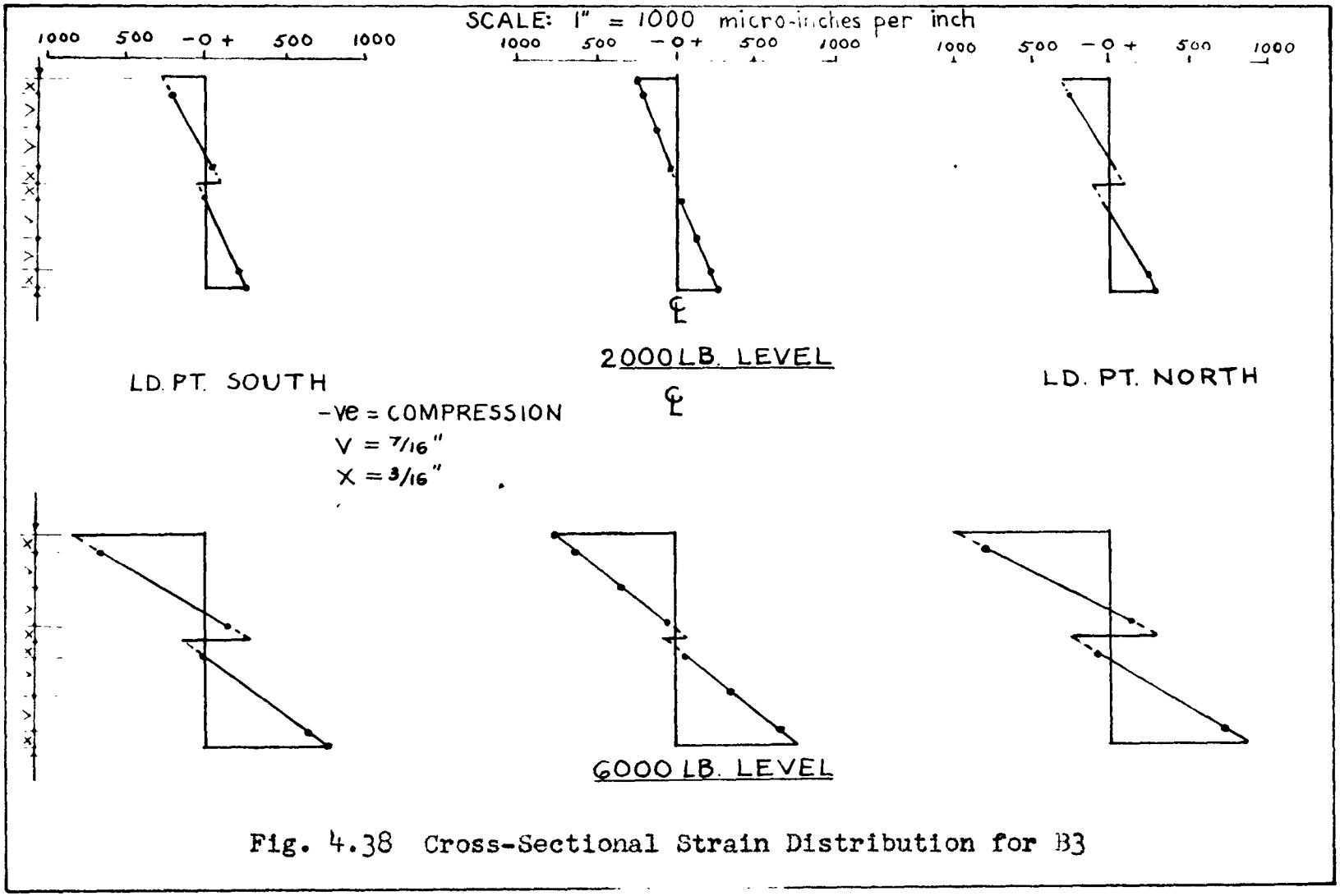

Fig. 4.38 Cross-Sectional Strain Distribution for B3

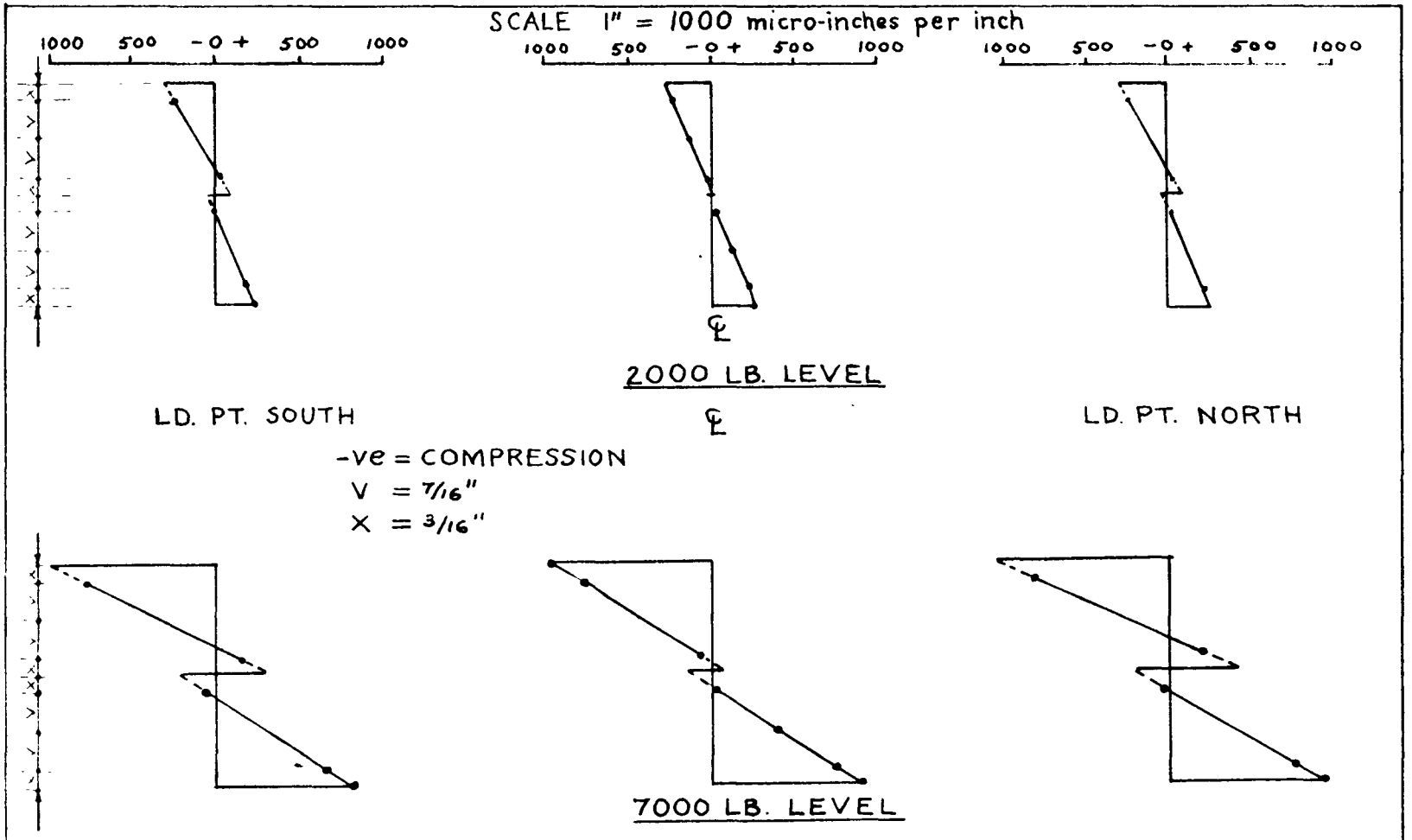

Fig. 4.39 Cross-Sectional Strain Distribution for B4

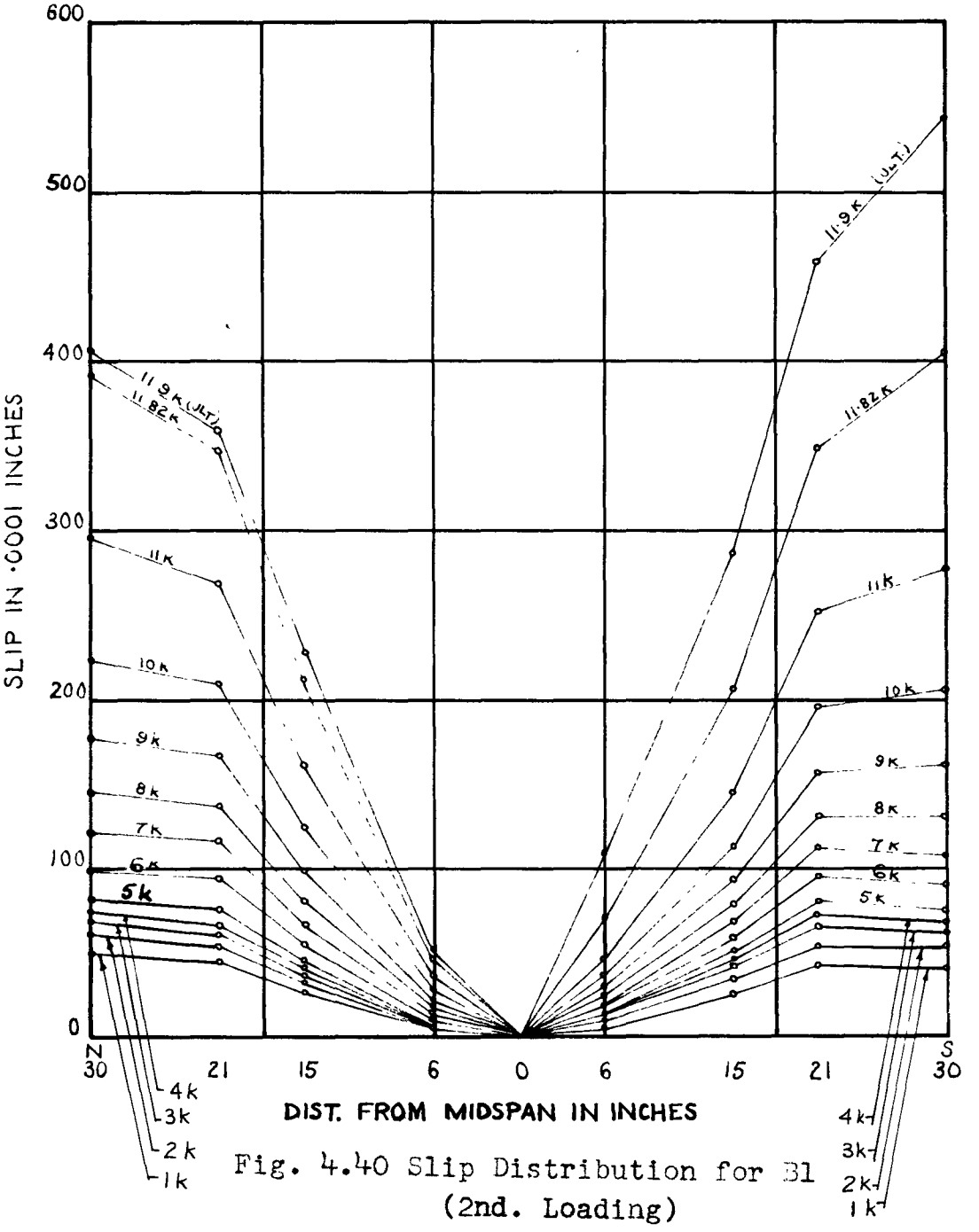

Fig. 4.40 Slip Distribution for B1 (2nd. Loading)

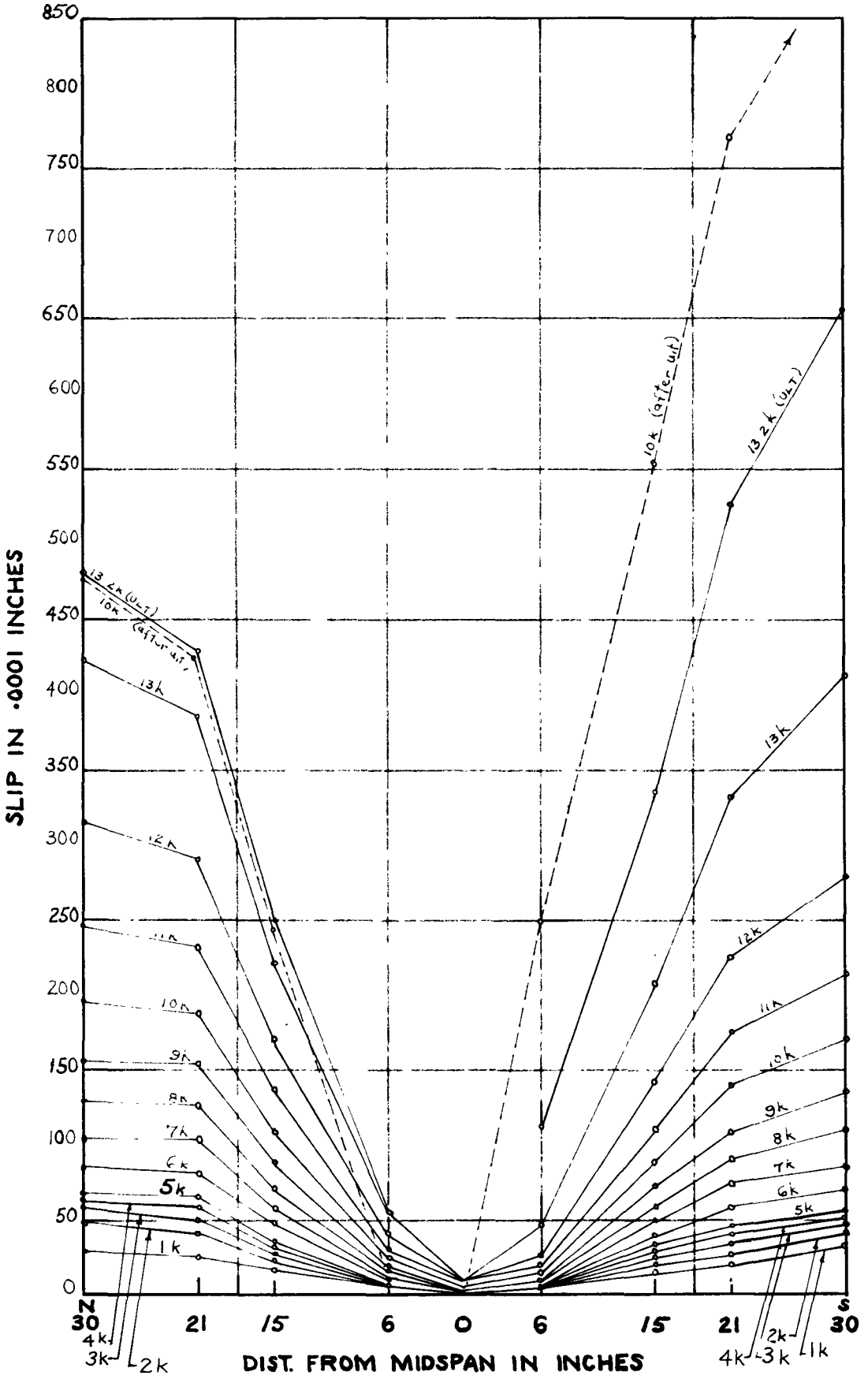

Fig. 4.41 Slip Distribution for B2 (2nd. Loading)

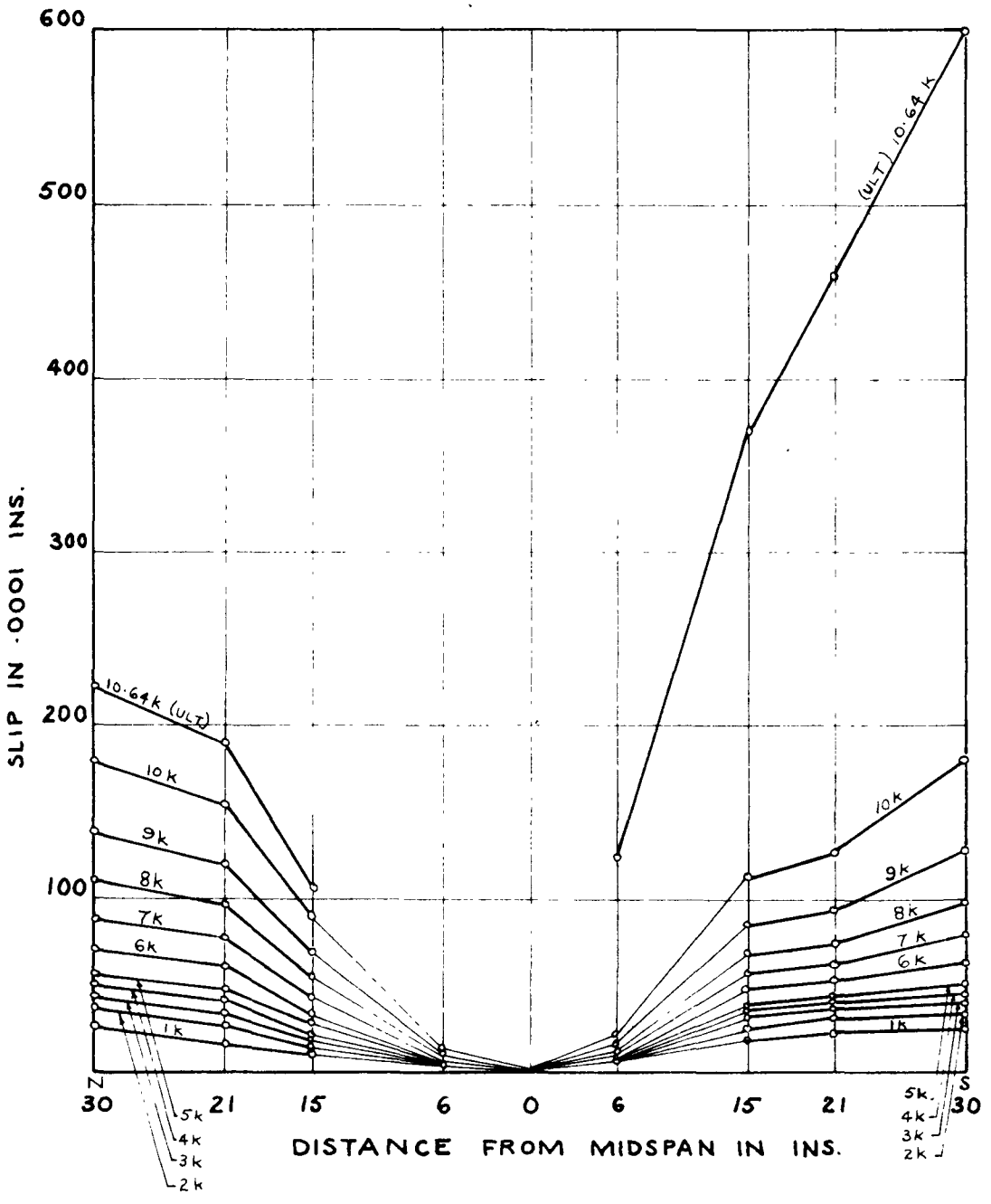

Fig. 4.42 Slip Distribution for B3 (2nd. Loading)

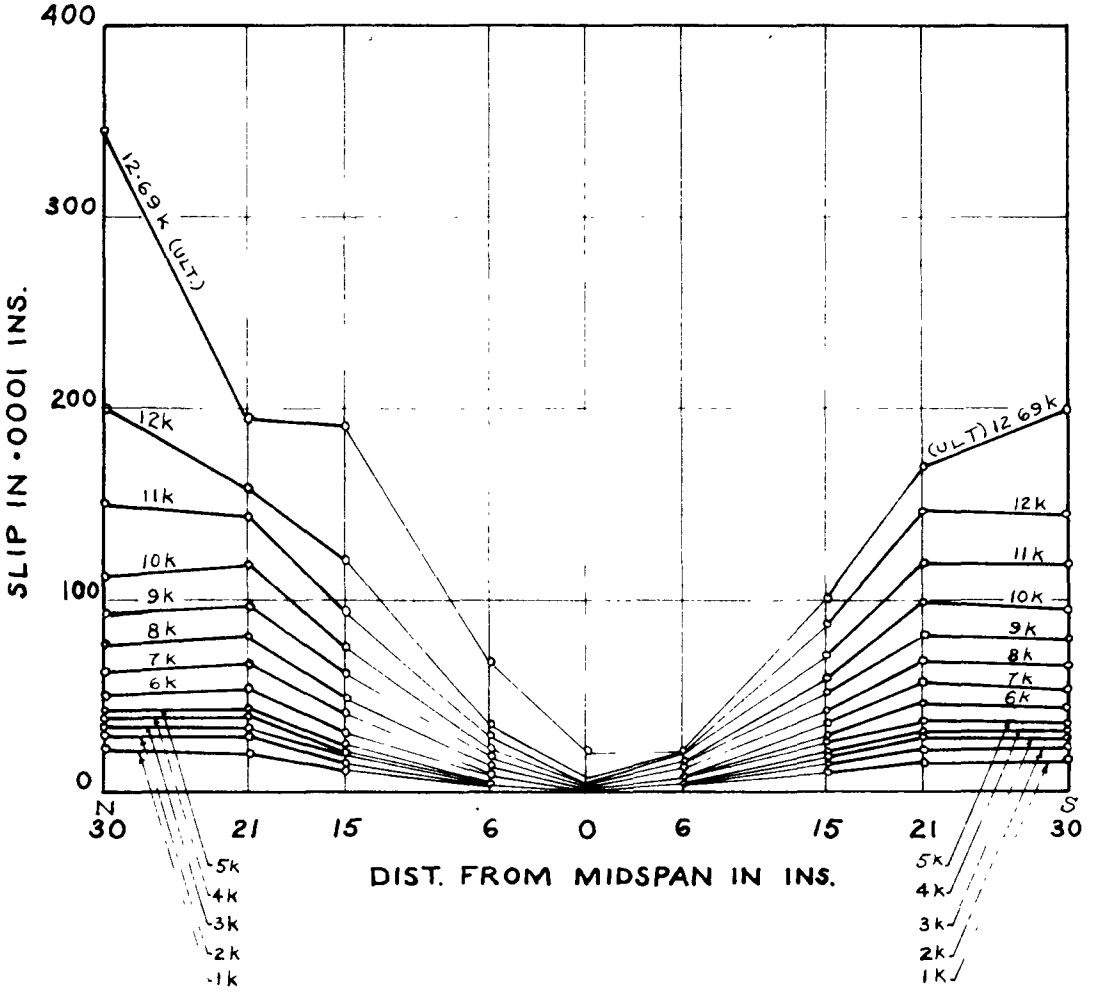

Fig. 4.43 Slip Distribution for B4 (2nd. Loading)

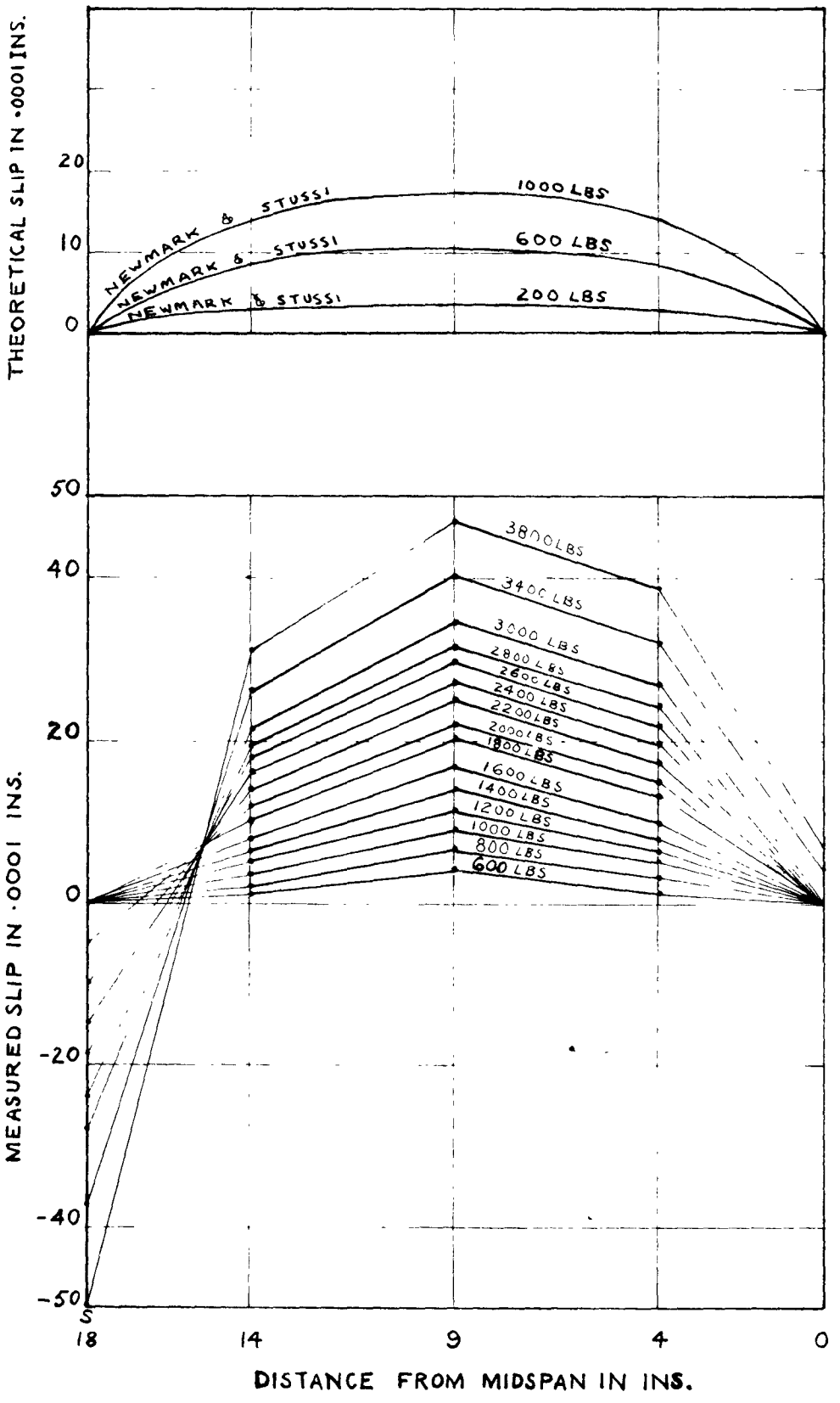

Fig. 4.44 Slip Distribution Curves for B5

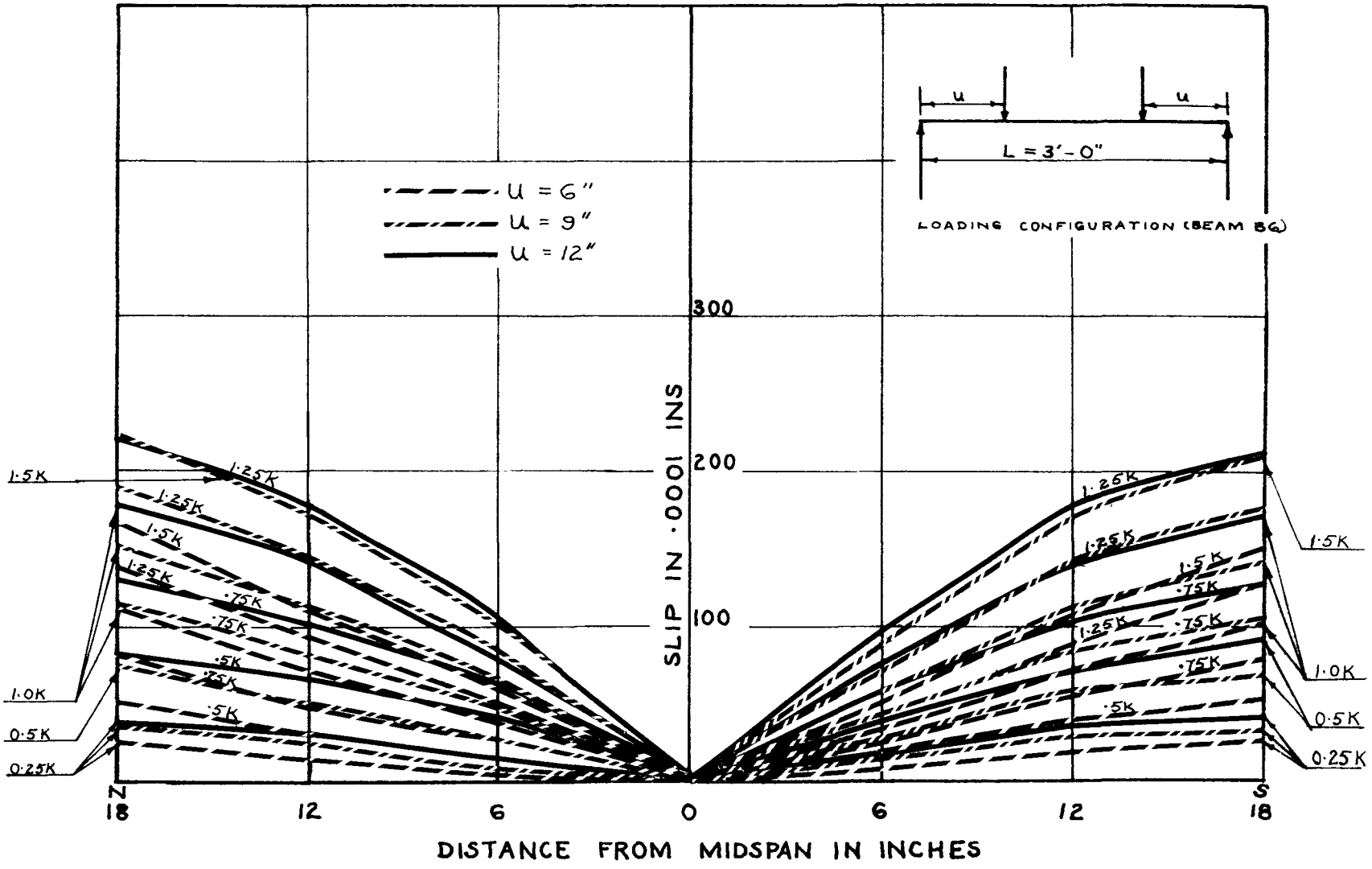

Fig. 4.45 Slip Distribution Curves for B6

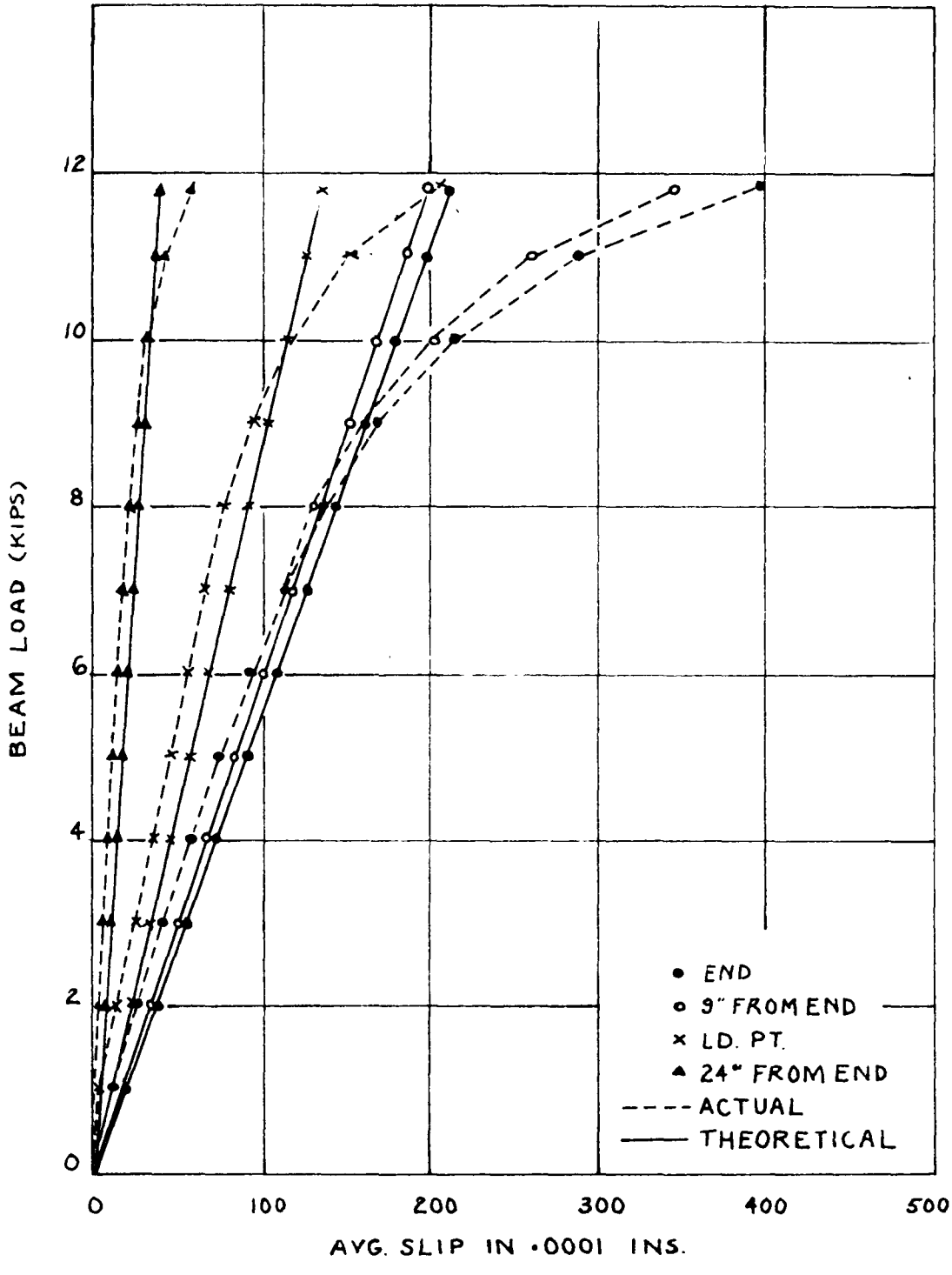

Fig. 4.46 Load-Slip Curves for B1 (Stussi)

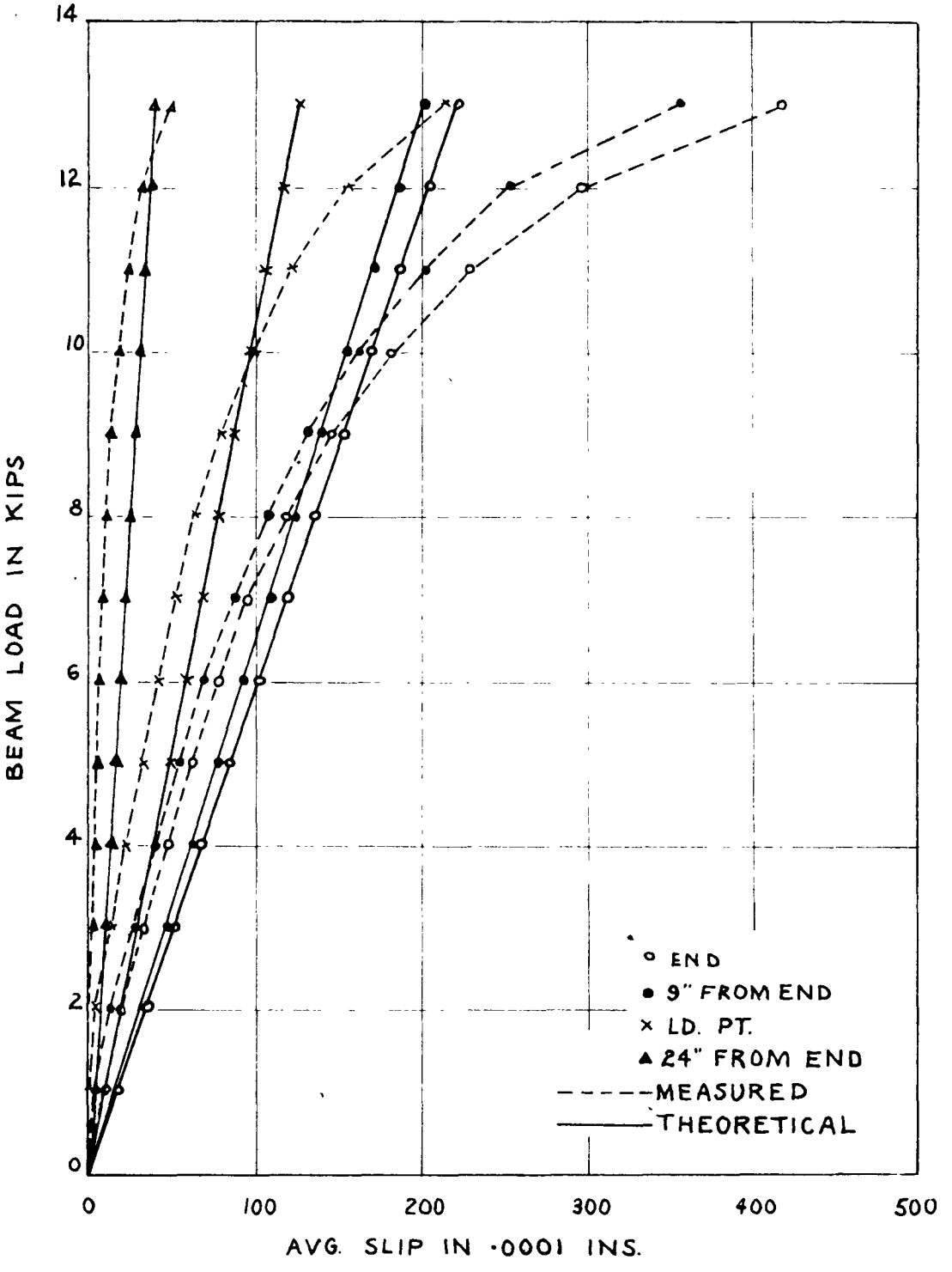

Fig. 4.47 Load-Slip Curves for B2 (Stussi)

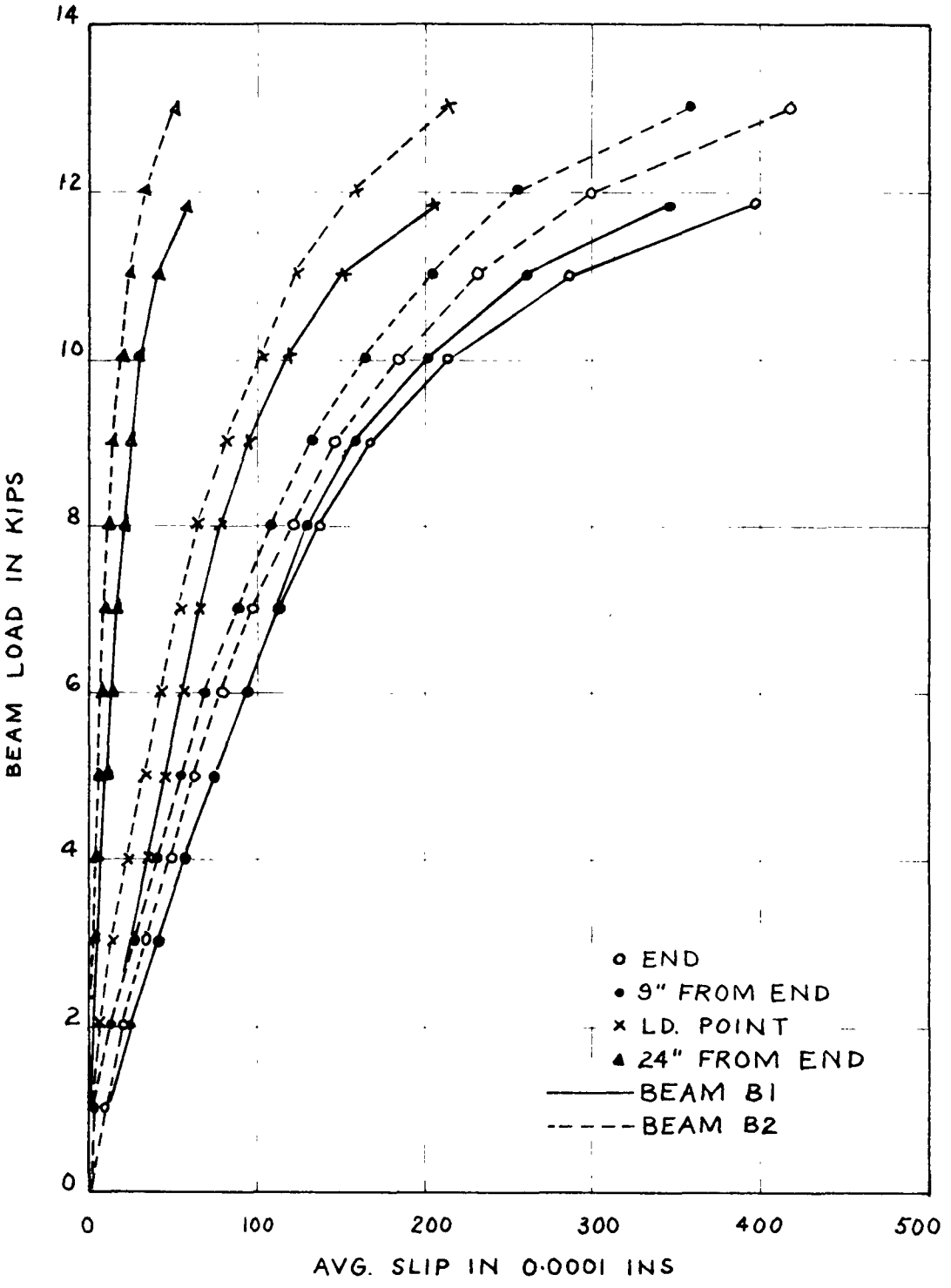

Fig. 4.48 Load-Slip Curves for B1 and B2

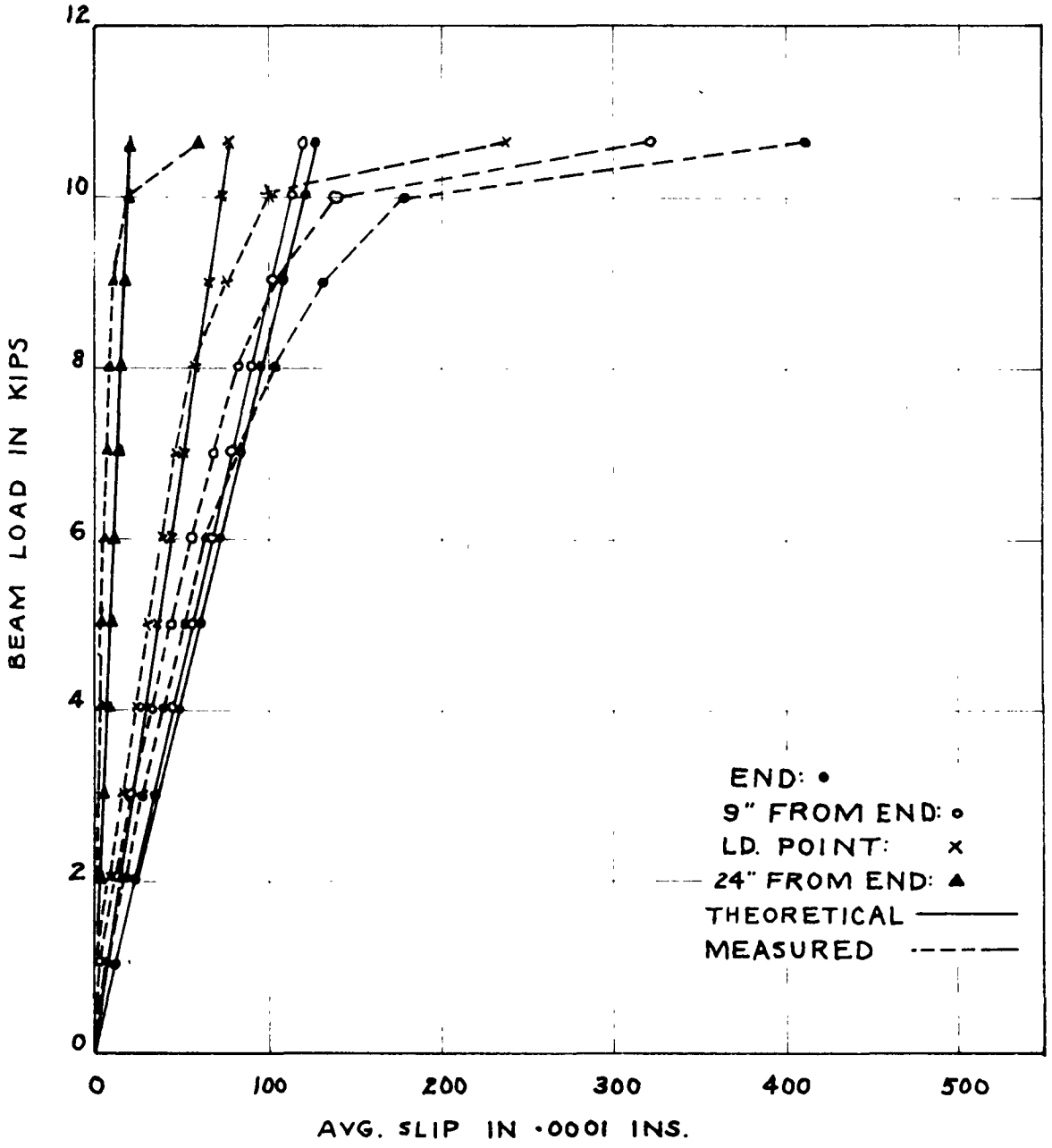

Fig. 4.49 Load-Slip Curves for B3 (Stussi)

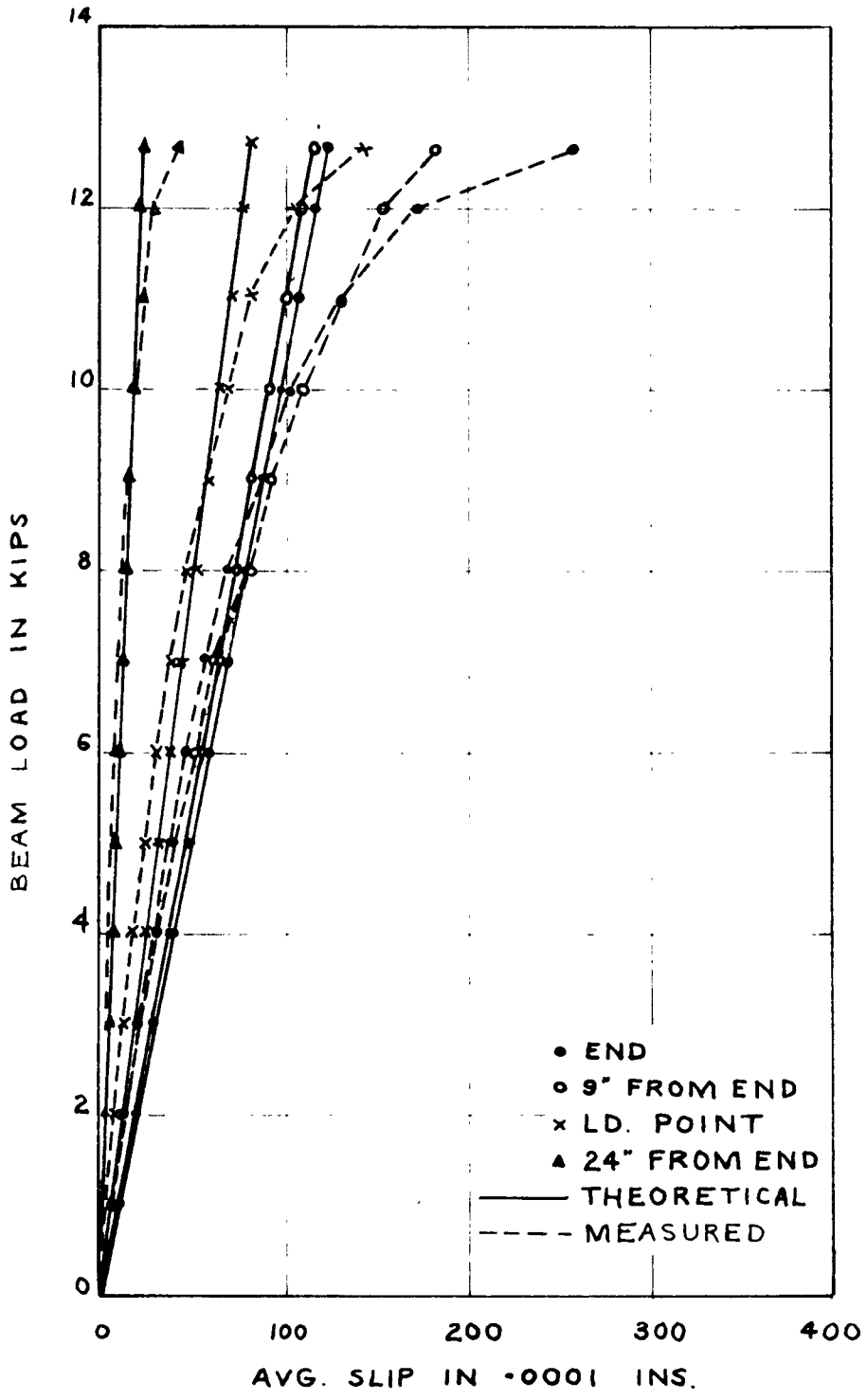

Fig. 4.50 Load-Slip Curves for B4 (Stussi)

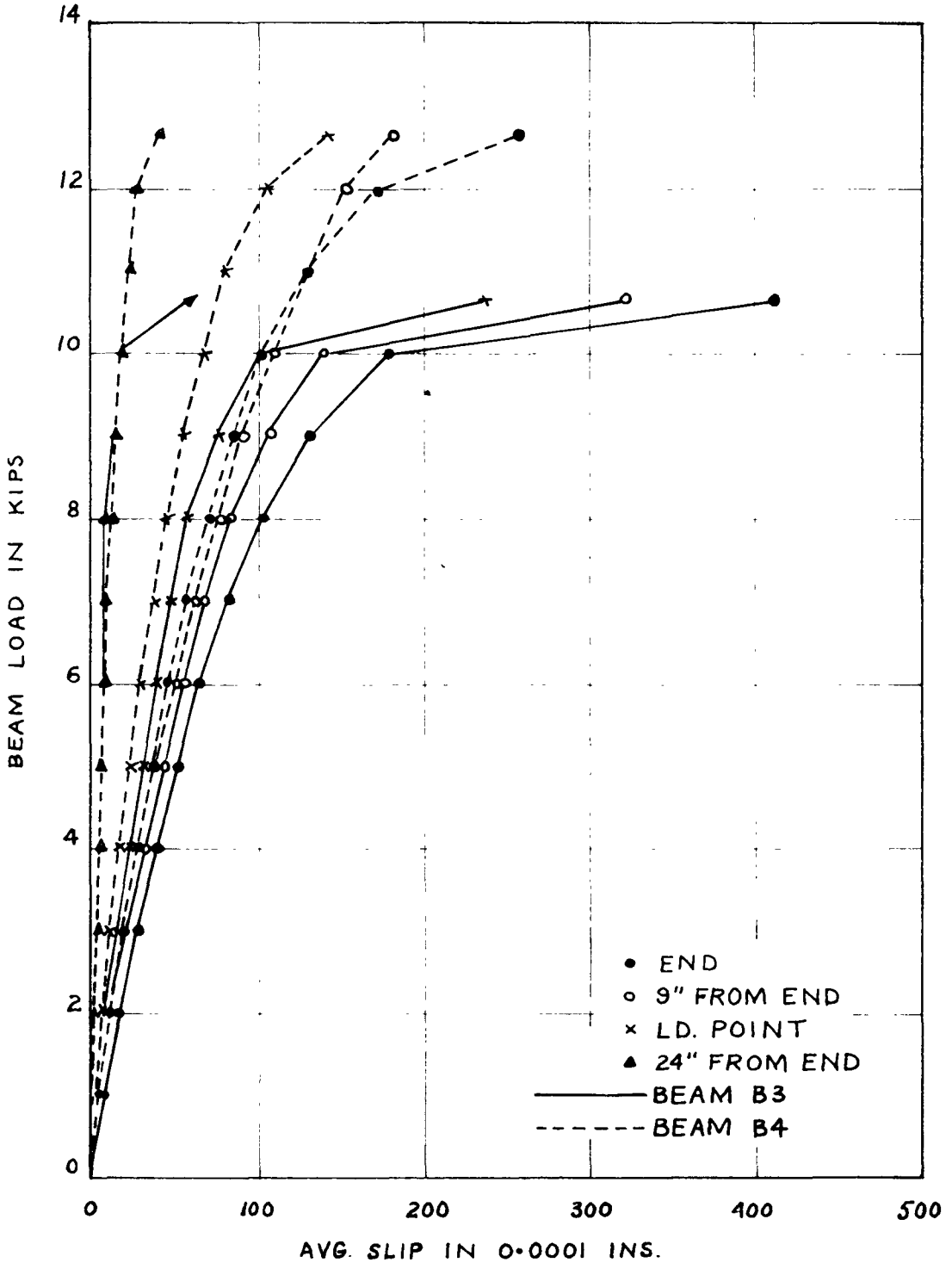

Fig. 4.51 Load-Slip Curves for B3 and B4

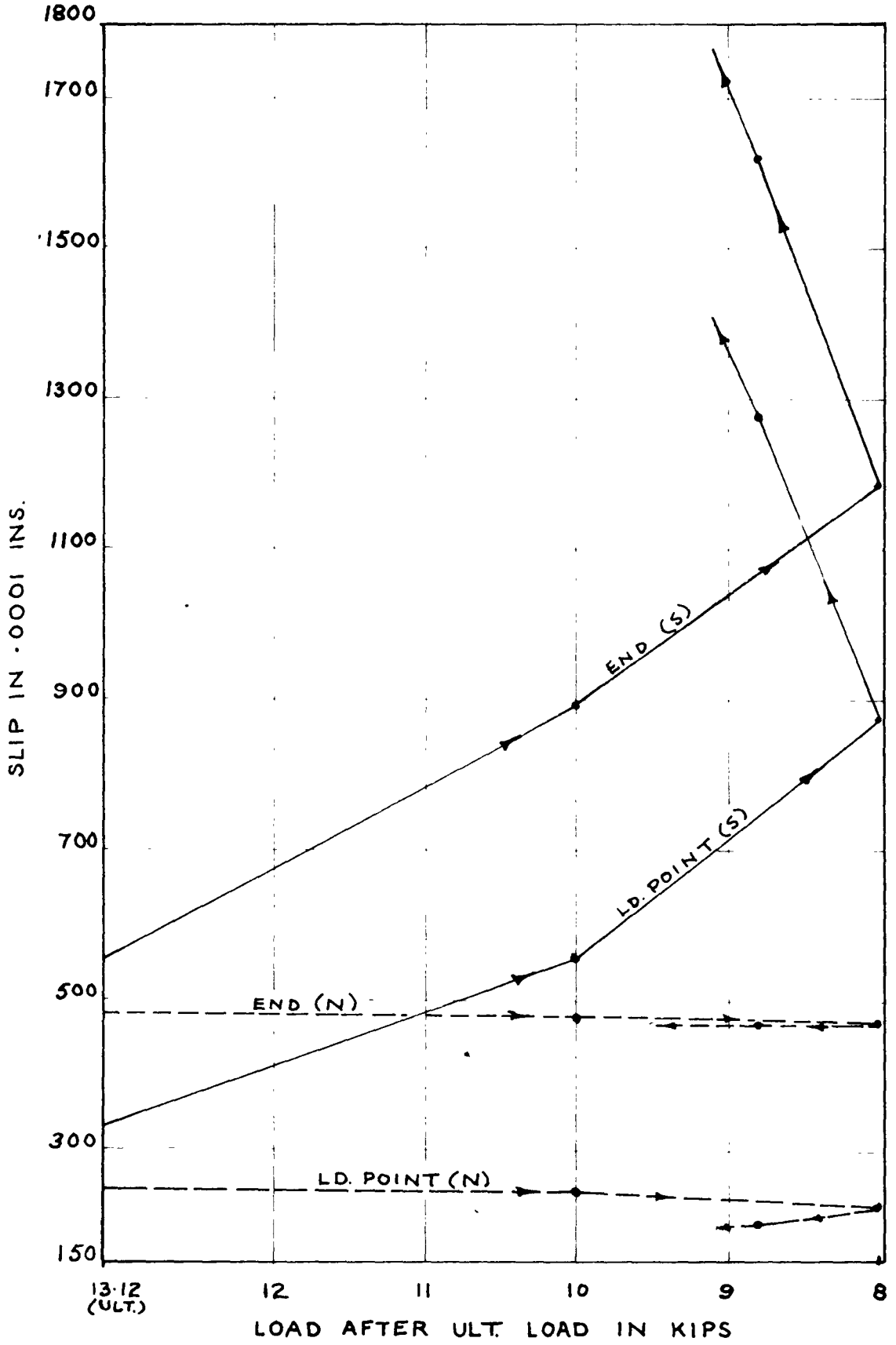

Fig. 4.52 Variation of Slip in B2 after Ultimate Load

CHAPTER 5

DISCUSSION AND SUMMARY

5.1 Discussion

Beam B6 was designed to demonstrate some of the features described in Fig. 2.1. The q/q' curves give an idea of the variation of slip along the length of the beam for different degrees of interaction. Fig. 4.45 shows good agreement with the theoretical slip variations for low degrees of interaction in Fig. 2.1. B6 indicated that for a given applied load there was a reduction in the measured slips as the points of application of the loads moved towards the points of support. As predicted in Fig. 2.1, and shown in Fig. 4.45, the largest slips occurred at the ends of the member and reduced to zero at midspan. This is also borne out in Figs. 5.20 and 5.21 where it is seen that the white rectangular meshes deformed most at the ends of the beam.

1/C values were computed for this beam on the basis of measured end slips in accordance with the Newmark theory[1]. These values ranged between 1.49×10^{-8} and 4.52×10^{-8} when the loads were applied at 12 inches on either side of midspan. This means that there was a very flexible connection in the member. Slips throughout the

length of the beam were then computed using these values of 1/Ç, and the results are shown graphically in Fig. 5.15. In this figure it is seen that between the load points there is good agreement between the computed slips and those measured. However, the theory indicates constant slips in the shear spans. This indication of the theory does not appear to be correct, because during loading the rectangular meshes on the shear connection deformed more at the ends of the beam than in the regions close to the load points in the shear spans. The deformation of the rectangular meshes was interpreted as a reflection of the slip distribution in the member, and therefore indicated that in the shear spans the magnitudes of the slips increased between the load points and the points of support. One reason for the theoretical disagreement in this regard may be that the theory is not suitable for slip computations in the shear spans when there is such a low degree of interaction.

The degree of qualitative agreement, which was obtained between the experimental performances of B6 and those theoretically predicted in Fig. 2.1, leads to the speculation that the Newmark theory also gives a good qualitative description of the behaviour of a simply supported composite beam with uniform loading, and having a very flexible connection. Nevertheless, it would be

best to verify the theoretical predictions of Fig. 2.2 by experimental observations.

An inspection of the load-deflection curves in Figs. 4.9, 4.10, 4.14 and 4.15 and of the load-strain curves in Figs. 4.21, 4.22, 4.24, 4.25, 4.29 and 4.30 reveals that, for analyses of B1 and B3 in accordance with the Newmark theory, better agreement with measured values was obtained with the use of a varying 1/C value than with a constant value of this coefficient. This is to be expected because the varying interaction coefficient provided lower values as the beam degenerated. Nevertheless, it is observed from Figs. 5.13 and 5.14 that even this detailed type of analysis failed to produce good quantitative agreement with measured slips.

In Figs. 5.9 to 5.12 the Newmark theory suggests that the load-slip characteristics may vary markedly for connectors along the length of the beam. If this aspect of the theory is correct, then it is either that the load-slip characteristics of a connector varies greatly with the location of that connector, or that generally there is a weakening of the connectors towards midspan. First of all, it does not seem reasonable that the location of a connector in a simply supported beam should alter its behaviour as significantly as Figs. 5.9 to 5.12 indicate.

Uplift forces did exist in the members tested; and these forces can weaken the shearing resistance of a shear connector. However, the derivation of this theory does not take into account uplift forces and should not, therefore, be expected to reveal the effects of such forces. It is thus thought that the theory does not give a good description of the load-slip characteristics of the shear connectors throughout the beam.

An attempt was made to apply the Newmark theory to beams B2 and B4 by varying the connector spacings in in the equations, since the connectors were not uniformly spaced in these members. After plotting results as shown in Figs. 5.3, 5.4, 5.7 and 5.8, it became clear that the applications were not valid. Some points, which had higher interaction coefficients than other points at a given load level, showed lower connector moduli than these other points at the same load level. In other words, the theory was showing the obvious need for varying the connector moduli proportionately as the spacings. When this was discovered, analysis along this line was discontinued for these members. Consequently, strain, deflection and slip analyses for B2 and B4 could not be based on the Newmark theory, whereas these quantities were validly computed by the Stussi method for these members.

Efficiency curves have been prepared for composite beams utilizing some of the geometric and elastic properties of B1. These efficiencies were based on composite deflections which were computed by the Newmark method of analysis. The curves are shown in Fig. 5.19, and a sample calculation is shown in Appendix A. There is general agreement between these curves and those published by Fazlur R. Khan[7].

5.2 Comparison Between the Newmark and Stussi Theories

Both the Stussi and Newmark theories are elastic theories, and they show good qualitative agreement with measured results in the elastic range for the members tested.

A comparison between the two methods cannot be made for all the members tested. In each beam equal size connectors were used; but there was a variation of the connector spacings in beams B2 and B4, and therefore full analysis only by the Stussi method was possible for these two members.

The load-deflection curves in Figs. 4.9, 4.10, 4.14 and 4.15, and the load-strain curves in Figs. 4.21 to 4.26 and Figs. 4.29 and 4.30 show good quantitative results by both methods for B1 and B3. In the case of B5,

Fig. 4.33 shows that the load-midspan strain curves were coincident for both theories, while in Fig. 4.19 the load-midspan deflection curves show better agreement for the Stussi curve, since this curve lies closer to the measured curve than does the Newmark. Fig. 4.34 shows that the Newmark strain distribution curve for the lower fibre of B5 lies closer to the measured curve than does the Stussi, but that both these theoretical curves coincide at, and close to, midspan.

Figs. 5.16 and 5.17 show slip distribution curves for B1 and B3 at various load levels. These slip computations for each beam were based on a constant connector modulus which was obtained from previous push-out tests. It is seen that the Newmark method produces larger numerical results than does the Stussi theory. A review of Figs. 4.46 and 4.49 would reveal that the Stussi results are larger than those measured; and therefore, it is evident that the Newmark theoretical values are even farther away from the experimental.

Fig. 5.18 shows identical results for both the Stussi and Newmark methods except at the end connections. This figure indicates the theoretical horizontal connector load distribution along beam B5. The Newmark method suggests that there was no load on the end connections of this beam, whereas the Stussi method indicates that large

negative forces were exerted on these connections. Fig. 4.44 shows that large negative end slips were recorded for this member, thus indicating that the Stussi theory gives a more realistic description of the loading of the end connections in an encastré beam than does the Newmark theory.

Generally, the Stussi method of analysis produced better quantitative results than did the Newmark method in the light of observed values.

5.3 Summary

Tests were conducted on six small-scale rectangular composite beams. The object of these tests was to obtain information regarding the suitability of the Newmark and Stussi theories for analyzing composite beams, and also to observe the influence of connector spacing on the overall performance of composite flexural members. All the tests were made with two concentrated loads applied to the slab component symmetrically about midspan, except in the case of beam B5 where a single concentrated load was applied at midspan.

There was generally good agreement between experimental observations and theoretical predictions. In addition, it was observed that connector spacing does have a significant effect on the behaviour of composite beams..

The beams tested had flexible connectors, and it is recognized that the results obtained from these tests cannot be applied directly to full-size beams with stiff connectors. There are indications that beams with stiff connections behave in a somewhat different manner from the predictions of the Newmark and Stussi theories. For instance, composite beams with stiff connections tested by Chapman[6] revealed slip distribution profiles which are different from those obtained by analyses in accordance with the Newmark and Stussi theories. Perhaps more parameters would have to be introduced into these theories when they are applied to composite beams with stiff connections. However, it can be said that these theories do provide a good description of the behaviour of composite beams with flexible connectors.

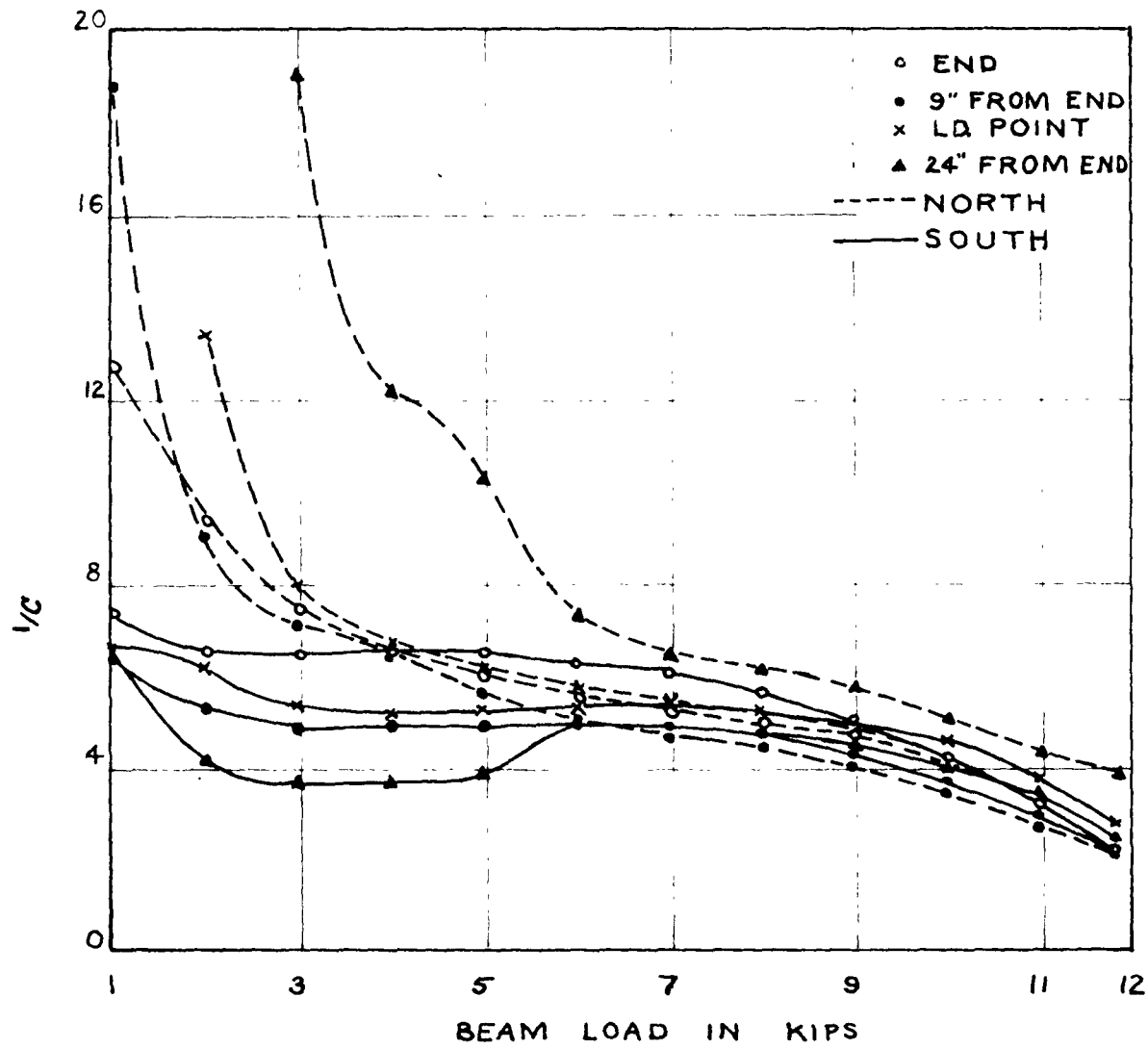

Fig. 5.1 Variation of 1/C in Beam B1

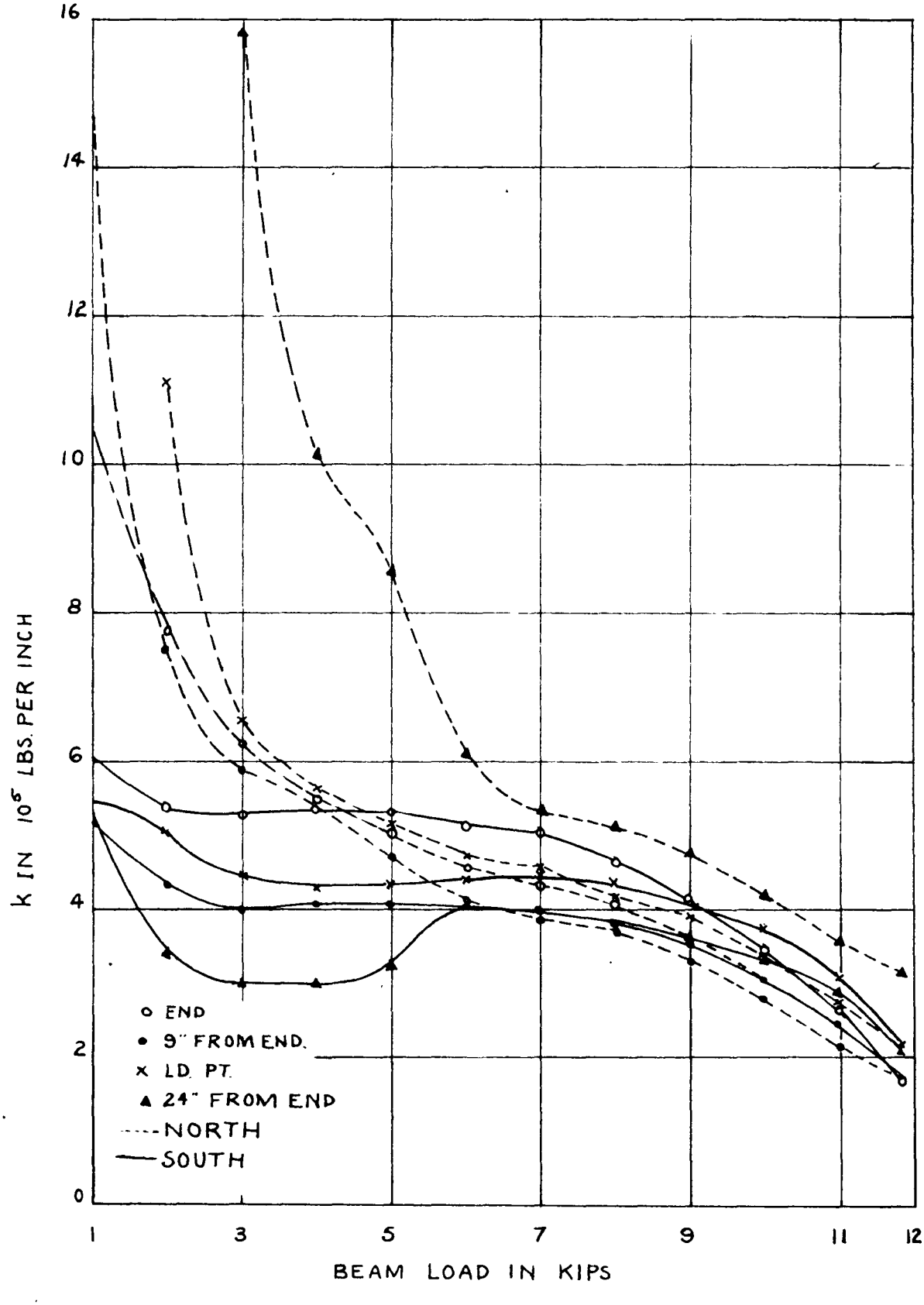

Fig. 5.2 Variation of k in Beam B1

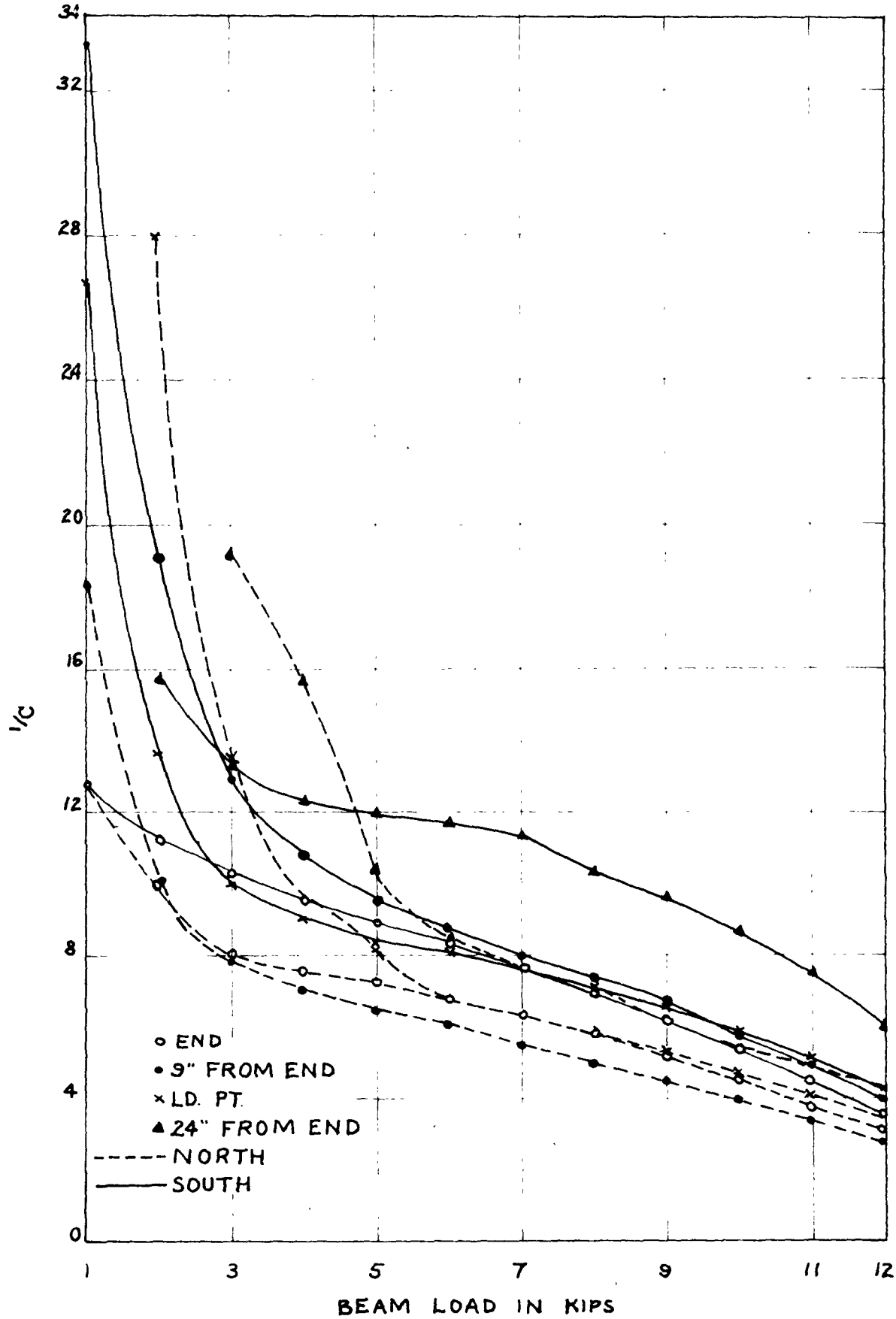

Fig. 5.3 Variation of 1/C in Beam B2

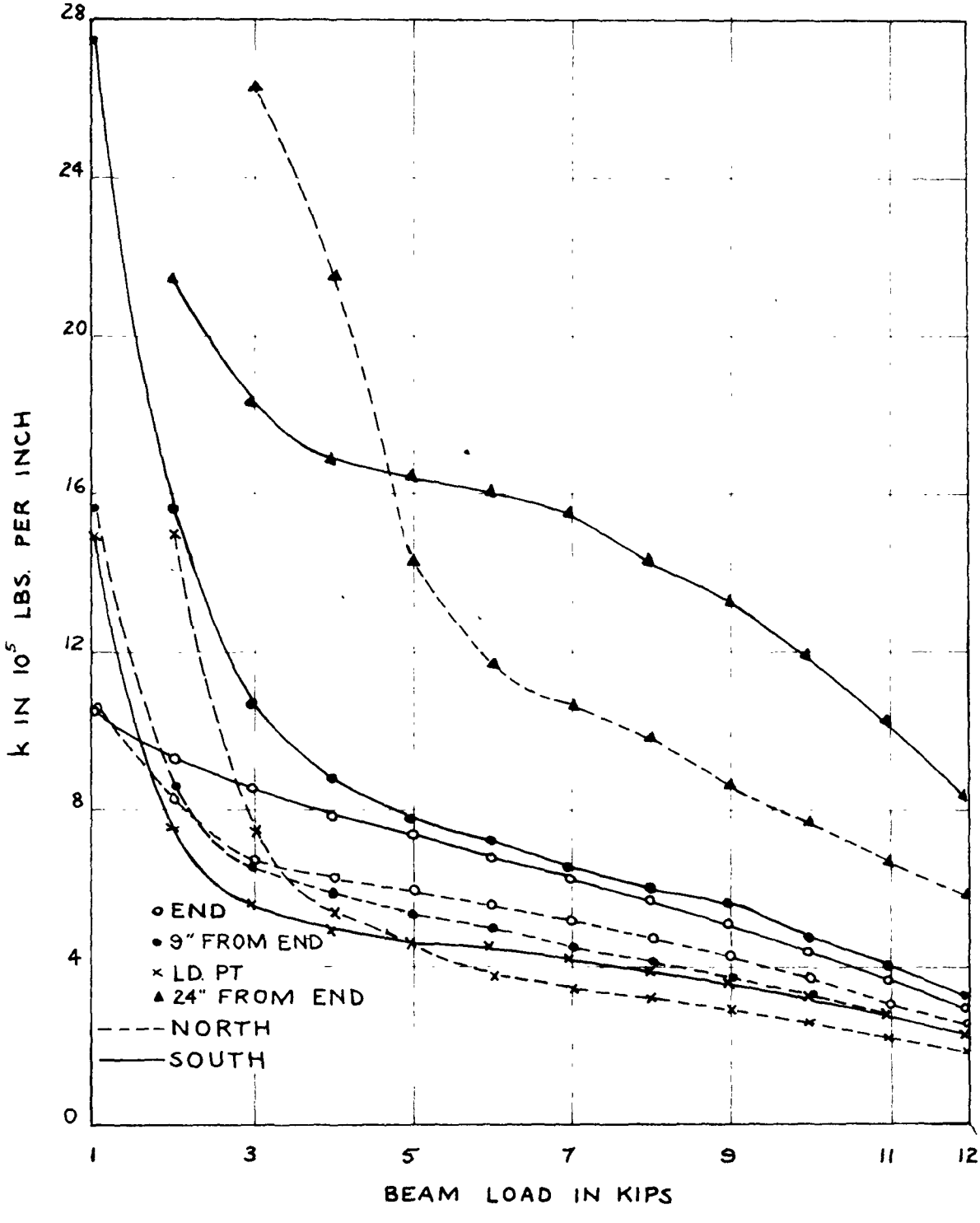

Fig. 5.4 Variation of k in Beam B2

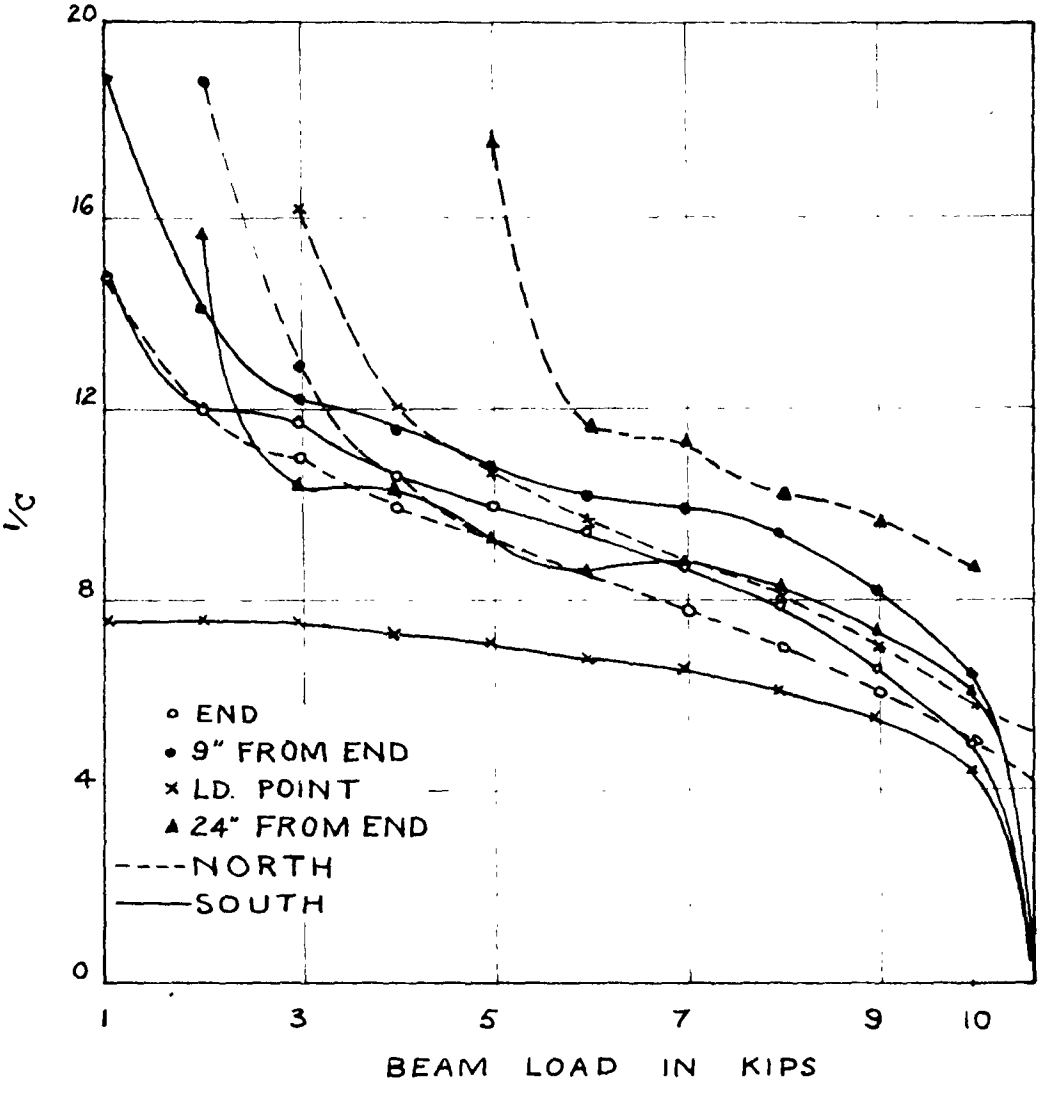

Fig. 5.5 Variation of 1/C in Beam B3

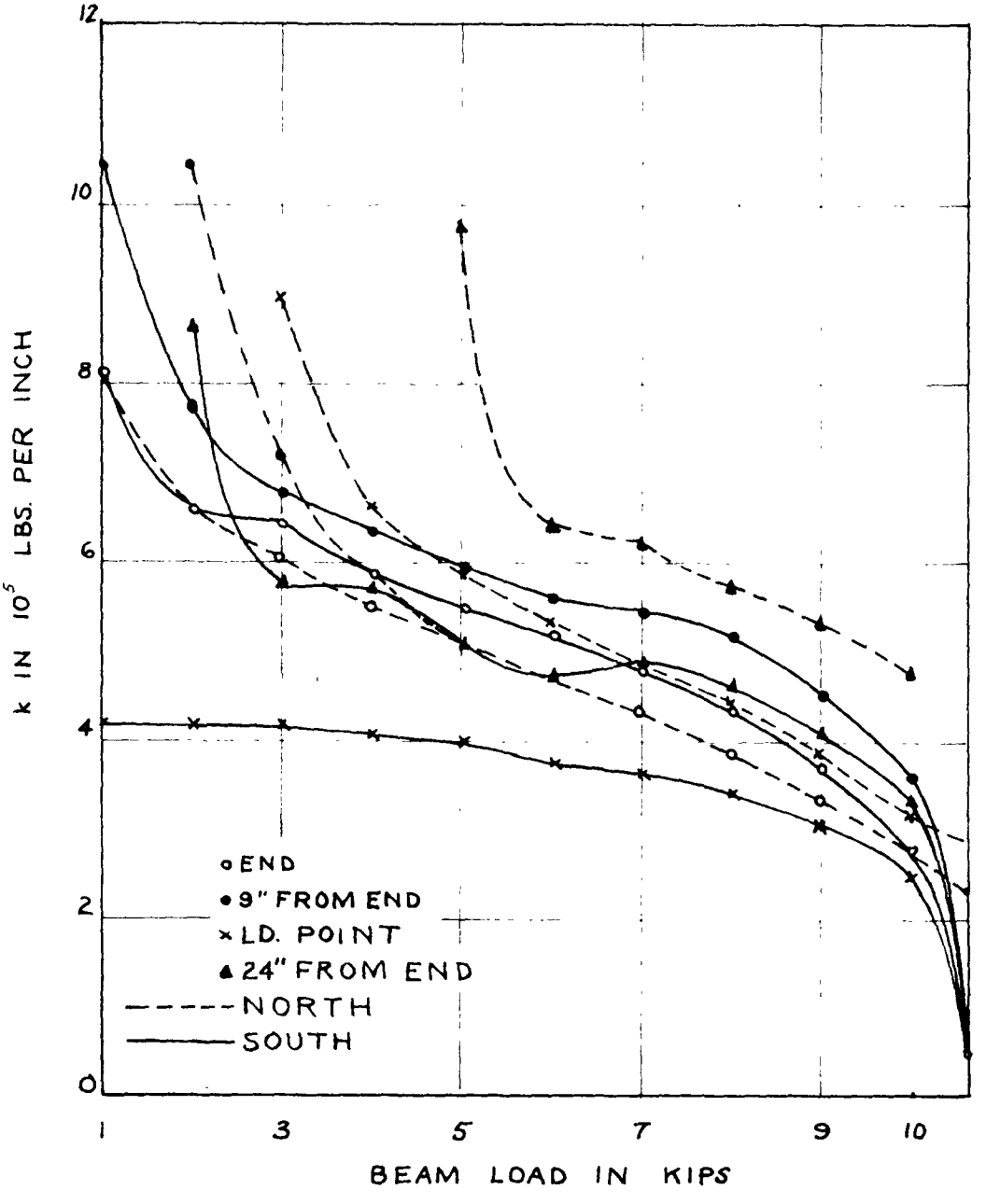

Fig. 5.6 Variation of k in Beam B3

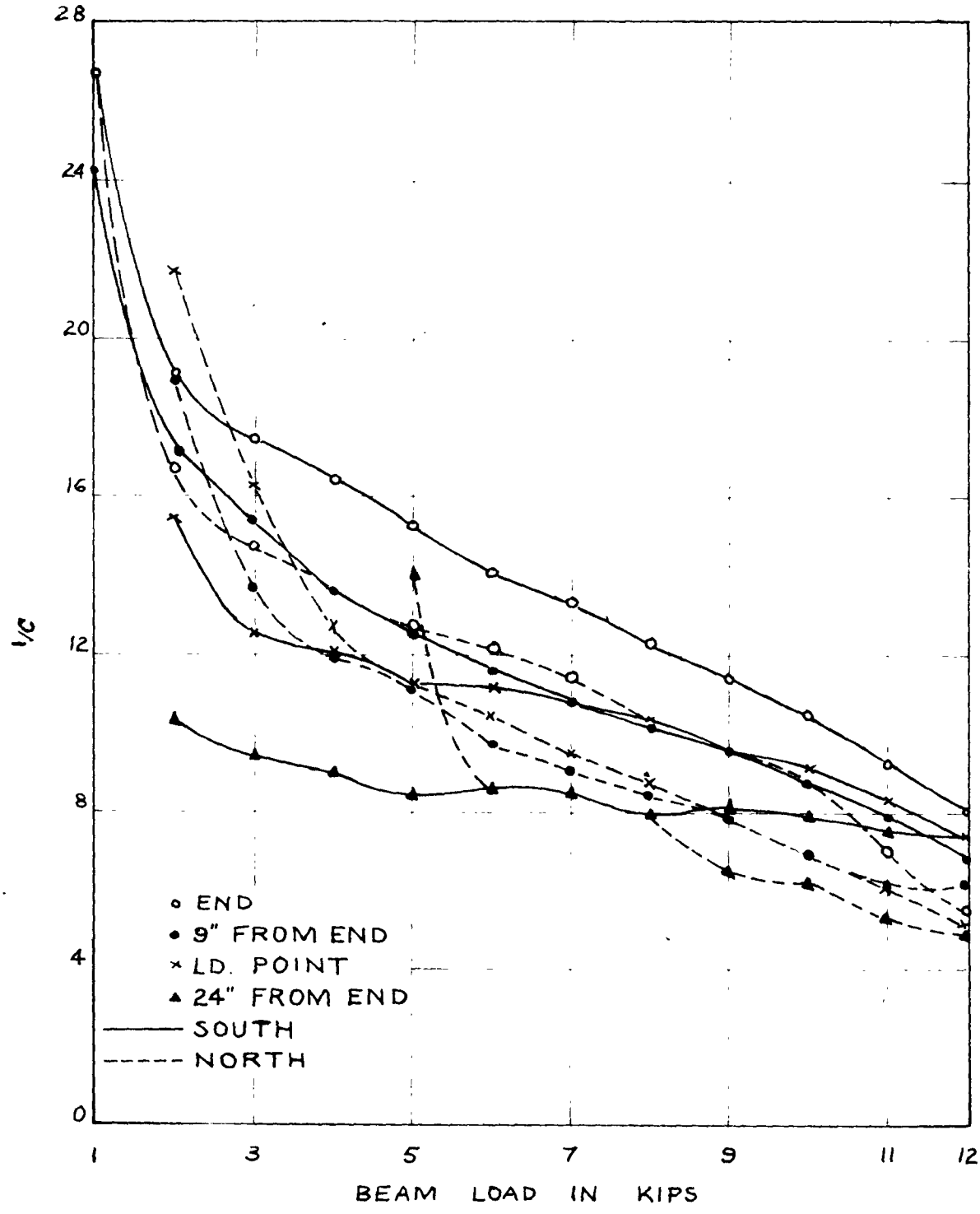

Fig. 5.7 Variation of 1/C in Beam B4

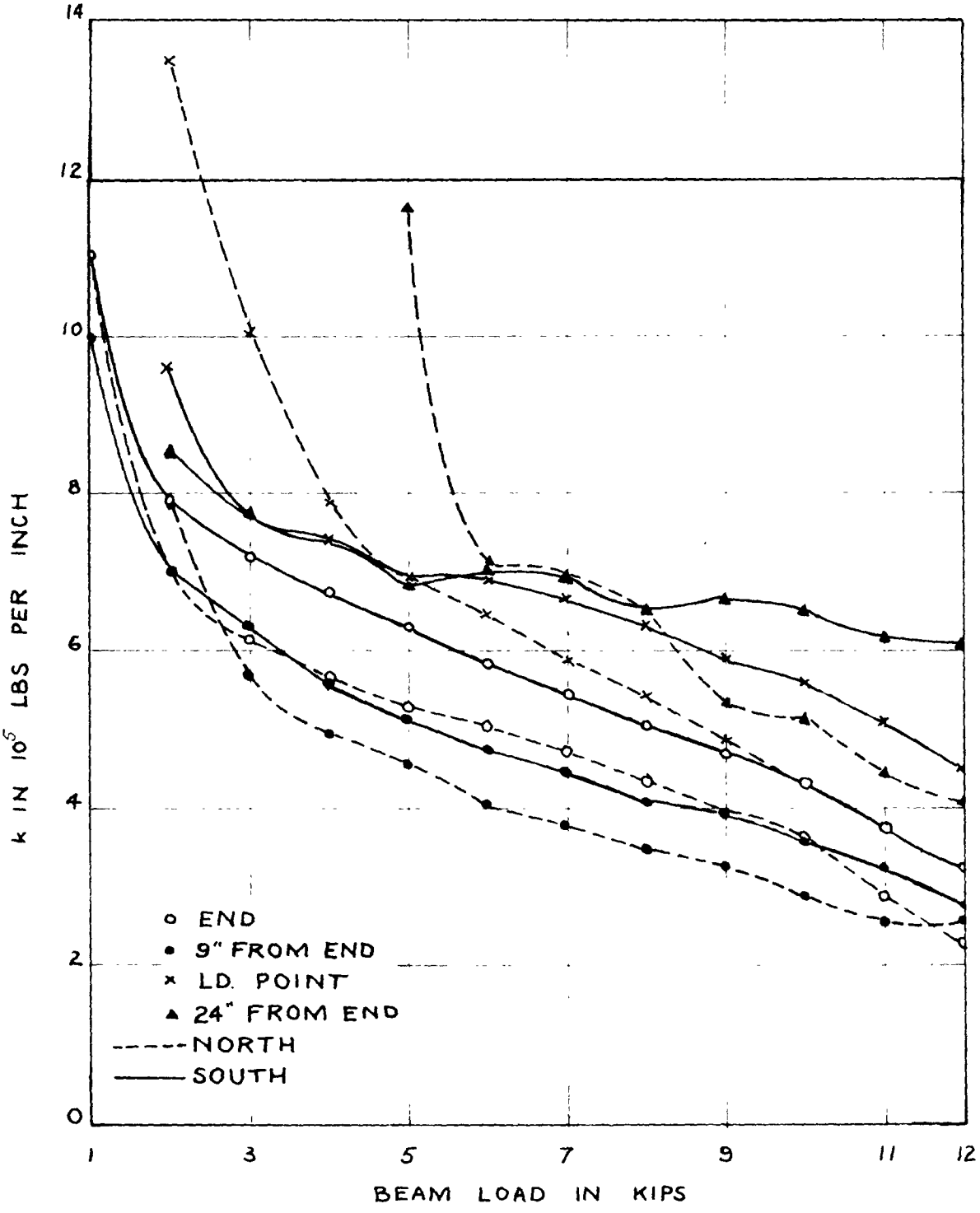

Fig. 5.8 Variation of k in Beam B4

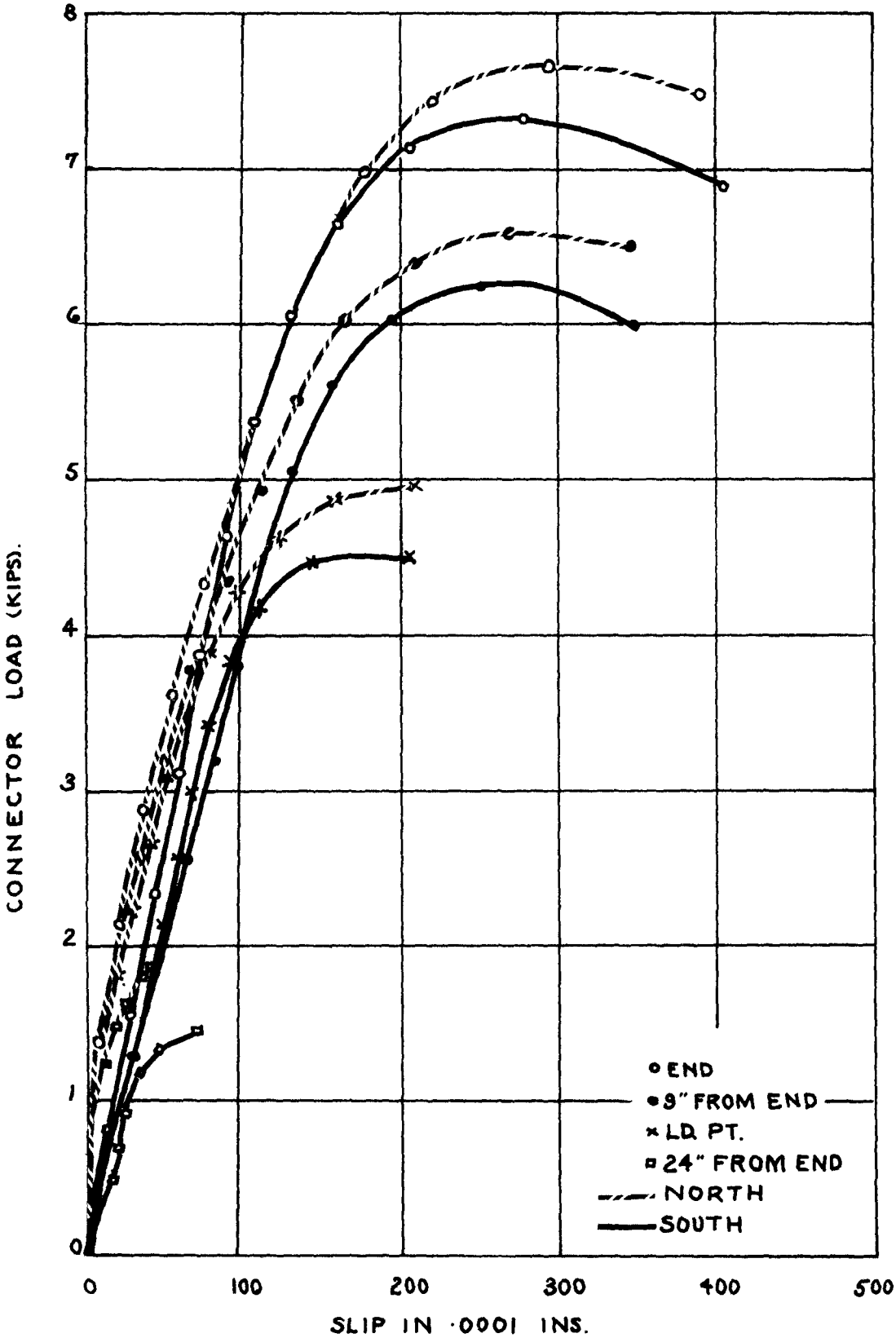

Fig. 5.9 Load-Slip Curves for Connectors in Beam B1 (Newmark)

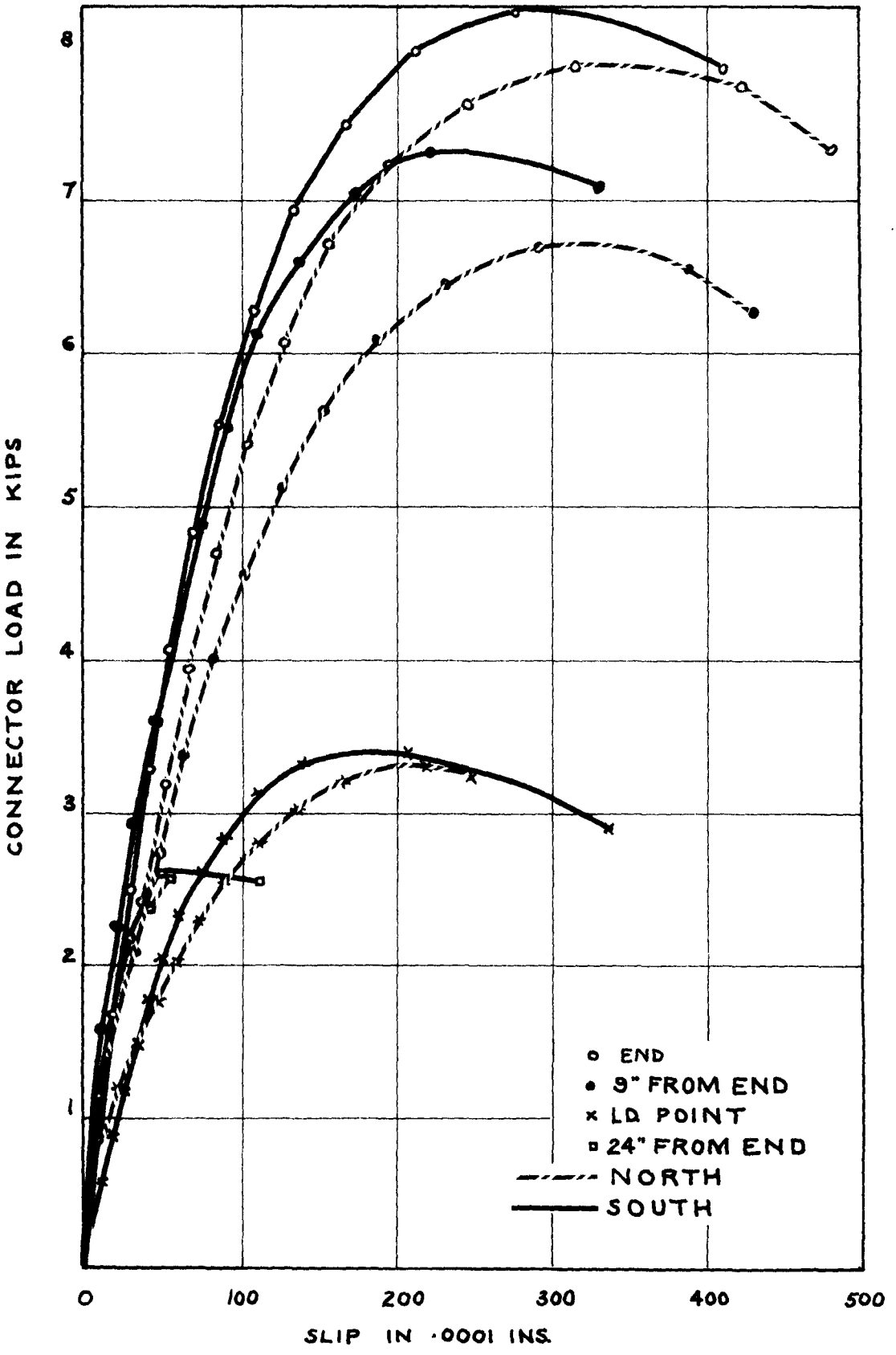

Fig. 5.10 Load-Slip Curves for Connectors in Beam B2 (Newmark)

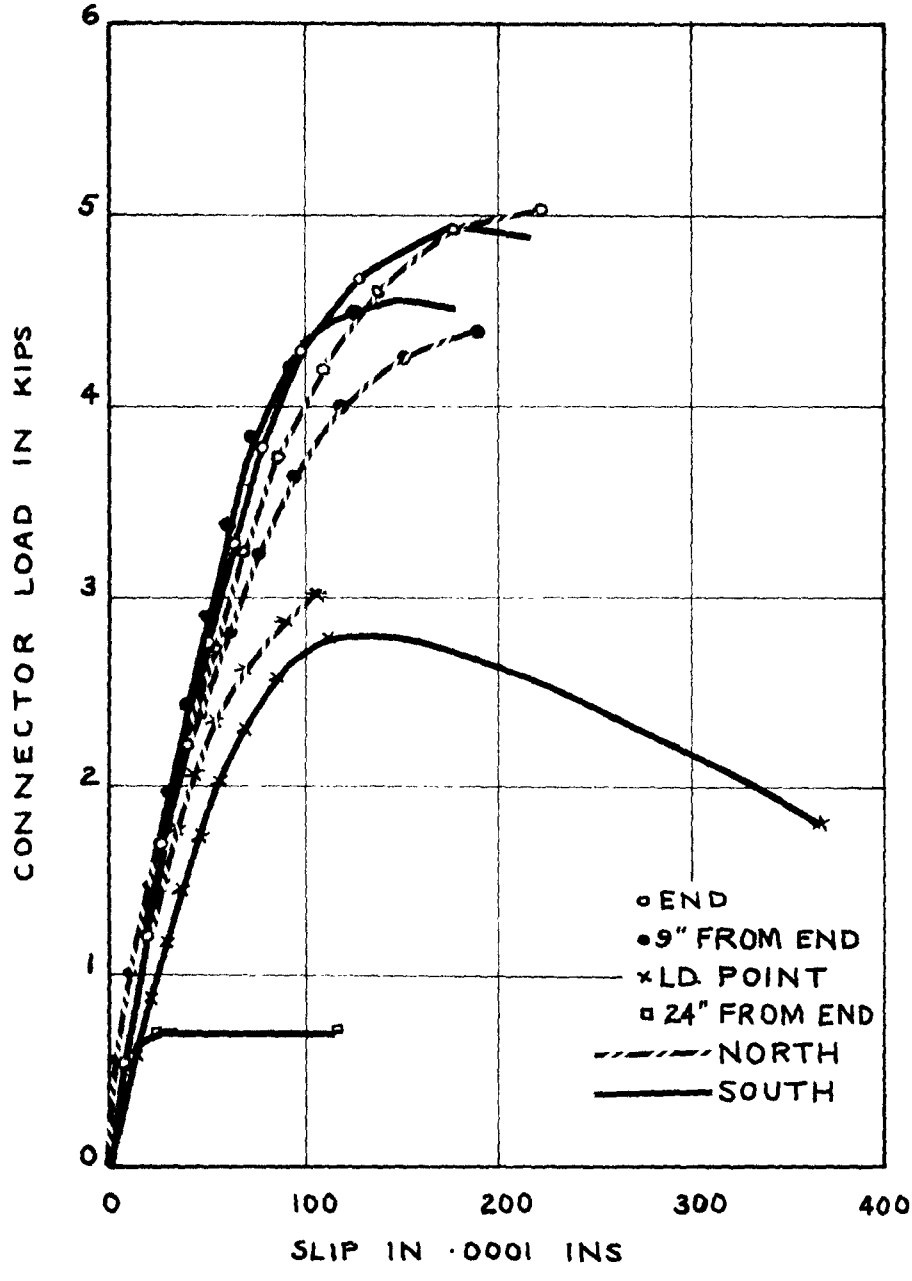

Fig. 5.11 Load-Slip Curves for Connectors in Beam B3 (Newmark)

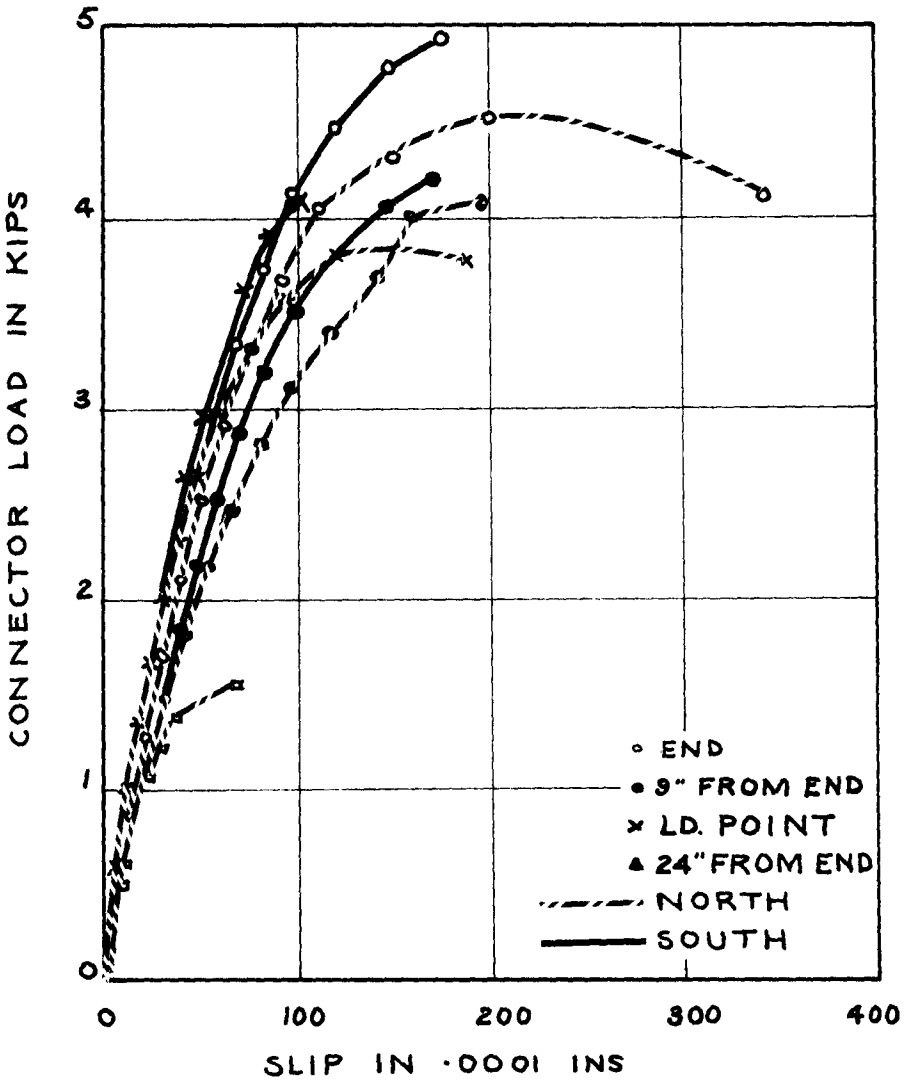

Fig. 5.12 Load-Slip Curves for Connectors in Beam B4 (Newmark)

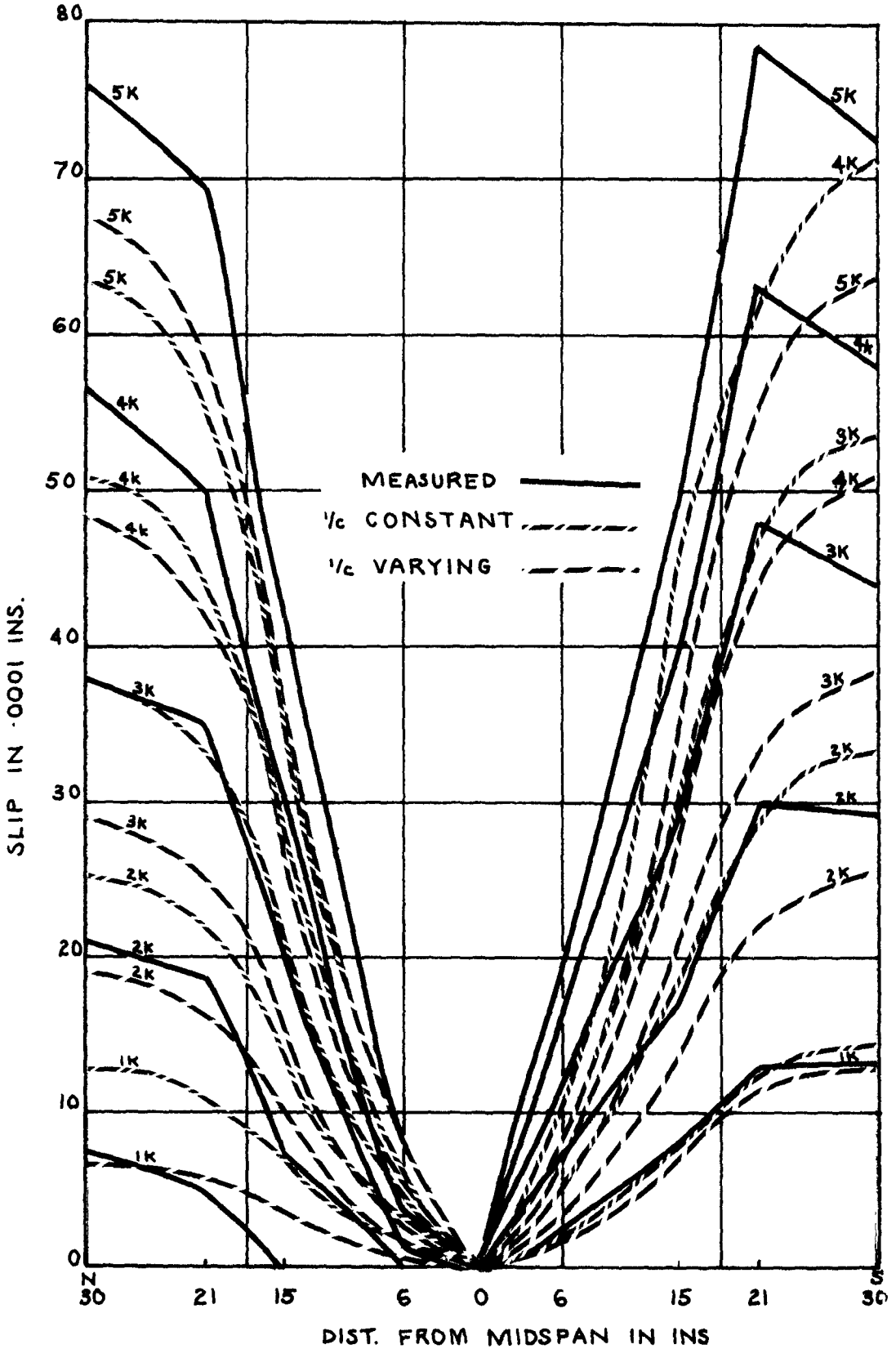

Fig. 5.13 Slip Distribution for Beam B1 (Newmark)

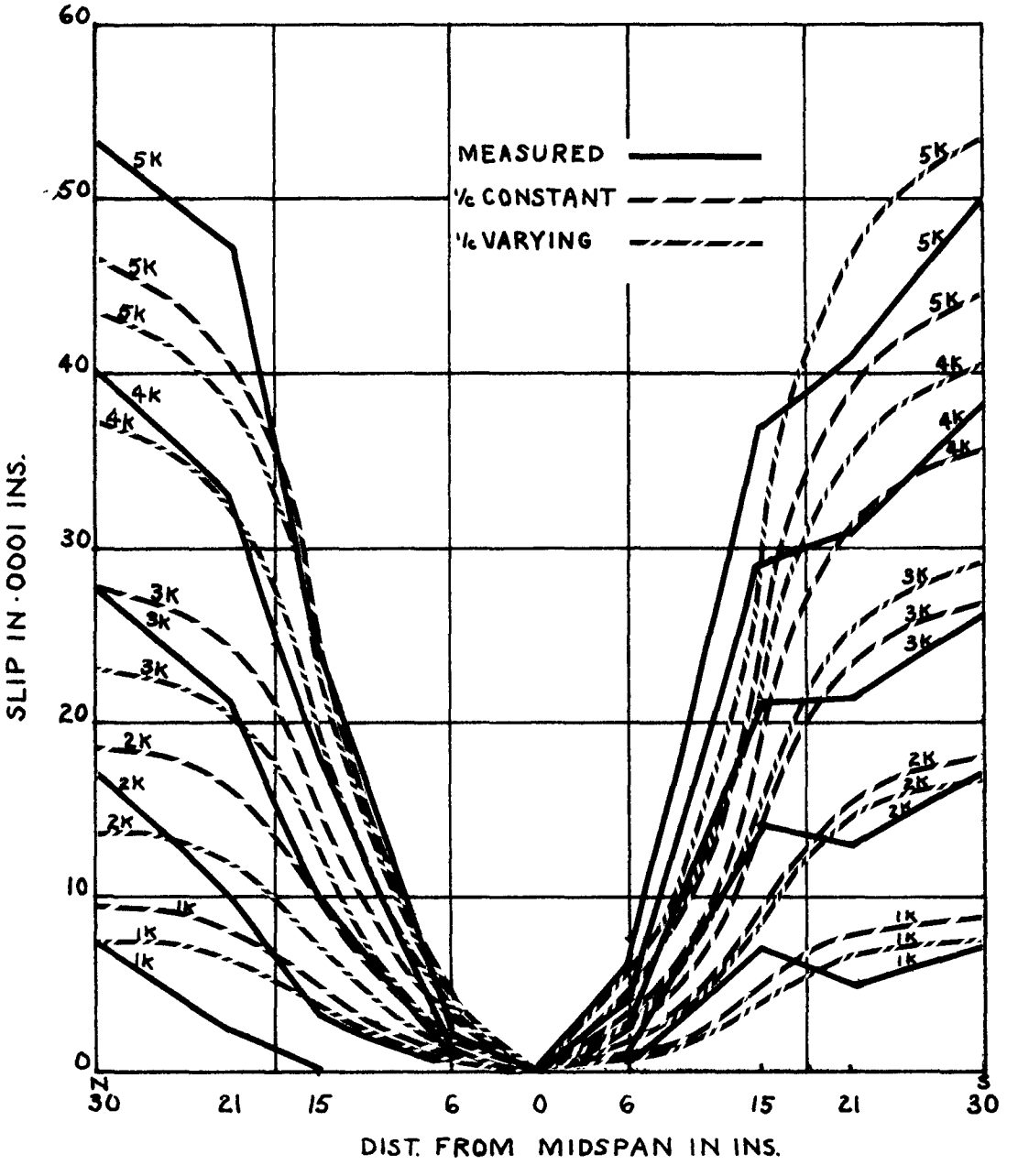

Fig. 5.14 Slip Distribution for Beam B3 (Newmark)

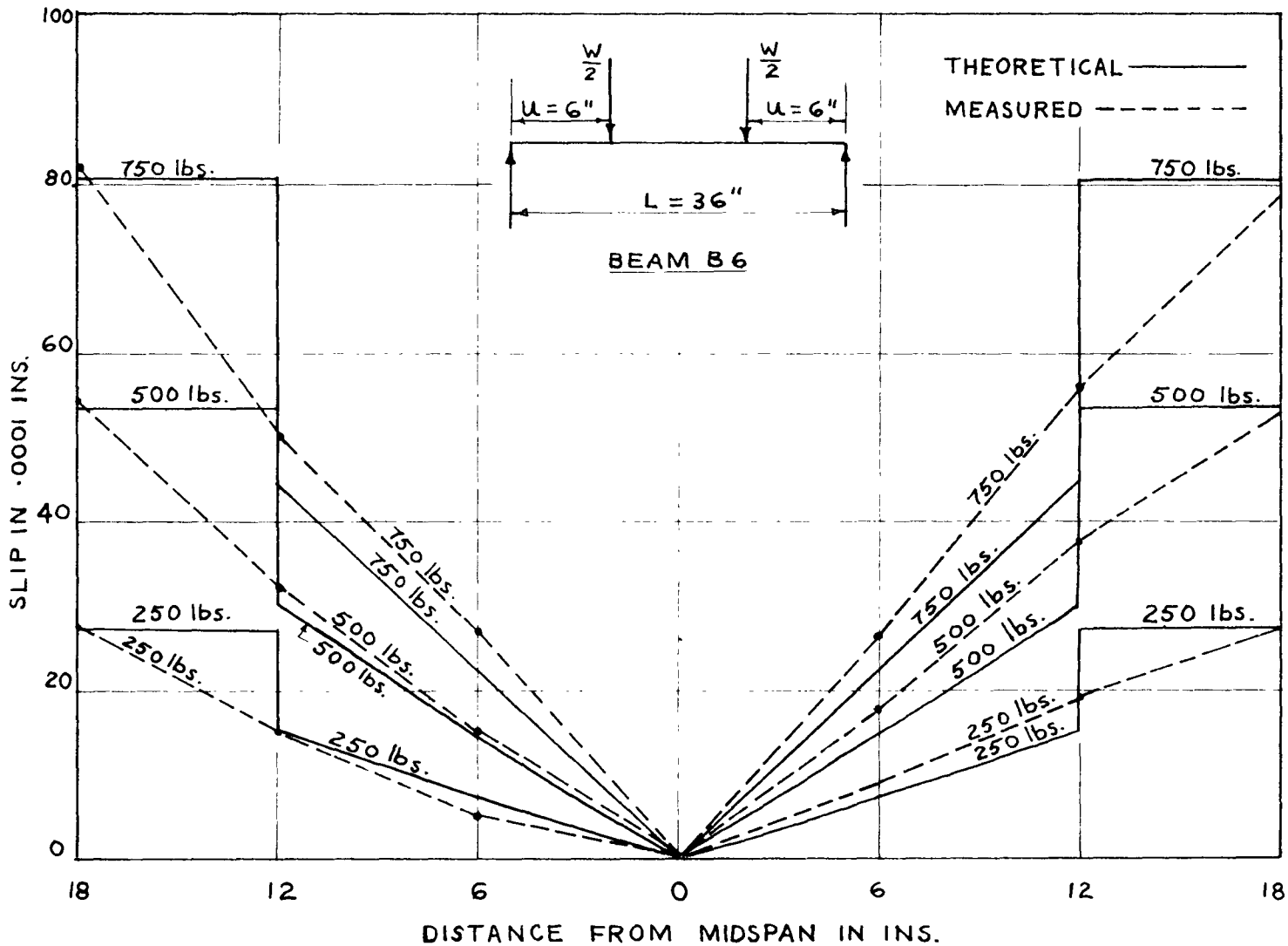

Fig. 5.15 Slip Distribution for Beam B6 (Newmark)

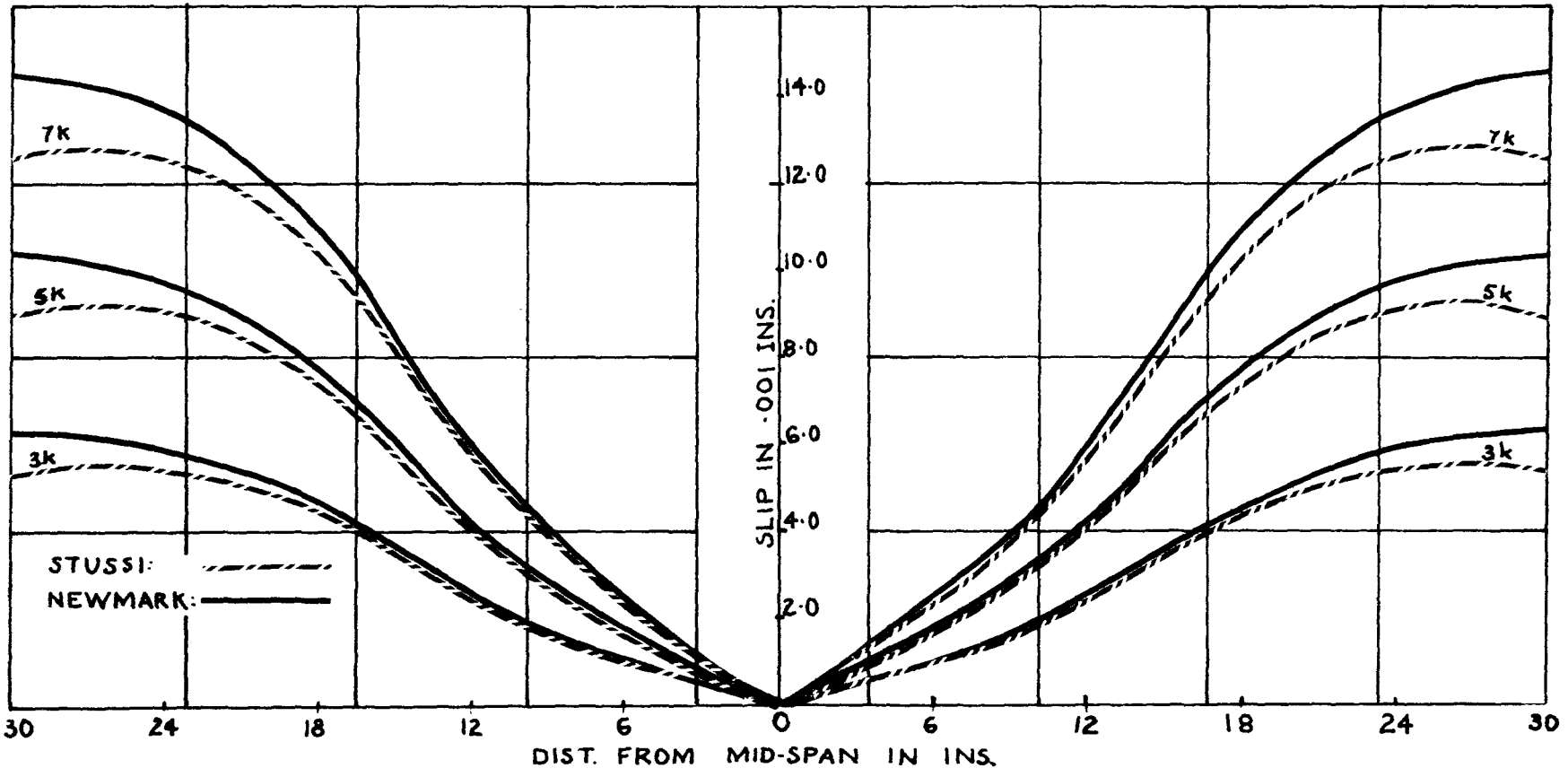

Fig. 5.16 Slip Distribution Curves for Beam B1

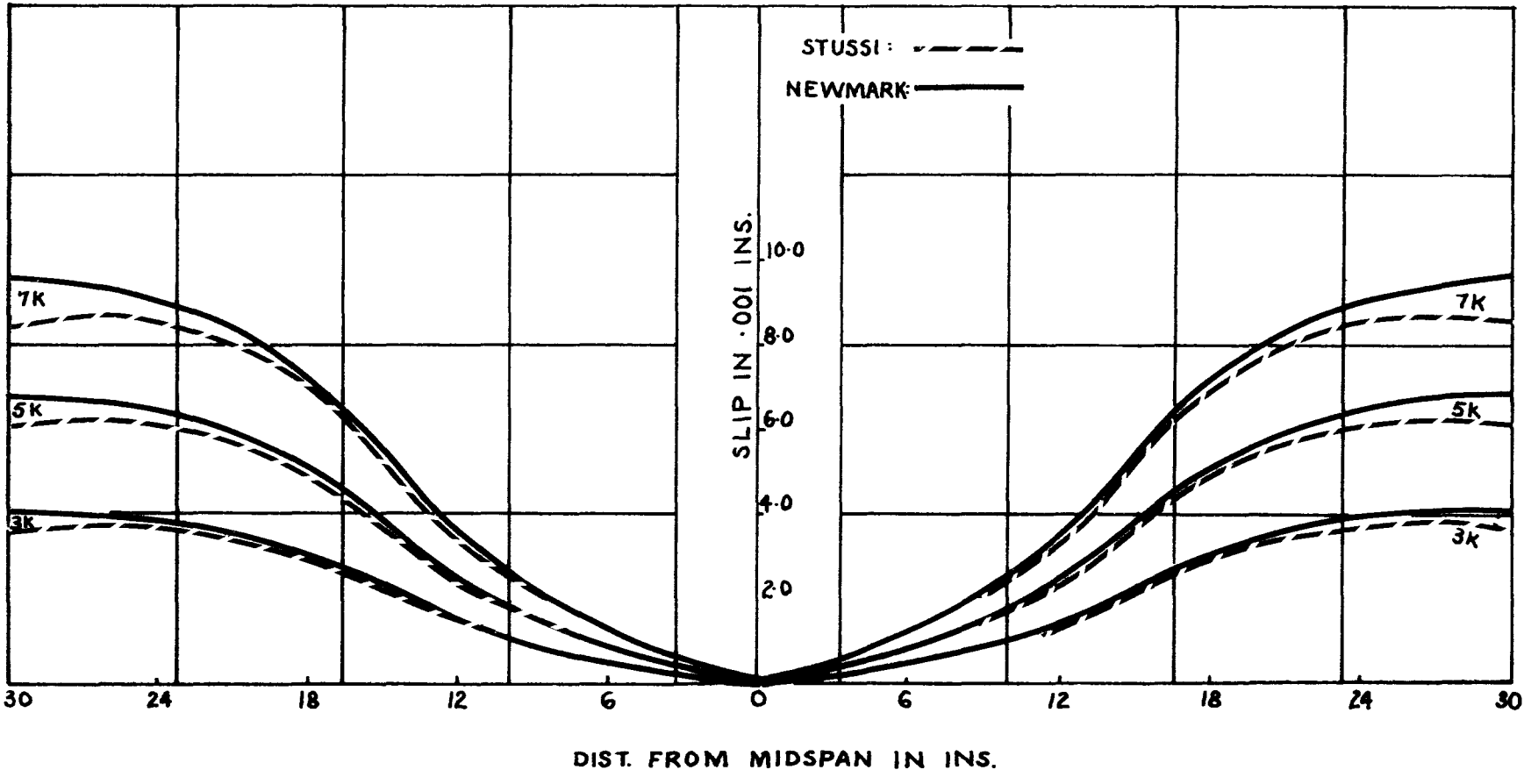

Fig. 5.17 Slip Distribution Curves for Beam B3

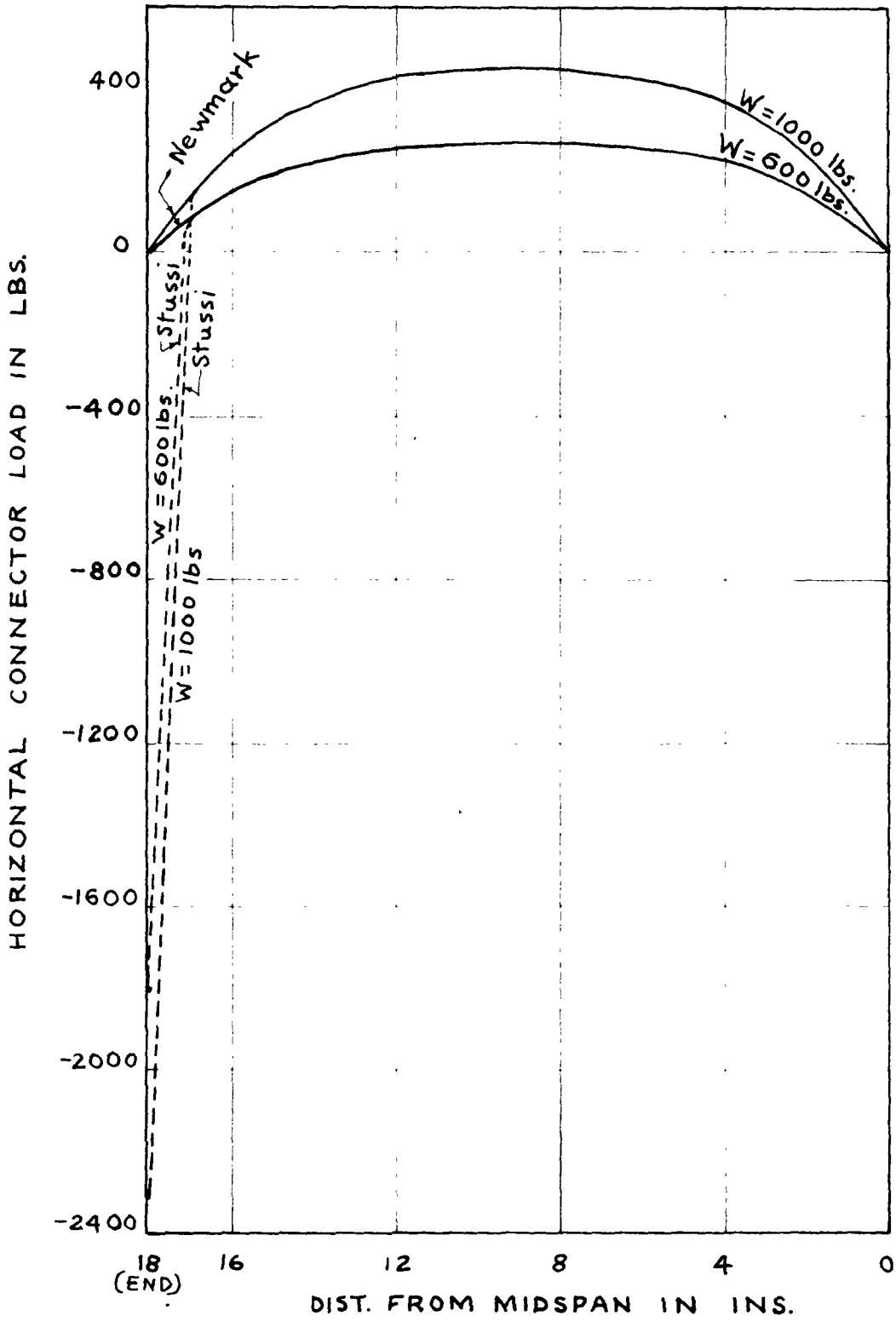

Fig. 5.18 Variation of Connector Load in Beam B5

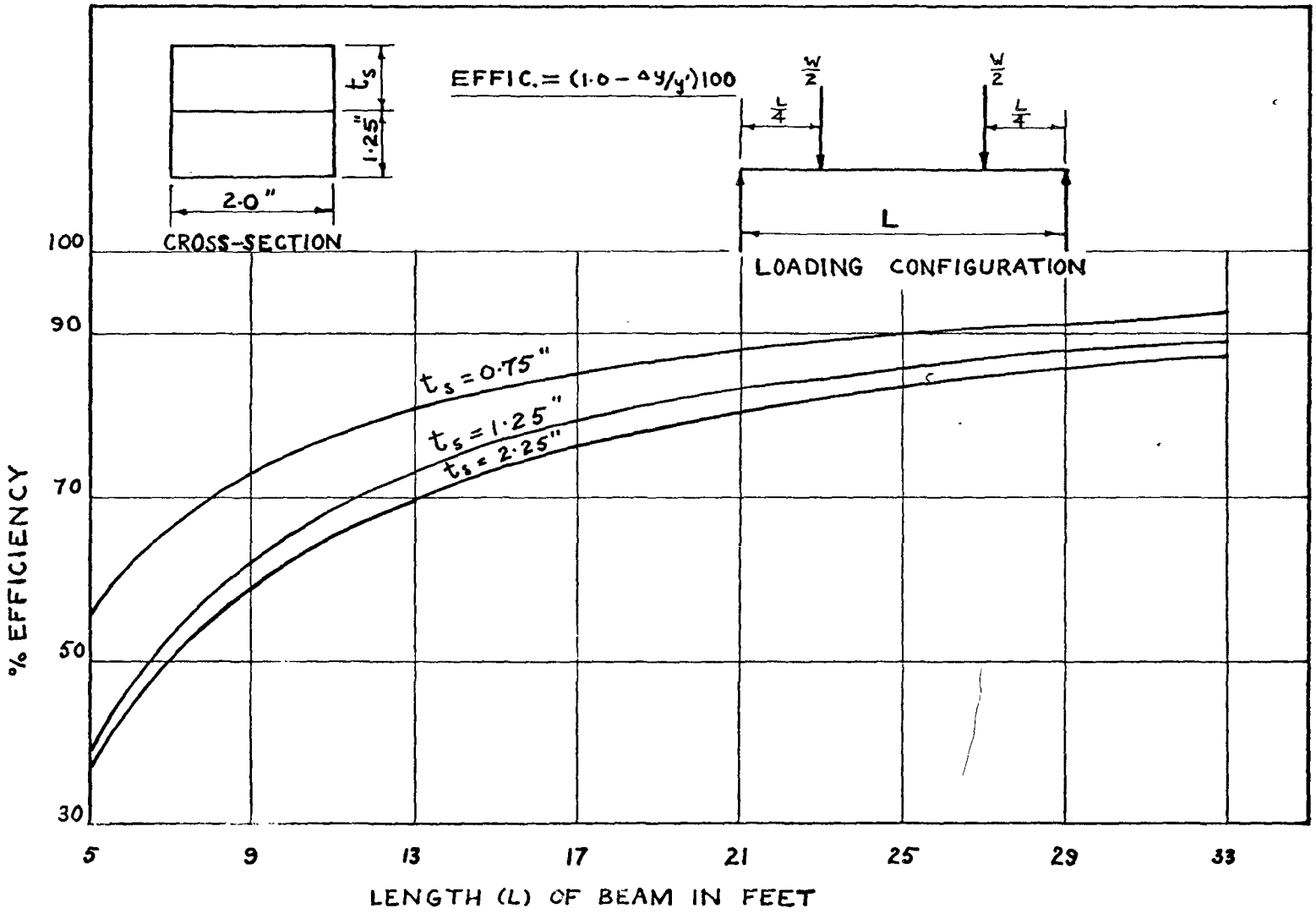

Fig. 5.19 Efficiency [illegible] Composite Beams (Based on Defln. Calculations)

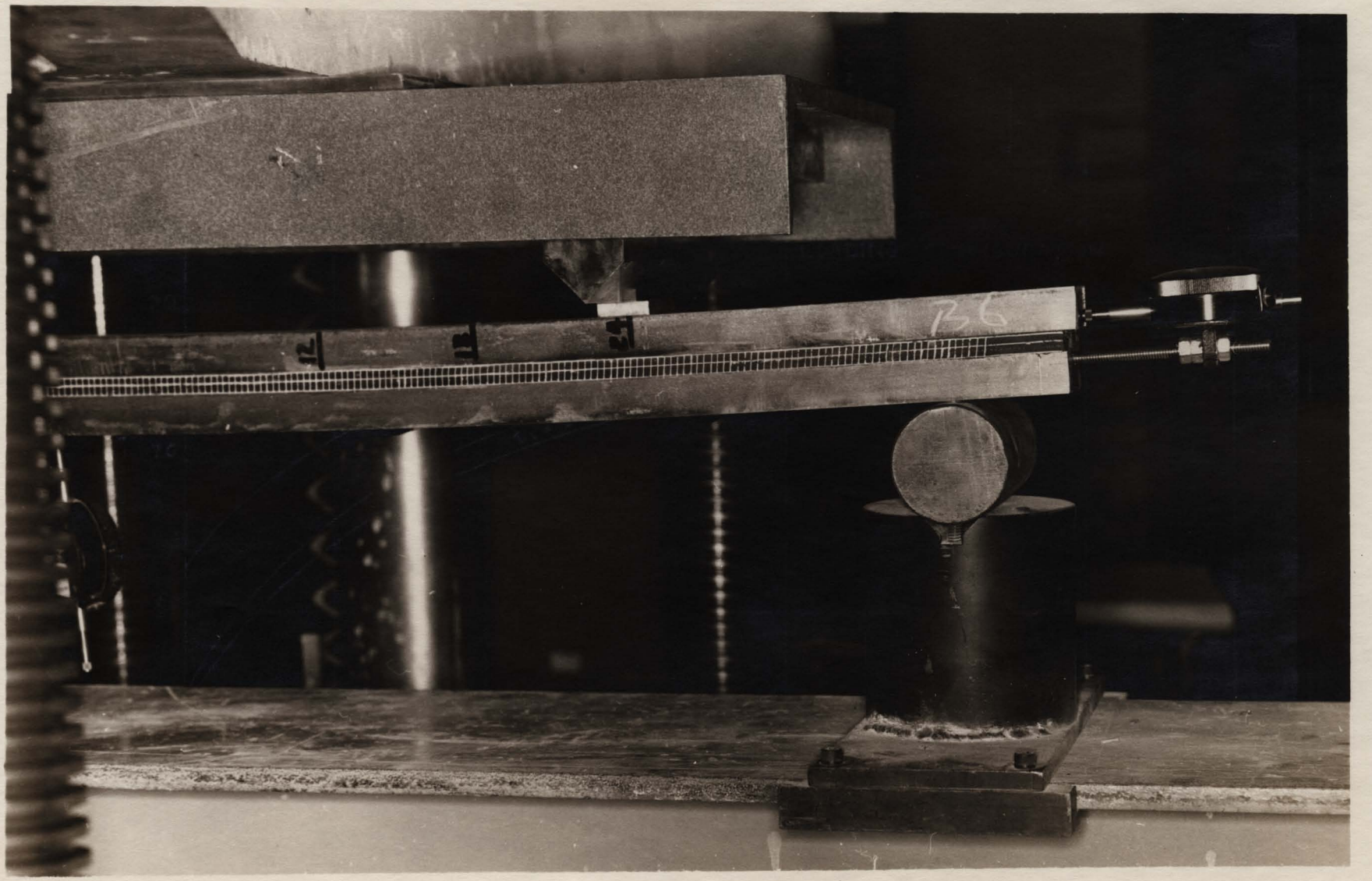

Fig. 5.20 Deformed Position of B6 at 1,000 lb. Load Level

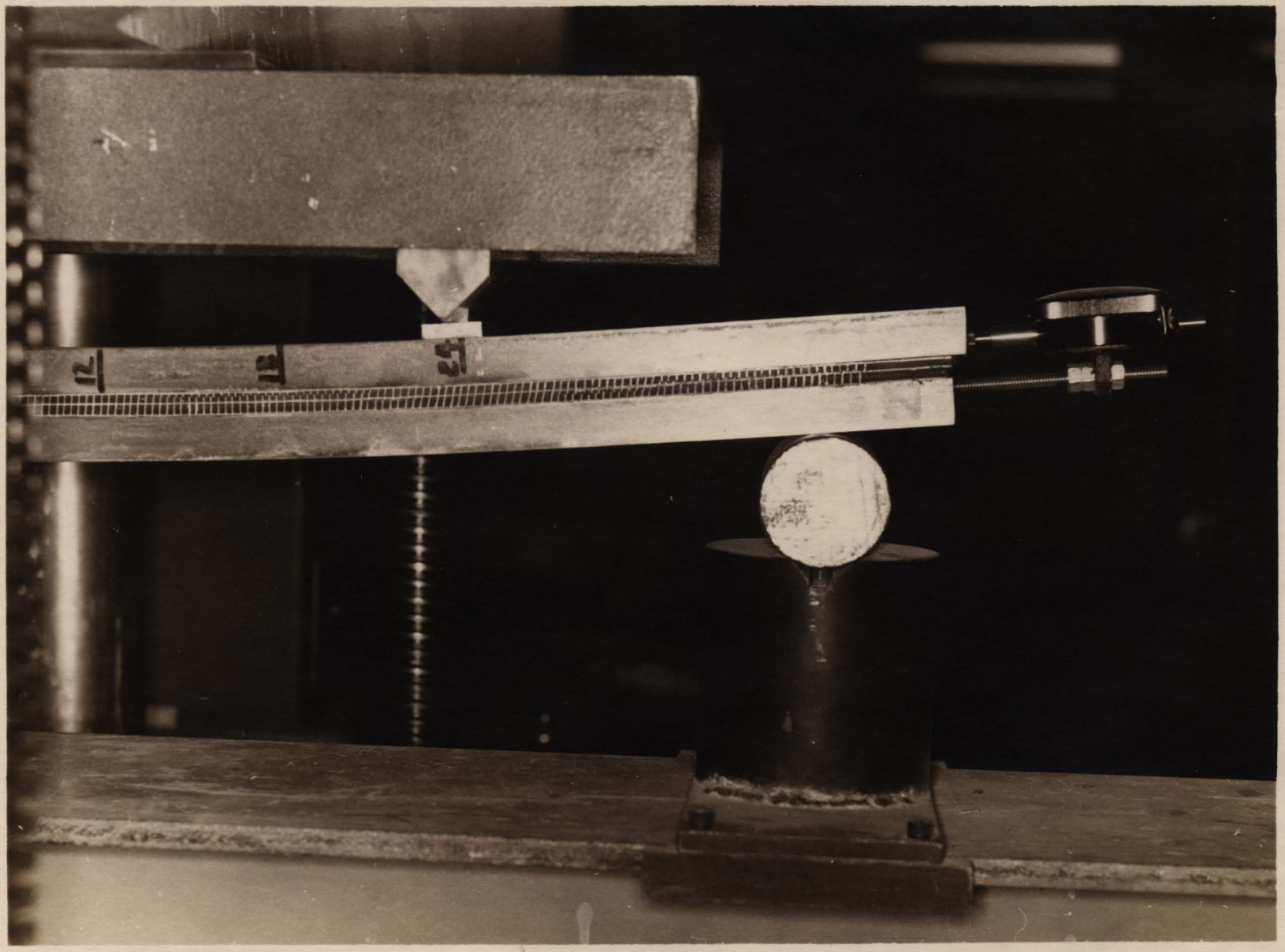

Fig. 5.21 Deformed Position of B6 at 9,000 lb. Load Level

CHAPTER 6

CONCLUSIONS AND RECOMMENDATIONS

6.1 Conclusions From Tests on Composite Beams

The conclusions which follow are based on the data obtained from the six beams tested.

1. The Newmark theory in its present form does not give a true account of the load-slip characteristics of the shear connectors throughout the beam.
2. Better load-slip performances are obtained in beam tests than in push-out tests for shear connectors.
3. Both the Stussi and Newmark theories give a good qualitative description of the behaviour of a composite beam in the elastic range.
4. The Stussi method gives a better quantitative account of the behaviour of a flexural composite member with flexible connections than does the Newmark method.
5. The Newmark theory is strictly applicable to the case of uniformly spaced connectors when connectors of equal capacity are used in the

composite beam. However, the Stussi approach is suitable also for variation of connector spacing. Generally, it can be said that the Stussi method is preferable to that of Newmark for the analysis of composite beams with flexible connections.

6. For a two-point loaded, simply supported beam where equal capacity connectors are used, a connector spacing arrangement based on the conventional shear force diagram appears to be the best of the three arrangements used in this investigation.
7. The composite behaviour of a simply supported beam with a two-point loading is a function of the load position.
8. The Newmark and Stussi methods of analysis are applicable to an encastré beam.

6.2 Recommendations for Future Studies

a) It is clear from the tests that uplift forces do exist in a composite flexural member, and that these forces do affect the behaviour of the beam. In order to make more accurate predictions of composite behaviour in beams, it would be necessary to have some idea of

the variation of uplift forces in these members. Therefore, it would be of advantage if future tests are conducted to study the magnitude and variation of such forces.

b) Theoretical predictions of the behaviour of composite beams with uniformly distributed loading are given in Fig. 2.2. Tests should be carried out on simply supported members with very flexible connections and bearing uniformly distributed loads to see what agreement would be obtained with the theory.

c) It is suggested that more detailed experiments be carried out on encastré beams. Care should be taken to improve the conditions of end fixity; and more slip and deflection measurements should be taken along such beams.

APPENDIX A

The notation in the Appendix is also the notation of the thesis.

A.1 Notation

The subscripts used with the notation of this Appendix have the following meaning:

b = beam component

t = slab component

L = section to the left of the point of application of the load

R = section to the right of the point of application of the load

Primed symbols indicate values for composite beam with complete interaction.

The following symbols have been adopted for use in this Appendix:

A_t, A_b	=	cross-sectional areas of the beam and slab components respectively.
c_t, c_b	=	distances between the respective centroidal axes of the slab and beam components and their respective extreme fibres.
E_t, E_b	=	moduli of elasticity of the slab and beam components respectively.
$\frac{1}{EA}$	=	$\frac{1}{E_tA_t} + \frac{1}{E_bA_b}$
ΣEI	=	$E_tI_t + E_bI_b$

$\overline{EI}$ = $\Sigma EI + \overline{EA}z^2$

$\frac{l}{C}$ = $\frac{k}{s}\frac{L^2}{\overline{EA}}\frac{\overline{EI}}{\Sigma EI\,\pi^2}$

F, F_L, F_R, F' = horizontal direct forces acting at the centroids of the slab and beam components.

I_t, I_b = second moments of area of the slab and beam components respectively.

k = modulus of shear connector (in lb/in).

L = span length of composite beam.

M = total internal stress couple of the composite beam.

M_t, M_b = internal stress couples of the slab and beam components respectively.

q, q_L, q_R, q' = horizontal shear per unit length of beam, transmitted between the slab and beam components.

Q = connector load.

s = connector spacing.

s_b = $y_b/\Sigma EI$

u = distance from the point of application of the load to the nearest end support.

W = applied load on composite beam.

x = distance of cross-section from the left support.

y, y' = flexural deflections.

y_t, y_b = vertical distances from the centroidal axes of the slab and beam components respectively.

z = distance between centroidal axes of slab and beam components.

γ = slip between the slab and beam components.

ε_t, ε_b = strains in the slab and beam components respectively

ε_{bb} = strain in the lower fibre of the beam component

A.2 Analysis by the Newmark Theory

The beams considered in Fig. A.1 are composite rectangular beams which are analyzed in accordance with the Newmark theory. The development of this theory leading to equations 1, 2, 3 and 4 hereunder was originally done by N.W. Newmark[1].

The general differential equation is:

$$\frac{d^2F}{dx^2} - F\frac{k}{s}\frac{\overline{EI}}{\overline{EA}\,\Sigma EI} = -\frac{k\,M\,z}{s\,\Sigma EI} \qquad (1)$$

where F is the horizontal direct force acting at the centroids of the slab and beam components,

and M is the total internal stress couple of the composite beam usually expressed in terms of the distance x of the section from the left support.

The strain equations are:

$$\varepsilon_b = \left[s_b - \frac{F}{F'}\frac{\overline{EA}z}{\overline{EI}}\left(s_b z - \frac{1}{E_b A_b}\right)\right] M \qquad (2)$$

$$\varepsilon_t = \left[s_t - \frac{F}{F'}\frac{\overline{EA}z}{\overline{EI}}\left(s_t z + \frac{1}{E_t A_t}\right)\right] M \qquad (3)$$

The deflection equation is:

$$y = y' + \frac{M L^2 C\,\overline{EA}\,z^2}{\overline{EI}\,\pi^2\,\Sigma EI}\frac{F}{F'} \qquad (4)$$

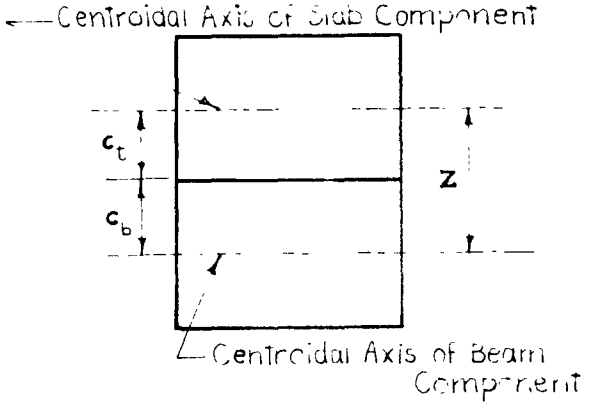

(a) Cross-Section

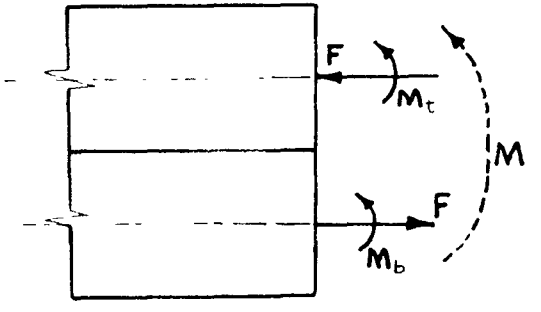

(b) Forces

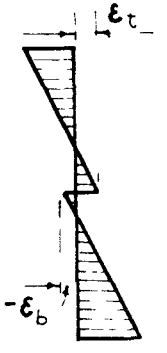

(c) Strain Distribution

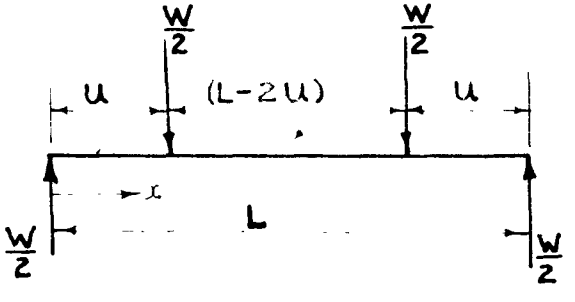

(d) Two-point Loading

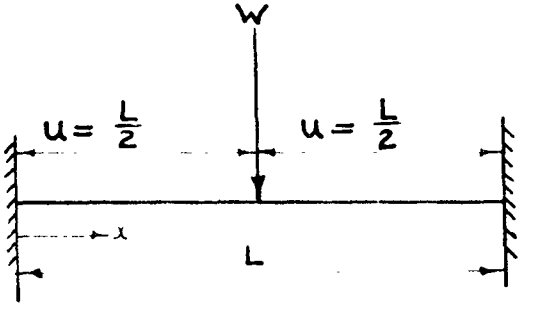

(e) Encastre Beam With Concentrated Load

Fig. A.1 Composite Rectangular Beams With Incomplete Interaction

Case A: A simply supported beam with two-point loading as shown in Fig. A.1(d).

The compatibility conditions assumed are:

at $x = 0$, $F_L = 0$

at $x = u$, $F_L = F_R$ and $\frac{dF_L}{dx} = \frac{dF_R}{dx}$

at $x = L/2$, $\frac{dF_R}{dx} = 0$

The solutions for F and q are:

for $x \leq u$

$$F_L = Z \frac{\overline{EA}}{\overline{EI}} \frac{W}{2} \left[x - \frac{\sqrt{c}L}{\pi} \frac{\sinh\left(\frac{\pi x}{\sqrt{c}L}\right) \cosh\left(\frac{\pi}{\sqrt{c}}\left(\frac{1}{2} - \frac{u}{L}\right)\right)}{\cosh\left(\frac{\pi}{2\sqrt{c}}\right)} \right]$$

$$F_L' = Z \frac{\overline{EA}}{\overline{EI}} \frac{W}{2} x$$

$$\frac{F_L}{F_L'} = 1.0 - \frac{\sqrt{c}L}{\pi x} \cdot \frac{\sinh\left(\frac{\pi x}{\sqrt{c}L}\right) \cosh\left(\frac{\pi}{\sqrt{c}}\left(\frac{1}{2} - \frac{u}{L}\right)\right)}{\cosh\left(\frac{\pi}{2\sqrt{c}}\right)}$$

$$q_L = Z \frac{\overline{EA}}{\overline{EI}} \frac{W}{2} \left[1.0 - \frac{\cosh\left(\frac{\pi x}{\sqrt{c}L}\right) \cosh\left(\frac{\pi}{\sqrt{c}}\left(\frac{1}{2} - \frac{u}{L}\right)\right)}{\cosh\left(\frac{\pi}{2\sqrt{c}}\right)} \right]$$

$$q_L' = Z \frac{\overline{EA}}{\overline{EI}} \frac{W}{2}$$

$$\frac{q_L}{q'_L} = 1{\cdot}0 - \frac{\cosh\left(\frac{\pi x}{\sqrt{c}L}\right)\cosh\left(\frac{\pi}{\sqrt{c}}\left(\frac{1}{2}-\frac{u}{L}\right)\right)}{\cosh\left(\frac{\pi}{2\sqrt{c}}\right)}$$

and for $u \leqslant x \leqslant L/2$

$$F_R = Z\frac{\overline{EA}}{\overline{EI}}\frac{w}{2}\left[u - \frac{\sqrt{c}L}{\pi}\frac{\sinh\left(\frac{\pi u}{\sqrt{c}L}\right)\cosh\left(\frac{\pi}{\sqrt{c}}\left(\frac{1}{2}-\frac{x}{L}\right)\right)}{\cosh\left(\frac{\pi}{2\sqrt{c}}\right)}\right]$$

$$F'_R = Z\frac{\overline{EA}}{\overline{EI}}\frac{w}{2}u$$

$$\frac{F_R}{F'_R} = 1{\cdot}0 - \left[\frac{\sqrt{c}L}{\pi u}\frac{\sinh\left(\frac{\pi u}{\sqrt{c}L}\right)\cosh\left(\frac{\pi}{\sqrt{c}}\left(\frac{1}{2}-\frac{x}{L}\right)\right)}{\cosh\frac{\pi}{2\sqrt{c}}}\right]$$

$$q_R = Z\frac{\overline{EA}}{\overline{EI}}\frac{w}{2}\left[\frac{\sinh\left(\frac{\pi u}{\sqrt{c}L}\right)\sinh\left(\frac{\pi}{\sqrt{c}}\left(\frac{1}{2}-\frac{x}{L}\right)\right)}{\cosh\left(\frac{\pi}{2\sqrt{c}}\right)}\right]$$

$$q'_R = Z\frac{\overline{EA}}{\overline{EI}}\frac{w}{2}$$

$$\frac{q_R}{q'_R} = \frac{\sinh\left(\frac{\pi u}{\sqrt{c}L}\right)\sinh\left(\frac{\pi}{\sqrt{c}}\left(\frac{1}{2}-\frac{x}{L}\right)\right)}{\cosh\frac{\pi}{2\sqrt{c}}}$$

where $\frac{1}{C} = \frac{k}{s}\frac{L^2}{\pi^2}\frac{\overline{EI}}{\overline{EA}\,\Sigma EI}$

Case B: An encastre beam with a concentrated load at midspan as shown in Fig. A.1(e).

The assumed compatibility conditions are:

at $x = 0$, $\gamma = 0$ and hence $\frac{dF_L}{dx} = 0$

at $x = L$, $\gamma = 0$ and hence $\frac{dF_R}{dx} = 0$

at $x = u$, $F_L = F_R$

The solutions for F and q are:

for $0 \leq x \leq L/2$

$$F_L = Z\frac{\overline{EA}}{\overline{EI}} W L \left[-\frac{\sqrt{c}\cosh\left(\frac{\pi x}{\sqrt{c}L}\right)}{\pi \sinh\left(\frac{\pi u}{\sqrt{c}L}\right)\sinh\frac{\pi}{\sqrt{c}}} \left\{ \sinh\left(\frac{\pi}{\sqrt{c}}\left(1.0 - \frac{u}{L}\right)\right)\left(2\frac{u^3}{L^3} - 3\frac{u^2}{L^2}\right.\right.\right.$$

$$\left. + 1.0 - \cosh\left(\frac{\pi u}{\sqrt{c}L}\right)\right) + \left(2\frac{u^3}{L^3} - 3\frac{u^2}{L^2}\right)\left(\sinh\left(\frac{\pi u}{\sqrt{c}L}\right) - \cosh\left(\frac{\pi u}{\sqrt{c}L}\right)\cdot\right.$$

$$\left.\left. \sinh\frac{\pi}{\sqrt{c}}\right)\right\} - \frac{\sqrt{c}\cosh\left(\frac{\pi x}{\sqrt{c}L}\right)\left(1.0 - \cosh\left(\frac{\pi u}{\sqrt{c}L}\right)\right)}{\pi \sinh\left(\frac{\pi u}{\sqrt{c}L}\right)} - \frac{\sqrt{c}}{\pi}\sinh\left(\frac{\pi x}{\sqrt{c}L}\right)$$

$$\left.\left(2\frac{u^3}{L^3} - 3\frac{u^2}{L^2} + 1.0\right) + 2\frac{u^3 x}{L^4} - 3\frac{u^2 x}{L^3} + \frac{x}{L} - \frac{u}{L} + \frac{2u^2}{L^2} - \frac{u^3}{L^3}\right]$$

$$F_L' = Z\frac{\overline{EA}}{\overline{EI}} W L \left[2\frac{u^3 x}{L^4} - 3\frac{u^2 x}{L^3} + \frac{x}{L} - \frac{u}{L} + 2\frac{u^2}{L^2} - \frac{u^3}{L^3} \right]$$

$$\frac{F_L}{F_L'} = 1.0 + \frac{1}{\left(2\frac{u^3x}{L^4} - 3\frac{u^2x}{L^3} + \frac{x}{L} - \frac{u}{L} + 2\frac{u^2}{L^2} - \frac{u^3}{L^3}\right)}\left[-\frac{\sqrt{c}\cosh\left(\frac{\pi x}{\sqrt{c}L}\right)}{\pi\sinh\left(\frac{\pi u}{\sqrt{c}L}\right)\sinh\frac{\pi}{\sqrt{c}}}\right\{$$

$$\sinh\left(\frac{\pi}{\sqrt{c}}\left(1.0-\frac{u}{L}\right)\right)\left(2\frac{u^3}{L^3} - 3\frac{u^2}{L^2} + 1.0 - \cosh\left(\frac{\pi u}{\sqrt{c}L}\right)\right) + \left(2\frac{u^3}{L^3} - 3\frac{u^2}{L^2}\right)$$

$$\left(\sinh\left(\frac{\pi u}{\sqrt{c}L}\right) - \cosh\left(\frac{\pi u}{\sqrt{c}L}\right)\sinh\frac{\pi}{\sqrt{c}}\right)\Bigg\} - \frac{\sqrt{c}\cosh\left(\frac{\pi x}{\sqrt{c}L}\right)\left(1.0-\cosh\left(\frac{\pi u}{\sqrt{c}L}\right)\right)}{\pi\sinh\left(\frac{\pi u}{\sqrt{c}L}\right)}$$

$$-\frac{\sqrt{c}}{\pi}\sinh\left(\frac{\pi x}{\sqrt{c}L}\right)\left(2\frac{u^3}{L^3} - 3\frac{u^2}{L^2} + 1.0\right)\Bigg]$$

$$q_L = z\frac{\overline{EA}}{EI}w\left[\frac{-\sinh\left(\frac{\pi x}{\sqrt{c}L}\right)}{\sinh\left(\frac{\pi u}{\sqrt{c}L}\right)\sinh\frac{\pi}{\sqrt{c}}}\left\{\sinh\left(\frac{\pi}{\sqrt{c}}\left(1.0-\frac{u}{L}\right)\right)\left(2\frac{u^3}{L^3} - 3\frac{u^2}{L^2} + 1.0\right.\right.\right.$$

$$\left.\left.\left.-\cosh\left(\frac{\pi u}{\sqrt{c}L}\right)\right) + \left(2\frac{u^3}{L^3} - 3\frac{u^2}{L^2}\right)\left(\sinh\left(\frac{\pi u}{\sqrt{c}L}\right) - \cosh\left(\frac{\pi u}{\sqrt{c}L}\right)\sinh\frac{\pi}{\sqrt{c}}\right)\right\}\right.$$

$$\left.-\frac{\sinh\left(\frac{\pi x}{\sqrt{c}L}\right)\left(1.0-\cosh\left(\frac{\pi u}{\sqrt{c}L}\right)\right)}{\sinh\left(\frac{\pi u}{\sqrt{c}L}\right)} - \cosh\left(\frac{\pi x}{\sqrt{c}L}\right)\left(2\frac{u^3}{L^3} - 3\frac{u^2}{L^2} + 1.0\right)\right.$$

$$\left.+2\frac{u^3}{L^3} - 3\frac{u^2}{L^2} + 1.0\right]$$

$$q_L' = 2\frac{\overline{EA}}{\overline{EI}} w \left[2\frac{u^3}{L^3} - 3\frac{u^2}{L^2} + 1.0 \right]$$

$$\frac{q_L}{q_L'} = 1.0 - \frac{1}{\left(2\frac{u^3}{L^3} - 3\frac{u^2}{L^2} + 1.0\right)} \left[\frac{\sinh\left(\frac{\pi x}{\sqrt{c}\,L}\right)}{\sinh\left(\frac{\pi u}{\sqrt{c}\,L}\right)\sinh\frac{\pi}{\sqrt{c}}} \left\{ \sinh\left(\frac{\pi}{\sqrt{c}}\left(1.0 - \frac{u}{L}\right)\right)\left(2\frac{u^3}{L^3} - 3\frac{u^2}{L^2} + 1.0 - \cosh\left(\frac{\pi u}{\sqrt{c}\,L}\right)\right) + \left(2\frac{u^3}{L^3} - 3\frac{u^2}{L^2}\right)\left(\sinh\left(\frac{\pi u}{\sqrt{c}\,L}\right) - \cosh\left(\frac{\pi u}{\sqrt{c}\,L}\right)\cdot \sinh\frac{\pi}{\sqrt{c}}\right) \right\} + \frac{\sinh\left(\frac{\pi x}{\sqrt{c}\,L}\right)\left(1.0 - \cosh\left(\frac{\pi u}{\sqrt{c}\,L}\right)\right)}{\sinh\left(\frac{\pi u}{\sqrt{c}\,L}\right)} + \cosh\left(\frac{\pi x}{\sqrt{c}\,L}\right)\cdot \left(2\frac{u^3}{L^3} - 3\frac{u^2}{L^2} + 1.0\right) \right]$$

Due to the symmetry of loading F_L, F_L', q_L and q_L' are are equal to F_R, F_R', q_R and q_R' respectively.

A.3 Sample Calculations

Sample calculations of strain and deflection for beam B1:

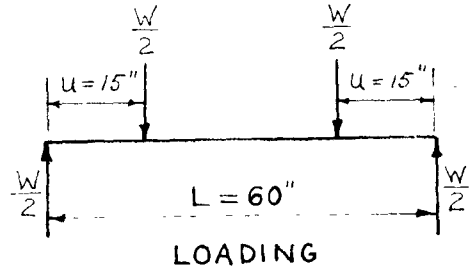

BEAM B1

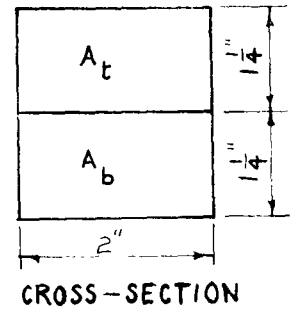

CROSS-SECTION

$A_t = A_b = 2'' \times 1\frac{1}{4}'' = 2.5$ sq. ins.

$Z = 1.25''$

$I_t = I_b = \frac{1}{12} \times 2 \times \left(\frac{5}{4}\right)^3 = 0.33$ in.^{4}

$E_t = E_b = 32.25 \times 10^6$ lbs./in^2

$$\frac{1}{\overline{EA}} = \frac{1}{E_t A_t} + \frac{1}{E_b A_b} = \frac{2}{32.25 \times 10^6 \times 2.5}$$

Therefore $\overline{EA} = 40.31 \times 10^6$

$\Sigma EI = E_t I_t + E_b I_b = 2(32.25 \times 10^6 \times 0.33) = 2.13 \times 10^7$

$\overline{EA} \cdot Z^2 = 40.31 \times 10^6 \times 1.56 = 6.29 \times 10^7$

$$\begin{array}{rl} \overline{EI} = \Sigma EI + \overline{EA} \cdot Z^2 = & 2.13 \times 10^7 \\ + & 6.29 \times 10^7 \\ \hline & 8.42 \times 10^7 \end{array} = 8.42 \times 10^7$$

I = second moment of area of composite section for complete interaction = $(2 \times 2.5^3)/12 = 2.61$ in.^{4}.

$EI = 32.25 \times 10^6 \times 2.61 = 8.42 \times 10^7$

$$s_b = y_b/\Sigma EI = \frac{0.625}{2.13 \times 10^7} = 2.93 \times 10^{-8}$$

Midspan moment = moment at quarter-span = $(W \times 15)/2 = M$

For midspan computations $x = 30''$, and for computations at load point $x = 15''$.

Strains

Referring to equation (2), strains at the lower

fibre of the beam component are computed from the following equations:

$$\varepsilon_{bb}(\text{quarter-span}) = \left[2{\cdot}78 \times 10^{-8} - 1{\cdot}48 \times 10^{-8} \times \frac{F_L}{F_L'}\right] \frac{W}{2} \times 15$$

$$\varepsilon_{bb}(\text{midspan}) = \left[2{\cdot}78 \times 10^{-8} - 1{\cdot}48 \times 10^{-8} \times \frac{F_R}{F_R'}\right] \frac{W}{2} \times 15$$

Deflection

$$y' = \frac{15W}{12EI}\left[3Lx - 3x^2 - u^2\right]$$

Referring to equation (4),

$$y(\text{midspan}) = W\left[3{\cdot}67 + \frac{9{\cdot}6}{1/C} \times \frac{F_R}{F_R'}\right] 10^{-5}$$

A few results are presented in Table A.1. The values for incomplete interaction are based on 1/C = 7.59. This value of 1/C was computed from the measured end slips of beam B1 as discussed in section 2.2.

Sample calculation of efficiency curves of beam in Fig. A.2:

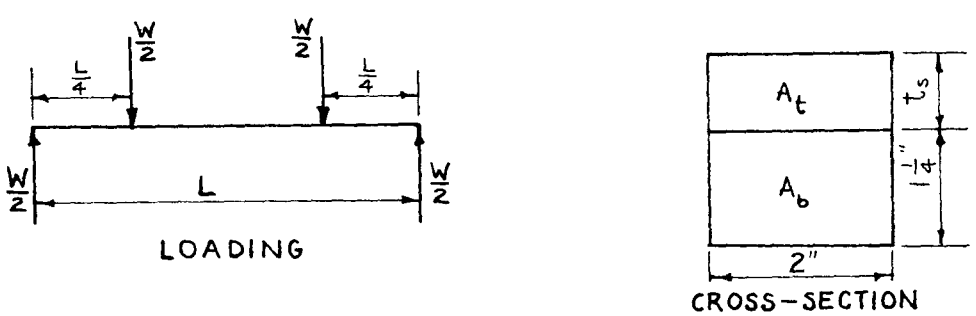

FIG. A.2

No. of connectors = 17

$s = L/(17 - 1)$ inches

$E_t = E_b = 32.25 \times 10^6$ lbs/in^2.

$k = 3.82 \times 10^5$ lbs/in.

$$\frac{1}{C} = \frac{k}{s} \frac{L^2 \overline{EI}}{\pi^2 EA \ \Sigma EI}$$

y'(midspan) = deflection due to complete interaction and is computed as shown before in the case of beam B1.

Δy(midspan) = increase in deflection due to loss of interaction = $\dfrac{M L^2 \overline{EA} z^2 F_R}{1/C \ \overline{EI} \ \Sigma EI \ F_R'}$

Efficiency = $(1.0 - (\Delta y/y')) 100$

TABLE A.1 - RESULTS OF BEAM B1

W in kips	ε_{bb} quarter-span in inches per inch			Midspan deflection in inches		
	Complete Interaction	Incomplete Interaction	Zero Interaction	Complete Interaction	Incomplete Interaction	Zero Interaction
1	0.00011	0.00014	0.00022	0.037	0.049	0.147
2	0.00022	0.00027	0.00045	0.074	0.098	0.295
3	0.00033	0.00041	0.00067	0.111	0.147	0.442
4	0.00045	0.00055	0.00089	0.147	0.196	0.589
5	0.00056	0.00069	0.00112	0.184	0.245	0.737

APPENDIX B

The notation in the Appendix is also the notation of the thesis.

B.1 Notation

The subscripts used with the notation of this Appendix have the following meaning:

b = beam component

t = slab component

The following symbols have been adopted for use in this Appendix:

A_t, A_b = cross sectional areas of the slab and beam components respectively

$A_{id} = \dfrac{2n_t A_t \cdot n_b A_b}{n_t A_t + n_b A_b}$

c_t, c_b = distances between the respective centroidal axes of the slab and beam components and the interface

C = a reference connector modulus (in lbs/in.)

C_i = modulus of connector at section i of the composite beam (in lbs/in.)

d_i = spacing between the shear connectors at sections i and (i+1) of the composite beam

d_i' = deformed length of d_i at the lower fibre of the slab component

d_i'' = deformed length of d_i at the upper fibre of the beam component

e_t, e_b = distances between the respective centroidal axes of the slab and beam components and their respective extreme fibres

E = a reference modulus of elasticity

E_t, E_b = moduli of elasticity of slab and beam components respectively

F_i = sum of horizontal connector forces from the left support up to section i of the composite beam

I_t, I_b = second moments of area of slab and beam components respectively

$I_n = I_{no} + A_{id} \cdot \frac{z^2}{2}$

$I_{no} = n_t I_t + n_b I_b$

L = span length of composite beam

M = total internal stress couple of composite beam

M_{ai} = total internal stress couple of composite beam at the middle of d_i

M_t, M_b = internal stress couples of the slab and beam components respectively

$n_b = E_b/E$

$n_t = E_t/E$

Q_x = horizontal component of connector force

Q_y = vertical component of connector force

W = total applied load on composite beam

z = distance between centroidal axes of beam and slab components

$\alpha = \frac{2 I_n \cdot C}{E \cdot I_{no} \cdot A_{id}}$

β = $\frac{z\ C}{E\ I_{no}}$

γ = slip between the slab and beam components

$\Delta\varepsilon_b$ = strain at the lower fibre of beam component due to M_b

$\Delta\varepsilon_t$ = strain at the upper fibre of slab component due to M_t

$\Delta\sigma_b$ = stress at the lower fibre of beam component due to M_b

$\Delta\sigma_t$ = stress at the upper fibre of slab component due to M_t

ε_{ts}, ε_{bs} = strains caused by F in slab and beam components respectively

σ_{ts}, σ_{bs} = stresses caused by F in slab and beam components respectively

B.2 Analysis by the Stussi Theory

The beam considered in Fig. B.1 is a composite rectangular beam. It consists of two rectangular components held together by shear connectors, and is analyzed in accordance with the Stussi theory[2].

The principal assumptions made in the analysis are as follows:-

1) The slab and beam components have equal curvature at all points.

2) The distribution of strains throughout the depth of the slab and beam components is linear.

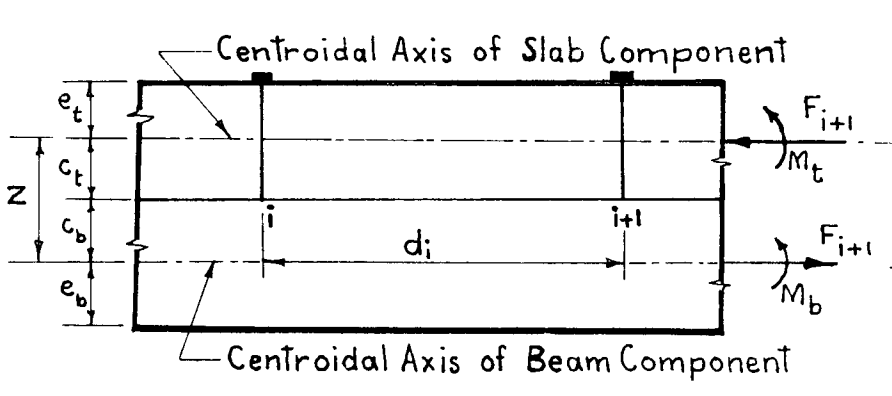

(a) Undeformed Beam

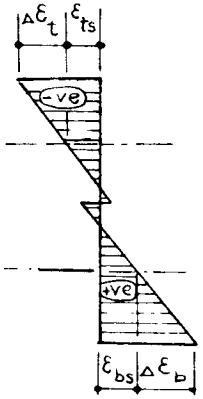

(b) Strain Distribution

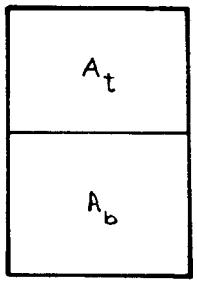

(c) Cross-Section

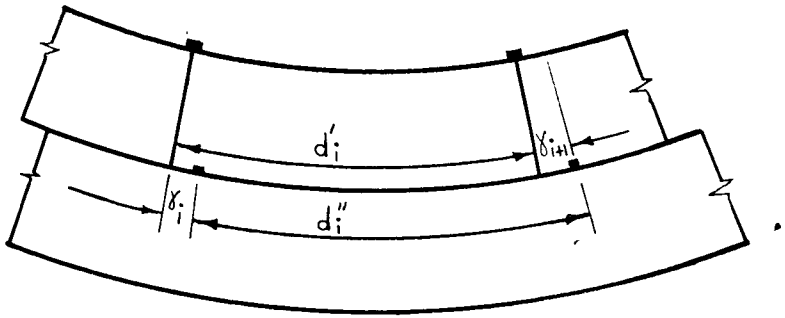

(d) Deformed Beam

A: Area

γ: Slip

d: Spacing of Connectors

ε: Strains

Fig. B.1 Composite Rectangular Beam

3) The deformation of the shear connectors is proportional to the connector loads.

Referring to Fig. B.1(d),

let

$\Delta d_i'$ = change in the length of the lower face of the top component

and

$\Delta d_i''$ = change in the length of the upper face of the bottom component

then

$$\Delta d_i' + \gamma_{i+1} = \Delta d_i'' + \gamma_i \quad \text{.....(1)}$$

If the total internal stress couple at the middle of $d_i = M_{ai}$, then the changes in length of the upper and lower faces considered are:

$$\Delta d_i' = \frac{d_i}{E_t}\left(\frac{M_{ait} \cdot c_t}{I_t} - \frac{F_i}{A_t}\right)$$

and

$$\Delta d_i'' = \frac{d_i}{E_b}\left(-\frac{M_{aib} \cdot c_b}{I_b} - \frac{F_i}{A_b}\right)$$

The deformation of the connectors is proportional to the connector forces Q_x.

Hence

$$\gamma_i = \frac{F_i - F_{i-1}}{C_i} = \frac{Q_{xi}}{C_i}$$

and

$$\gamma_{i+1} = \frac{F_{i+1} - F_i}{C_{i+1}} = \frac{Q_{x(i+1)}}{C_{i+1}}$$

Referring to Fig. B.1(b),

$$\frac{M_{ait} \cdot c_t}{I_t} - \frac{F_i}{A_t} = \frac{\Delta\sigma_t \cdot c_t}{e_t} - \sigma_{ts}$$

and

$$-\frac{M_{aib} \cdot c_b}{I_b} + \frac{F_i}{A_b} = -\frac{\Delta\sigma_b \cdot c_b}{e_b} + \sigma_{bs}$$

Hence

$$\Delta d_i' + \gamma_{i+1} = \frac{d_i}{E_t}\left(-\sigma_{ts} + \frac{\Delta\sigma_t \cdot c_t}{e_t}\right) + \frac{F_{i+1} - F_i}{C_{i+1}}$$

and

$$\Delta d_i'' + \gamma_i = \frac{d_i}{E_b}\left(\sigma_{bs} - \frac{\Delta\sigma_b \cdot c_b}{e_b}\right) + \frac{F_i - F_{i-1}}{C_i}$$

Equation (1) can now be written as:

$$\frac{d_i}{E_t}\left(-\sigma_{ts} + \frac{\Delta\sigma_t \cdot c_t}{e_t}\right) + \frac{F_{i+1} - F_i}{C_{i+1}} = \frac{d_i}{E_b}\left(\sigma_{bs} - \frac{\sigma_b \cdot c_b}{e_b}\right) + \frac{F_i - F_{i-1}}{C_i} \quad \text{.....(2)}$$

The total internal stress couple $M = F \cdot z + \frac{\Delta\sigma_t I_t}{e_t} + \frac{\Delta\sigma_b I_b}{e_b}$

and

$$F = \sigma_{ts} \cdot A_t = \sigma_{bs} \cdot A_b$$

Due to equal curvature of beam and slab components,

$$\frac{\Delta\sigma_t}{e_t E_t} = \frac{\Delta\sigma_b}{e_b E_b} \quad \text{----------(3)}$$

hence

$$M = F \cdot z + \frac{\Delta\sigma_t}{e_t E_t}\left(E_t I_t + E_b I_b\right) = F \cdot z + \frac{\Delta\sigma_b}{e_b E_b}\left(E_t I_t + E_b I_b\right)$$

$$\frac{\Delta\sigma_t}{e_t} = \frac{(M - F \cdot z) E_t}{E_t I_t + E_b I_b} \quad \text{and} \quad \frac{\Delta\sigma_b}{e_b} = \frac{(M - F \cdot z) E_b}{E_t I_t + E_b I_b}$$

Equation (2) can now be written as:

$$d_i\left(-\frac{F_i}{E_tA_t}+\frac{M_{ai}-F_i\cdot z}{E_tI_t+E_bI_b}c_t\right)+\frac{F_{i+1}-F_i}{C_{i+1}} = d_i\left(\frac{F_i}{E_bA_b}-\frac{M_{ai}-F_i\cdot z}{E_tI_t+E_bI_b}c_b\right) + \frac{F_i-F_{i-1}}{C_i} \quad \ldots\ldots\ldots (4)$$

Denoting

$$n_t = E_t/E \quad \text{and} \quad n_b = E_b/E$$

where

E is an arbitrary reference value for the modulus of elasticity,

and defining

$$I_{no} = n_tI_t + n_bI_b ,$$

$$A_{id} = \frac{2\, n_tA_t\, n_bA_b}{n_tA_t+n_bA_b}$$

and $$I_n = I_{no} + A_{id}\cdot\frac{z}{2}^2$$

Rearranging equation (4), the following equation for computing the longitudinal shear force F is obtained:

$$-\frac{F_{i-1}}{C_i} + F_i\left[\frac{1}{C_{i+1}}+\frac{1}{C_i}+2\frac{d_i\cdot I_n}{E\, I_{no}\cdot A_{id}}\right] - \frac{F_{i+1}}{C_{i+1}} = \frac{d_i\cdot z}{E\, I_{no}}M_{ai} \quad \ldots\ldots (5)$$

The solution of equation (5) for F enables the computation of the stresses in the components from the relations:-

$$\sigma_{ts} = \frac{F}{A_t}, \qquad \Delta\sigma_t = \frac{M-Fz}{I_{no}}n_te_t ,$$

$$\sigma_{bs} = \frac{F}{A_b}, \text{ and } \quad \Delta\sigma_b = \frac{M-Fz}{I_{no}}n_be_b .$$

B.3 Sample Calculations

Sample calculations of slip, strain and deflection for B2:

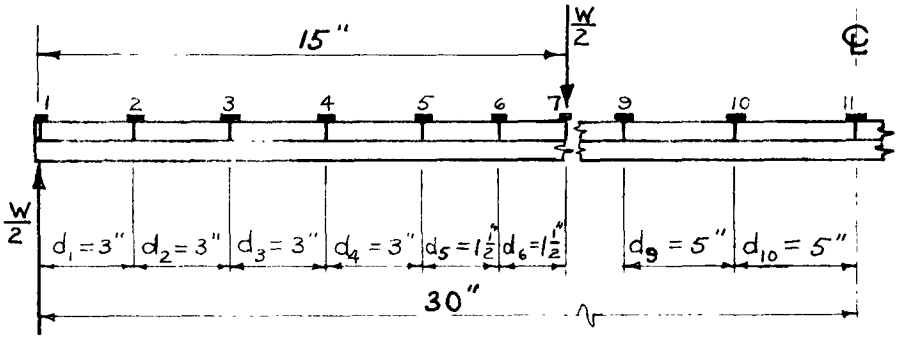

LOADING

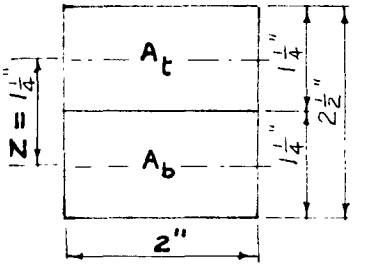

CROSS-SECTION

BEAM B-2

$C_1 = C_2 = C_3 = \cdots\cdots C_{11} = C = 3.44 \times 10^5$ lbs/in.

$Z = 1.25"$

$A_t = A_b = 2" \times \left(\frac{5}{4}\right)" = 2.5$ sq. ins.

$I_t = I_b = \frac{1}{12} \times 2 \times \left(\frac{5}{4}\right)^3 = 0.33$ in.^{4}

$E_b = E_t = E = 32.25 \times 10^6$ lbs/in^2

$n_b = \frac{E_b}{E} = 1.0 = n_t$

$$I_{no} = n_b I_b + n_t I_t = 0.66$$

$$A_{id} = \frac{2 n_t A_t \cdot n_b A_b}{n_t A_t + n_b A_b} = 2.5$$

$$I_n = I_{no} + \left(A_{id} \cdot \frac{z^2}{2}\right) = 0.66 + \frac{2.5}{2} \times \left(\frac{5}{4}\right)^2 = 2.62$$

Applying equation (5) to d_1 and d_2 gives:

$$F_1\left[\frac{1}{C_2} + \frac{1}{C_1} + \frac{2 d_1 I_n}{E I_{no} A_{id}}\right] - \frac{F_2}{C_2} = \frac{d_1 z M_{a1}}{E I_{no}}$$

and

$$\frac{-F_1}{C_2} + F_2\left[\frac{1}{C_3} + \frac{1}{C_2} + \frac{2 d_2 I_n}{E I_{no} A_{id}}\right] - \frac{F_3}{C_3} = \frac{d_2 z M_{a2}}{E I_{no}}$$

where

$$M_{a1} = \frac{W}{2} \times 1.5$$

and

$$M_{a2} = \frac{W}{2} \times 4.5$$

Making

$$\alpha = \frac{2 I_n C}{E I_{no} A_{id}} \quad \text{and} \quad \beta = \frac{z C}{E I_{no}}$$

The above equations relating to d_1 and d_2 may be written as:

$$F_1 = \left((d_1 M_{a1} \beta) + F_2\right) / (2.0 + d_1 \alpha) \quad \text{..... (a)}$$

and

$$F_2 = \left((d_2 M_{a2} \beta) + F_1 + F_3\right) / (2.0 + d_2 \alpha) \quad \text{..... (b)}$$

Similarly the following equations may be written:

$$F_3 = \left((d_3 M_{\alpha 3}\beta) + F_2 + F_4\right) / (2.0 + d_3\alpha) \quad \text{(c)}$$

$$\vdots \qquad \vdots \qquad \vdots$$

$$F_9 = \left((d_9 M_{\alpha 9}\beta) + F_8 + F_{10}\right) / (2.0 + d_9\alpha) \quad \text{(i)}$$

$$F_{10} = \left((d_{10} M_{\alpha 10}\beta) + F_9 + F_{11}\right) / (2.0 + d_{10}\alpha) \quad \text{(j)}$$

In equation (j) due to the symmetry of loading, $F_{11} = F_{10}$.

Therefore, this equation becomes:

$$F_{10} = \left((d_{10} M_{\alpha 10}\beta) + F_9\right) / (1.0 + d_{10}\alpha) \quad \text{(j')}$$

The Gauss Seidel Iteration can be applied to the above simultaneous equations so that the values of F may be obtained.

Slip:

$$\text{Slip at connector No.1} = \frac{Q_{x1}}{C_1} = \frac{F_1}{C_1}$$

$$\text{Slip at connector No.2} = \frac{Q_{x2}}{C_2} = \frac{F_2 - F_1}{C_2}$$

$$\vdots \qquad \vdots \qquad \vdots$$

$$\text{Slip at connector No.10} = \frac{Q_{x10}}{C_{10}} = \frac{F_{10} - F_9}{C_{10}}$$

Strain:

Strain at the lower fibre of the beam component at midspan $= \frac{M_{11} - F_{11} \cdot z}{I_{no}} \cdot n_b e_b = \frac{\left(\frac{W}{2} \times 15 - F_{10} \cdot z\right)}{0.66} \times 0.625$

Deflection:

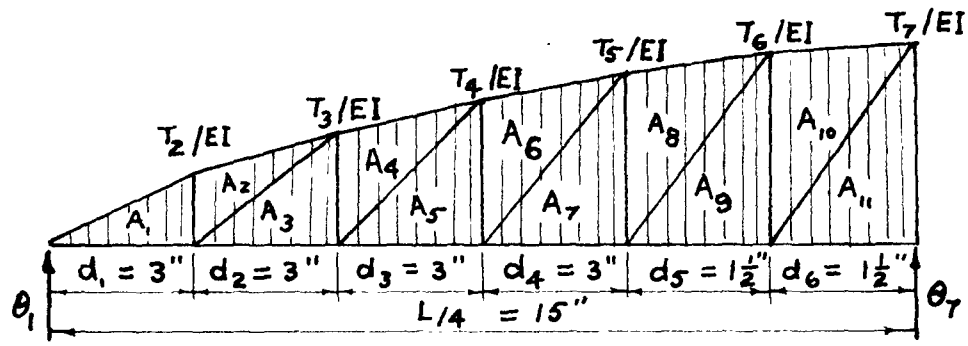

FIG. B·2

Fig. B.2 represents the equivalent conjugate beam over quarter span of beam B2.

Considering the beam component only,

$$T_2 = \frac{M_2 - F_2 z}{2}, \quad T_3 = \frac{M_3 - F_3 z}{2}, \ldots\ldots T_7 = \frac{M_7 - F_7 z}{2}$$

Load point deflection = quarter-span deflection =

$$\theta_1 \times 15 - (A_1 \times 13 + A_2 \times 11 + \ldots\ldots A_{10} \times 1 + A_{11} \times .5)$$

Computer programming has been used in the above computations, and a few results are shown in Table B.1.

Beam B5:

In the case of B5 an infinitely stiff end connection is assumed, hence $C_1 = \infty$.

Therefore, applying equation (5) to d_1 and d_2 of this member, the following equations are obtained:

$$F_1\left[\frac{1}{C_2} + \cancel{\frac{1}{C_1}}_{\,0} + \frac{2\,d_1\,I_n}{E I_{no} A_{id}}\right] - \frac{F_2}{C_2} = \frac{d_1 z M_{a1}}{E I_{no}}$$

and

$$-\frac{F_1}{C_2} + F_2\left[\frac{1}{C_3} + \frac{1}{C_2} + \frac{2 d_2 I_n}{E I_{no} A_{id}}\right] - \frac{F_3}{C_3} = \frac{d_2 z M_{a2}}{E I_{no}}$$

The rest of the analysis for B5 is similar to the case of B2.

TABLE B.1 - RESULTS OF BEAM B2

W in kips	Quarter-span deflection in inches			End slips in .0001 ins.	Midspan strains* at bottom of beam in ins./in. Incomplete Interaction
	Complete Interaction	Incomplete Interaction	Zero Interaction		
1	0.027	0.038	0.107	17.1	0.00012
2	0.054	0.077	0.214	34.1	0.00025
3	0.080	0.115	0.321	51.2	0.00037
4	0.107	0.153	0.429	68.3	0.00050
5	0.134	0.191	0.536	85.3	0.00062

* Strains for complete and zero interaction are the same as those at midspan for beam B1 as shown in Table A.1 of Appendix A.

REFERENCES

1. Siess, C.P., Viest, I.M., and Newmark, N.M., "Small-Scale Tests of Shear Connectors and Composite Beams," Bulletin No. 396, University of Illinois Engineering Experiment Station, 1952.

2. Stussi, F., "Zusammengesetzte Vollwandtrager," Publications, International Association for Bridge and Structural Engineering, Vol. VIII, pp. 249 - 269, 1947.

3. Viest, I.M., Siess, C.P., Appleton, J.H., and Newmark, N.M., "Full-Scale Tests of Channel Shear Connectors and Composite T-Beams," Bulletin No. 405, University of Illinois Engineering Experiment Station, 1952.

4. Slutter, R.G., and Adams, R.G., "Tests of Composite Beams with Holorib Composite Slabs," Fritz Engineering Laboratory Report No. 200.63.408.2, Lehigh University, 1964.

5. Chapman, J.C., "Composite Construction in Steel and Concrete - The Behaviour of Composite Beams," The Structural Engineer, Vol. 42, No. 4, April, 1964.

6. Chapman, J.C., and Balakrishnan, S., "Experiments on Composite Beams," The Structural Engineer, Vol. 42, No. 11, November, 1964.

7. Khan, Fazlur R., "Inland Hi-Bond Composite Beam Design", Design Manual No. 272, 1964.

8. Robinson, H., "Proposed Method of Establishing Design Criteria for Composite Steel and Concrete Beams Incorporating Cellular Steel Decking," Mc Master University, Hamilton, 1964.

9. Dai, K.H., and Siess, C.P., "Analytical Study of Composite Beams with Inelastic Shear Connection," Structural Research Series No. 267, University of Illinois, 1963.

10. Lane, V.P., "The Influence of Cell Geometry on the Behaviour of Composite Cellular Beams," M. Eng. thesis Mc Master University, November, 1964.